THIRD ANNUAL
CLIMATE ASSESSMENT
1991

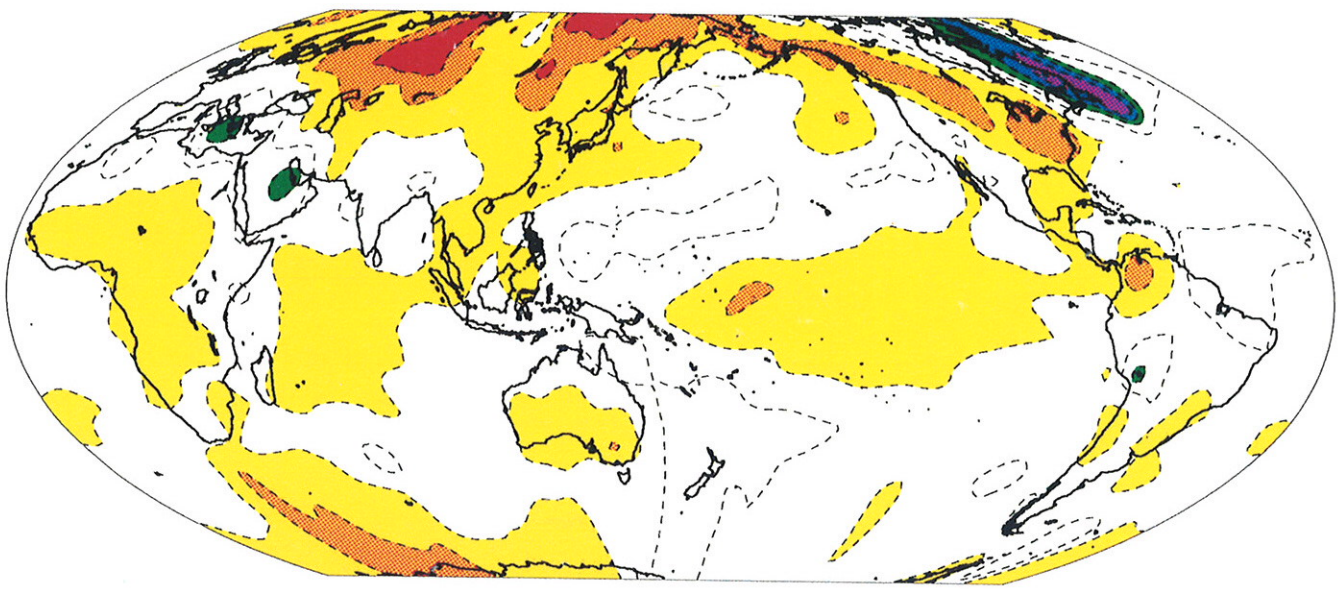

U.S. DEPARTMENT OF COMMERCE
National Weather Service
National Meteorological Center
Climate Analysis Center

COVER - Surface temperature anomalies for 1991. Analysis is based on station data over land and sea surface temperature data over the water. Anomalies for station data are from the 1951-1980 base period, while SST anomalies are computed as departures from the COADS/ICE climatology (Reynolds, 1988).

Climate Analysis Center
Camp Springs, Md
March 1992

THIRD ANNUAL
CLIMATE ASSESSMENT
1991

EDITORS: M. S. Halpert
C. F. Ropelewski

TECHNICAL ASSISTANCE:
J. D. Kopman

U. S. DEPARTMENT OF COMMERCE
NATIONAL OCEANIC AND ATMOSPHERIC ADMINISTRATION
NATIONAL WEATHER SERVICE
NATIONAL METEOROLOGICAL CENTER

Table of Contents

ACKNOWLEDGMENTS

This summary could not have been possible without the cooperation and contributions from several scientists representing a cross-section of the NOAA climate community. We also acknowledge the contributions from several scientists outside of NOAA. Each of the contributors have our sincere thanks for their timely and useful input. We also thank the internal reviewers (D. Rodenhuis, V. Kousky, R. Lehman, M. Gelman, L. Mannello) for their comments and suggestions. This report is partially supported by the Climate and Global Change sponsored Global Climate Perspectives System (GCPS) Project.

EXECUTIVE SUMMARY

The global climate of 1991 was influenced by a number of complex and competing influences, not all of them well understood. The detection of global warming was made more complicated by the short term competing influences of:

o a moderate El Niño/Southern Oscillation (ENSO) episode

and

o a major volcanic eruption (Mount Pinatubo).

The ocean-atmosphere system, after a prolonged build-up phase, moved into an ENSO mode during the spring of 1991. By this time, virtually all of the standard ENSO indicators suggested that a warm episode was in progress. Soon after the onset of the ENSO episode, Mt. Pinatubo erupted in mid-June. The aerosols associated with the Pinatubo eruption covered the global tropics by July and was associated with a $2^{o}C$ rise in stratospheric temperatures by the end of September. The effect of Mt. Pinatubo aerosols on tropospheric mean temperatures is more difficult to assess, since estimates of global temperature indicated that the 1991 temperature anomalies, although positive, were not as large as those observed during the first part of 1990 i.e., before the volcanic eruption. Nonetheless, 1991 was the second warmest year on record for the globe.

The typical precipitation and temperature pattern associated with ENSO episodes had established themselves in most locations by the end of August. Among the notable ENSO-related anomalies were extremely dry conditions over Indonesia, strong convective rainfall over the central equatorial Pacific, wet conditions over the southern United States and a warmer-than-normal early winter (December 1991) over northwestern North America.

Temperature patterns over the globe had many characteristics reminiscent of the entire decade of the 1980's. As in the past decade, the largest positive temperature anomalies were found over central and eastern Eurasia, and northwestern North America. Negative temperature anomalies were found over northeastern Canada and western Greenland. The main difference from the persistent temperature pattern of the 1980's was that an area of positive temperatures anomalies extended further eastward across the United States. The generally warmer-than-normal Northern Hemisphere temperatures were also accompanied by lower than average snow cover area and Arctic sea ice for the year.

CONTRIBUTORS

Air Resources Laboratory/ERL/NOAA

J. K. Angell

Climate Analysis Center/NMC/NWS/NOAA

G. D. Bell
D. R. Garrett
M. E Gelman
M. S. Halpert
J. E. Janowiak
J. D. Kopman
V. E. Kousky
A. J. Miller
D. Miskus
C. F. Ropelewski
P. Sabol
R. Tinker

Johnson Research Center, University of Alabama in Huntsville

J. R. Christy

NASA Marshall Space Flight Center

R. W. Spencer

National Climate Data Center NESDIS/NOAA

R. R. Heim Jr.

Satellite Research Laboratory NESDIS/NOAA

L. L. Stowe

List of Figures

Introduction

The purpose of this report is to present a technical resource which can be used to address questions concerning changes to the global climate system. Much of the data that is used in this summary is from preliminary reports; however, we do not expect that completed analyses will substantially change our preliminary results.

This year the most significant event has been the development of the El Nino/Southern Oscillation in the tropical Pacific. In addition, the question of global warming remains a critical issue and there is also a new sensitivity to changes in stratospheric ozone. However, the aerosols produced by the eruption of Mt. Pinatubo in mid-June, 1991 have added another factor of uncertainty to the interpretation of the observations.

This Assessment is being published for the third consecutive year. Our intention is to draw upon the NOAA-wide observational program and the early analyses which are available. In this we admit to being only partially successful, but we hope to produce a broader perspective in future years. In the meantime, there are some related publications which may augment this annual review.

Monthly ENSO Advisories	-	Climate Analysis Center
Antarctic Winter Summary 1991	-	Climate Analysis Center
Climate Variations Bulletin	-	National Climate Data Center
National Hydrologic Outlook Spring Flood Potential and Water Supply	-	Office of Hydrology/NWS

Southern Oscillation

By late 1990 surface and subsurface oceanic anomaly patterns in the western equatorial Pacific were indicating conditions favorable for the development of a warm episode. Sea surface temperatures were about 0.5°C above normal and the oceanic thermocline was deeper than normal. However, surface easterly winds, during early 1991, were near or slightly stronger than normal, and enhanced equatorial convection failed to develop in the central equatorial Pacific.

During the March - June transition season, the low-level easterlies weakened considerably and sea surface temperature anomalies increased substantially in the central equatorial Pacific, as once again conditions evolved toward a warm episode. Further development was delayed until the following transition season (September - November) when the easterlies weakened further and enhanced equatorial convection developed near the date line. By the end of 1991, all of the tropical Pacific indices were indicating that a warm episode was in progress and beginning to enter its mature phase.

As in the two previous warm episodes (1982-83, 1986-87), an important factor in establishing persistent enhanced convection in the central equatorial Pacific, during late 1991, was an eastward shift of the warmest water to the vicinity of the date line (**Fig. 1**). The evolution of warm episode conditions during late 1991 was similar in many respects to that observed during the early stages of the 1986-1987 warm episode. In both cases persistent enhanced convection first appeared in the central equatorial Pacific during the September - November period, as low-level easterlies (westerlies) became weaker than normal (established) in the central (western) equatorial Pacific. Also, subsurface thermal features, associated with a deepening (shoaling) thermocline in the eastern (western) equatorial Pacific (**Fig. 2**), evolved in a manner similar to that observed in late 1986.

However, by December 1991 certain differences were becoming evident in the evolution of the current warm episode as compared to the previous warm episode. By the end of 1991, the region of enhanced equatorial convection had shifted east of the date line (**Fig. 3**) and low-level easterlies throughout the central and eastern equatorial Pacific were at their weakest since the 1982-1983 warm episode. In spite of this, significant warming along the South American coast had not developed by the end of the year (**Fig. 4**).

The global precipitation and temperature anomaly patterns, generally associated with warm episodes, began to appear by the end of the year. Drier than normal conditions developed over most of Indonesia, the Philippines and northern Australia, while enhanced rainfall occurred over the islands in the central equatorial Pacific. Other features evident by the end of 1991,

including wetter than normal conditions over northern Mexico and the southern United States and warmer than normal conditions over western Canada and the northern border states of the contiguous United States, have been consistently observed during the mature phase of past warm episodes (Ropelewski and Halpert 1986,1987).

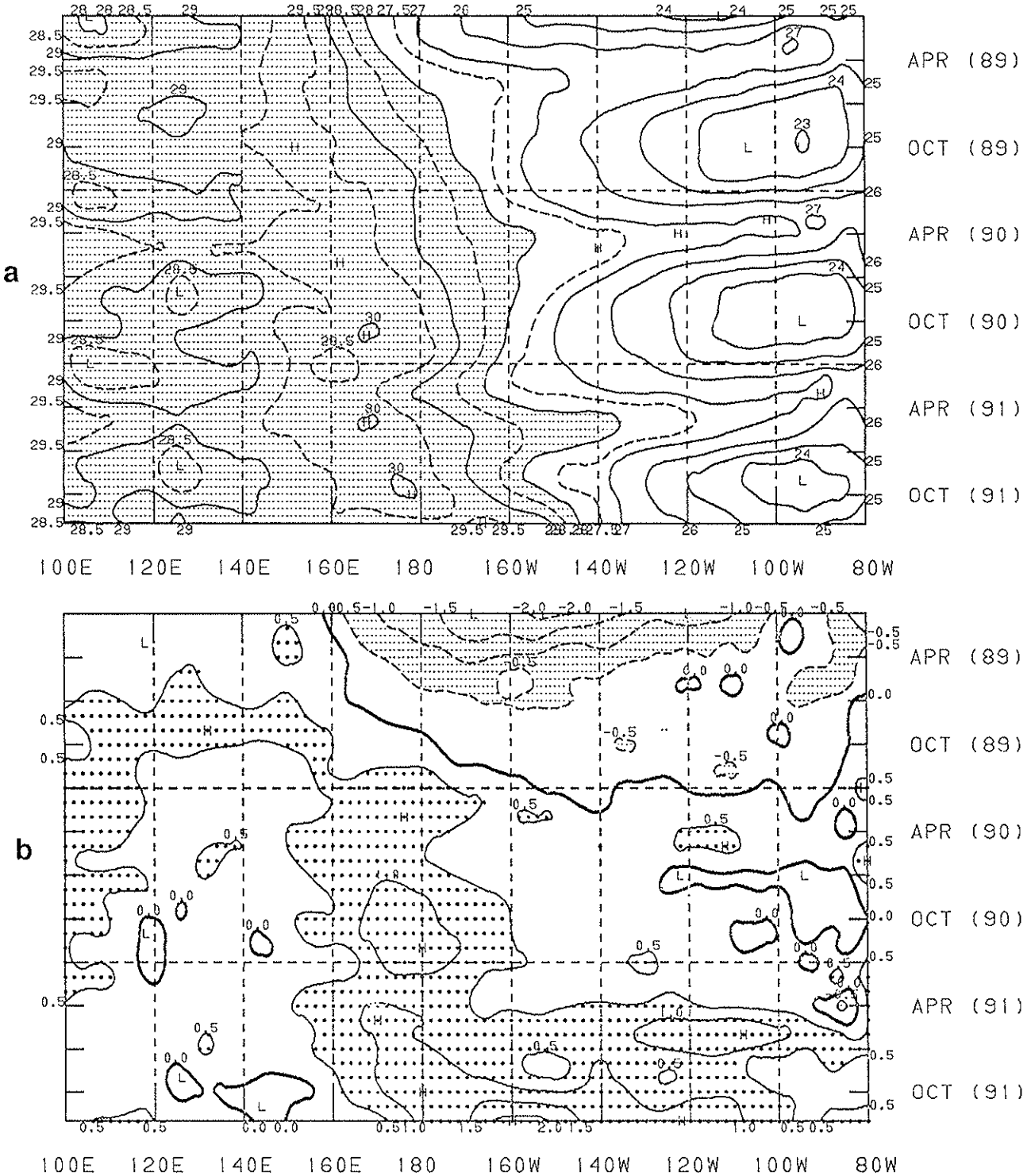

Fig. 1. Time-longitude section of monthly sea surface temperature a) mean and b) anomalous. Contour interval is 1°C and 0.5°C, respectively. SST values greater than 28°C and anomalies less than -0.5°C are shaded. Stippled areas indicate anomaly values greater than 0.5°C. Anomalies are computed based on the COADS/ICE climatology (Reynolds 1988). A 1-2-1 filter in time is used on all points prior to the current month.

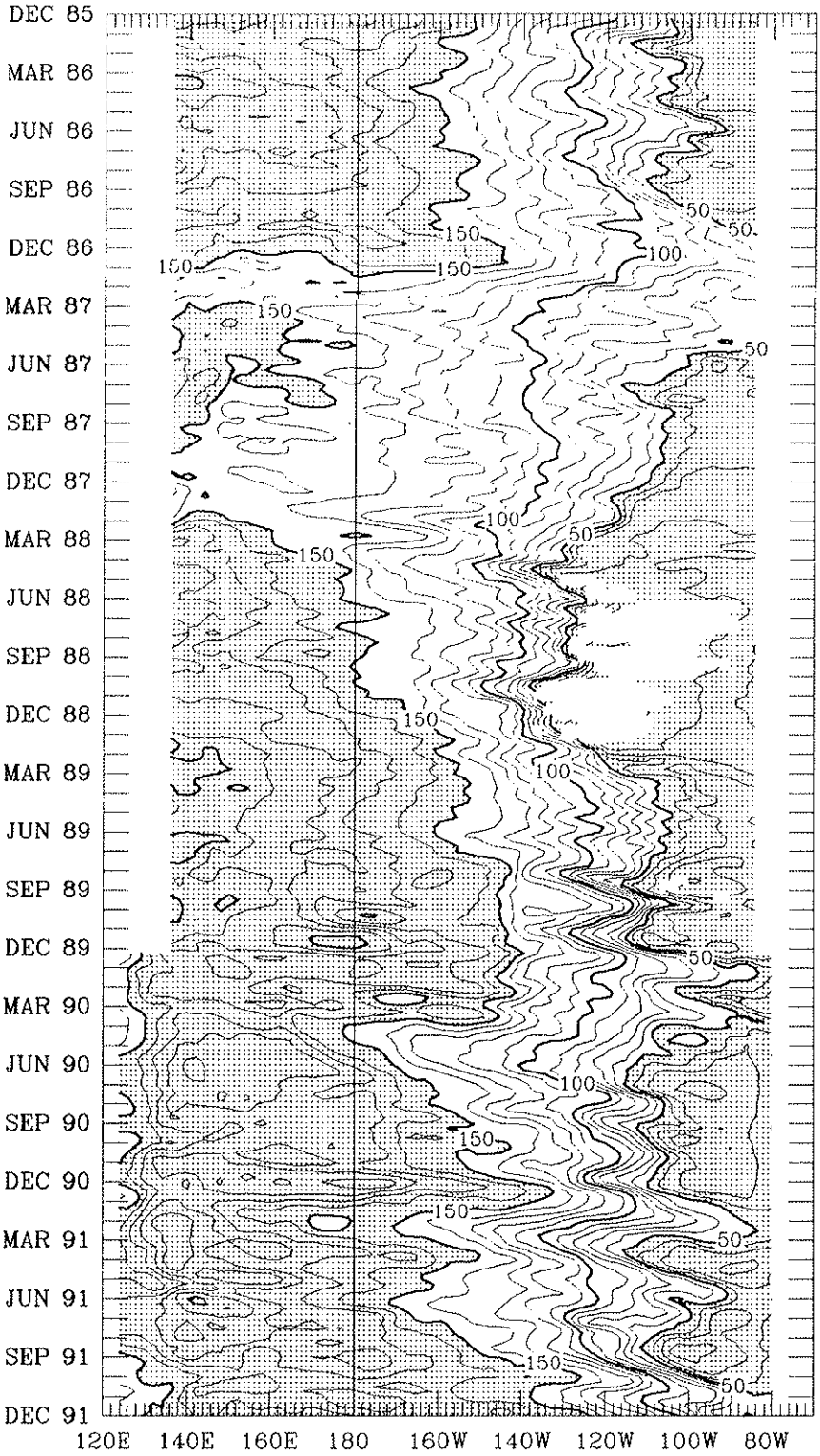

Fig. 2. Depth of the 20°C isotherm along the equator in the Pacific Ocean. Data are derived from an analysis system which assimilates oceanic observations into an oceanic GCM (Leetmaa and Ji 1989). The contour interval is 10 m with shading for values less than 50 m and also for values greater than 150 m.

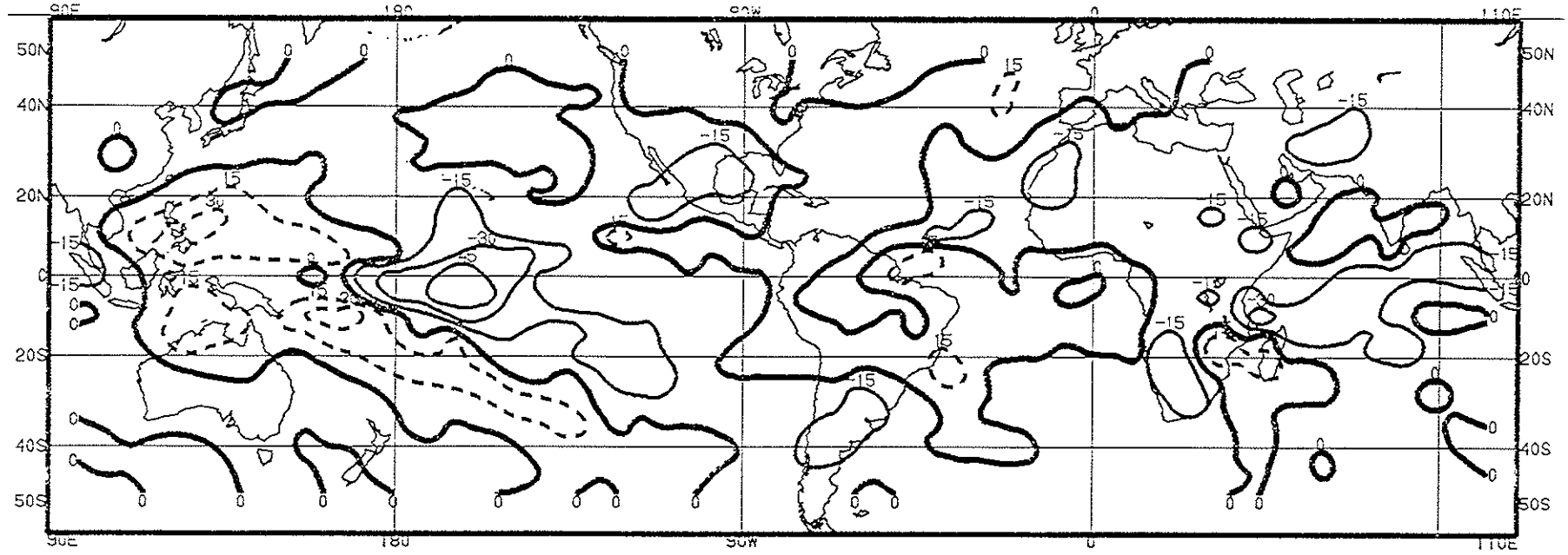

Fig. 3. Outgoing longwave radiation anomalies for December 1991 (NOAA 11 and 12 AVHRR IR window channel measurements by NESDIS/SRL). Data are accumulated and averaged over 2.5° areas and interpolated to a 5° Mercator grid for display. Contour interval is 20 Wm^{-2}. Contours of 280 Wm^{-2} and above are dashed. Anomalies are computed as departures from the 1979-1988 base period mean. Anomaly contour interval is 15 Wm^{-2}. Positive anomalies are dashed.

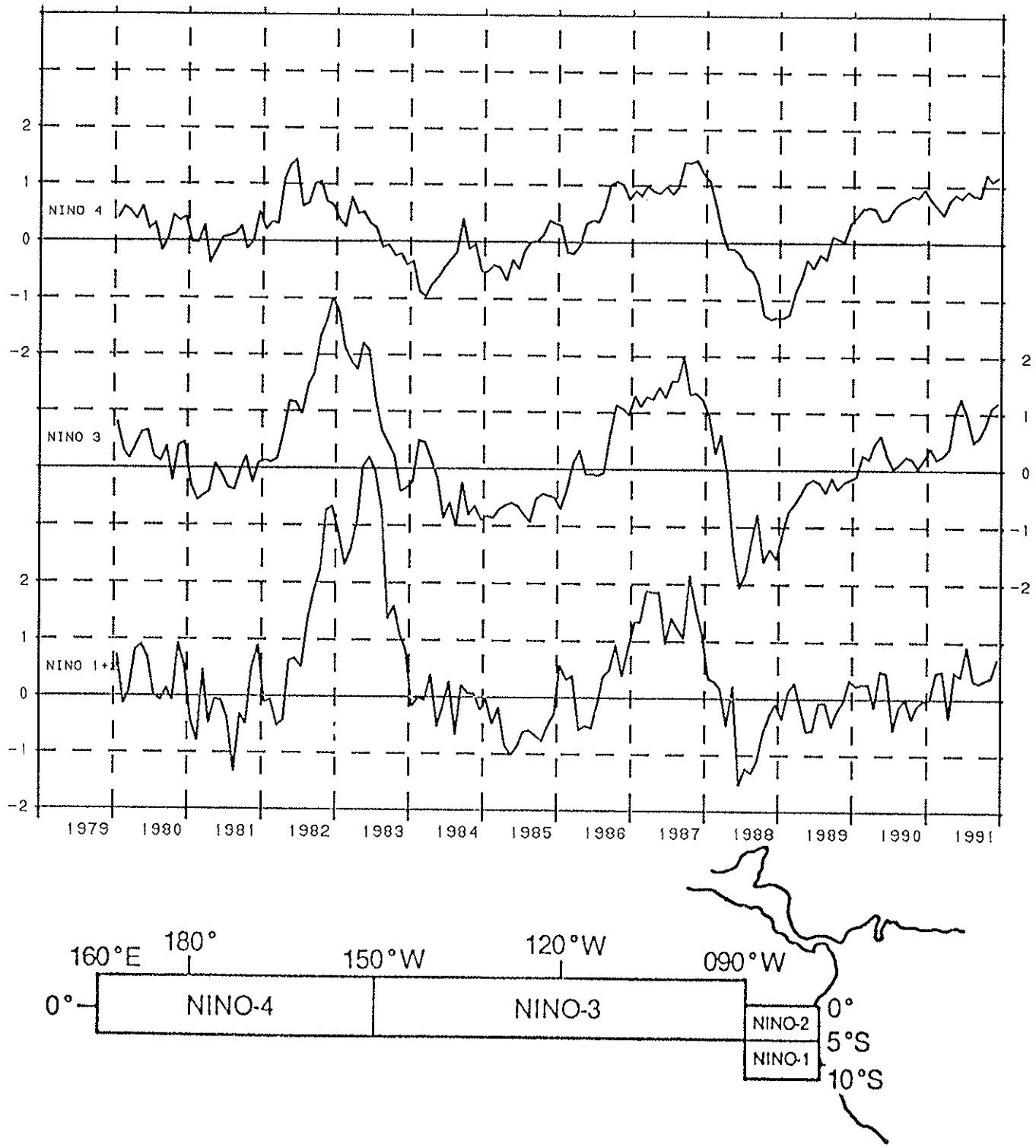

Fig. 4. Equatorial Pacific sea surface temperature anomaly indices (°C) for the areas indicated at the bottom of the figure. Niño 1+2 is the average over the Niño 1 and Niño 2 areas. Anomalies are computed with respect to the COADS/ICE climatology (Reynolds 1988).

SURFACE TEMPERATURE

Surface temperatures during 1991 averaged above the 1951-1980 average over most regions of the globe, continuing the trend that developed during the decade of the 1980's. In the Northern Hemisphere, positive temperature anomalies greater than 1.0°C were found over large areas of North America and over Siberia and Eastern Europe (**Fig. 5**). Smaller positive anomalies occurred over Africa and throughout Southeast Asia. Tropical Pacific sea surface temperatures (SSTs) were also above normal in association with a developing El Nino/Southern Oscillation (ENSO) warm episode. Positive SST anomalies also covered much of the Indian Ocean. In contrast, negative temperature anomalies less than -1.0°C were found over northeastern North America and Baffin Island, with smaller negative anomalies found over the Mediterranean region.

This pattern of temperature anomalies resembles that which persisted during the 1986 - 1990 period (Fig. 6, Halpert and Ropelewski, 1991). This anomaly pattern is also similar to that observed over North America and Asia during 1990 (**Fig. 7**), although positive anomalies greater than 1.0°C covered larger areas of northern Asia during 1990. One major difference between 1990 and 1991 occurred over Europe, where positive anomalies greater than 1.0°C during 1990 can be contrasted with normal to slightly below normal temperatures during 1991.

The pattern of temperature anomalies over Southern Hemisphere land areas during 1991 (**Fig. 6**) is remarkably similar to that observed during 1990 (**Fig. 8**). During both years, positive temperature anomalies were found over all land areas except for a small area of South America. Most of Australia experienced temperature anomalies greater than 0.5°C above normal during both years. Differences between the 1991 and 1990 patterns are found over the Pacific and Indian Oceans, where positive anomalies were greater during 1991.

A time series of the estimated global surface temperature anomalies over land (**Fig. 9**) indicates that 1991 was the second warmest year, exceeded only by 1990. This is also true for just the Northern Hemisphere (**Fig. 10a**), while the time series for the Southern Hemisphere (**Fig. 10b**) shows that a number of years during the 1980's had positive values similar to the 1991 anomaly.

Figure 11 shows the time series of global surface temperature anomalies over land separated into January through June (**Fig. 11a**) and July through December (**Fig. 11b**). It is evident that both halves of the year have been above normal throughout the 1980's, and that the first part of the year has experienced the larger positive anomalies. This trend has continued into the 1990's, with the values for the January through June period significantly warmer than the anomalies for the latter half of the year. During 1991, the anomaly for the

January - June period is the second warmest value in the record, surpassed only by the value for 1990. Although the decrease in the magnitude of positive temperature anomalies during the latter half of 1991 has been attributed to aerosols associated with the eruption of Mt. Pinatubo, similar decreases in temperature anomalies have occurred during the latter half of the year for every year since the mid 1980's.

The time series of the estimated global surface temperature anomalies over land shows that all months of 1991 had median temperature anomalies that were above normal (**Fig. 12a**). Also, four months during 1991 (March, April, July, and August) featured above normal temperatures for at least 70% of the 2^{o} latitude by 2^{o} longitude land areas used in this analysis. The 1991 monthly time series is similar to the time series for 1990 (**Fig. 12b**). The major difference between the two time series occurs in the January - March period, when the positive extremes were significantly greater during 1990. While the time series indicate the warmth that was prevalent during both years, they also show that more than 30% of the 2^{o} latitude by 2^{o} longitude land areas with data experienced below normal temperatures during most months.

The time series for the Northern Hemisphere, divided into the two halves of the year (**Fig. 13**), are very similar to the global time series. The time series of anomalies for the Southern Hemisphere (**Fig. 14**) also show larger anomalies during the first half of the year. For that part of the year, the 1991 value is larger than the 1990 anomaly and is comparable in magnitude to the previous warmest value which occurred in 1983.

As one would expect, based on the magnitudes of the seasonal standard deviations, anomalies were largest during the December 1990 - February 1991 period over the Northern Hemisphere (**Fig. 15a**). Large negative anomalies were found over northeastern North America, while large positive anomalies spanned northern and northeastern Asia. Positive anomalies greater than $2.0^{o}C$ were found across parts of northern Asia during all seasons (**Figs. 15 - 16**). Anomalies across central North America varied throughout the year, with positive anomalies greater than $2.0^{o}C$ during the March - May season (**Fig. 15b**). The area of anomalies greater than $2.0^{o}C$ was restricted to northern Canada during June - August (**Fig. 16a**). During the September - November season, however, this entire region experienced significant negative anomalies (**Fig. 16b**). Anomalies over Europe were generally small throughout all four seasons.

Seasonal time series averaged over the United States (**Figs. 17-18**) show that only the September - November season averaged below the long-term mean during 1991. This was the first season that averaged below normal for the contiguous United States since the September - November season of 1989. The December 1990 - February 1991 and the June - August 1991 seasons were each slightly warmer than normal. However, United States

temperatures during the March - May season were much above normal. This was the seventh abnormally warm spring in a row.

In the Southern Hemisphere, temperature anomalies over the southern half of Australia were generally positive, but small, during all four seasons (**Figs. 19 - 20**). Across South America, the largest positive anomalies occurred during the March - May season in Argentina and Chile. Below normal temperatures were found in Bolivia during all four seasons, while temperatures were near normal during the entire year over southern Africa.

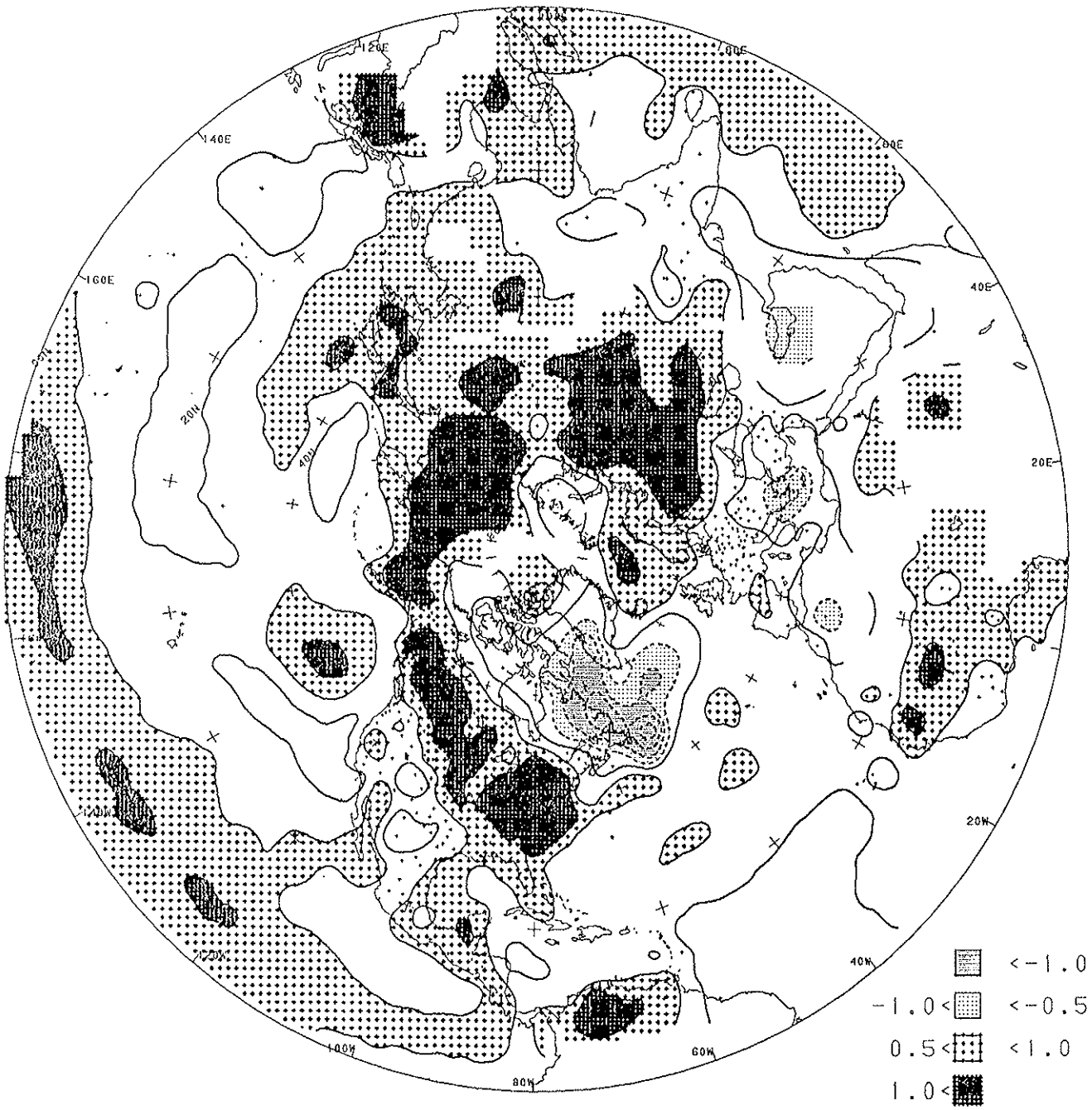

Fig. 5. Northern Hemisphere surface temperature anomaly for 1991. Analysis based on station data over land and sea surface temperature (SST) over the water. Anomalies for station data are from the 1951-1980 base period, while SST anomalies are computed as departures from the COADS/ICE climatology (Reynolds, 1988). Small plus signs indicate locations of data over land. Contour interval is 0.5°C, with negative anomalies dashed.

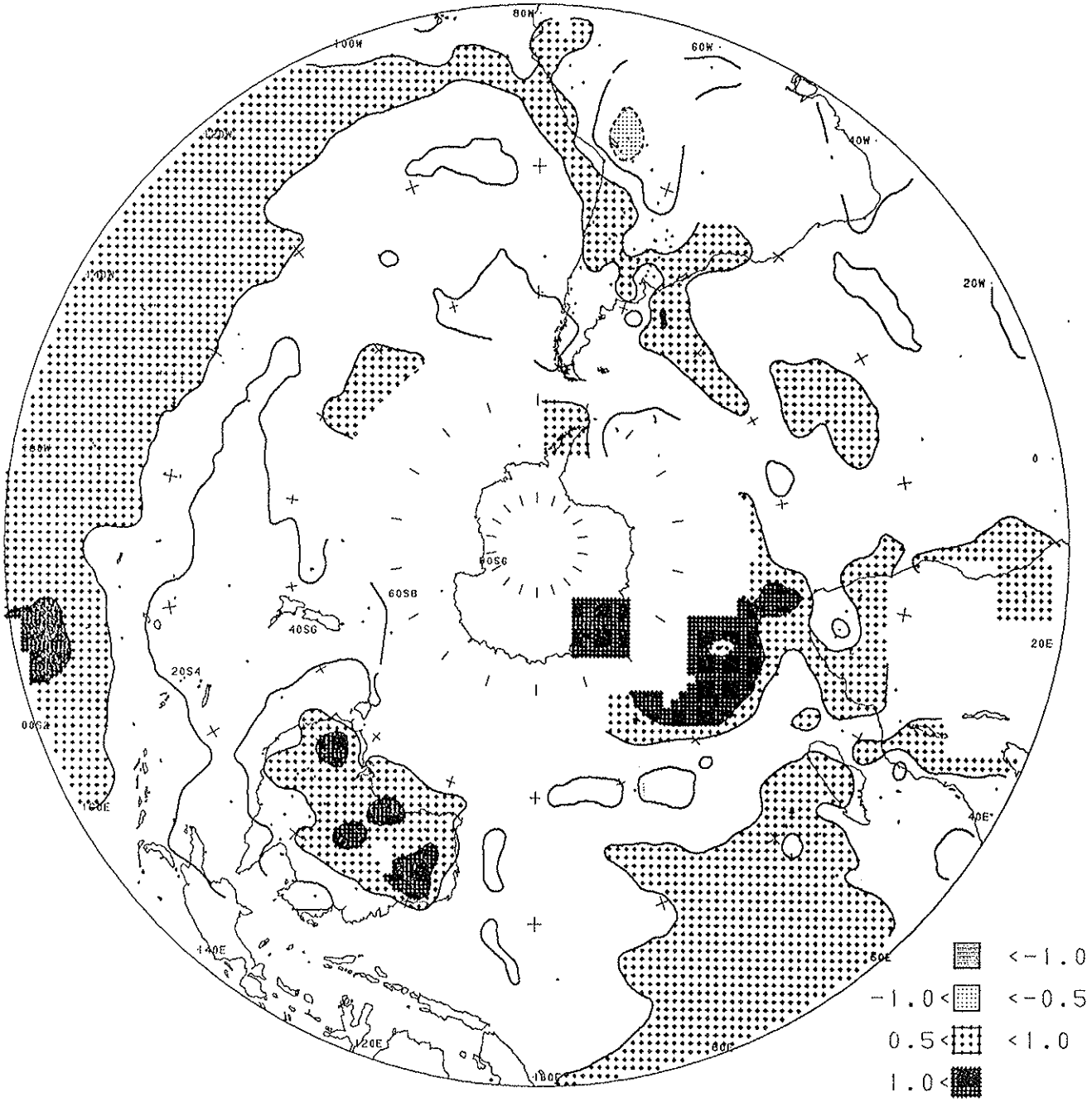

Fig. 6. Southern Hemisphere surface temperature anomaly for 1991. Analysis based on station data over land and sea surface temperature (SST) over the water. Anomalies for station data are from the 1951-1980 base period, while SST anomalies are computed as departures from the COADS/ICE climatology (Reynolds, 1988). Small plus signs indicate locations of data over land. Contour interval is 0.5°C, with negative anomalies dashed.

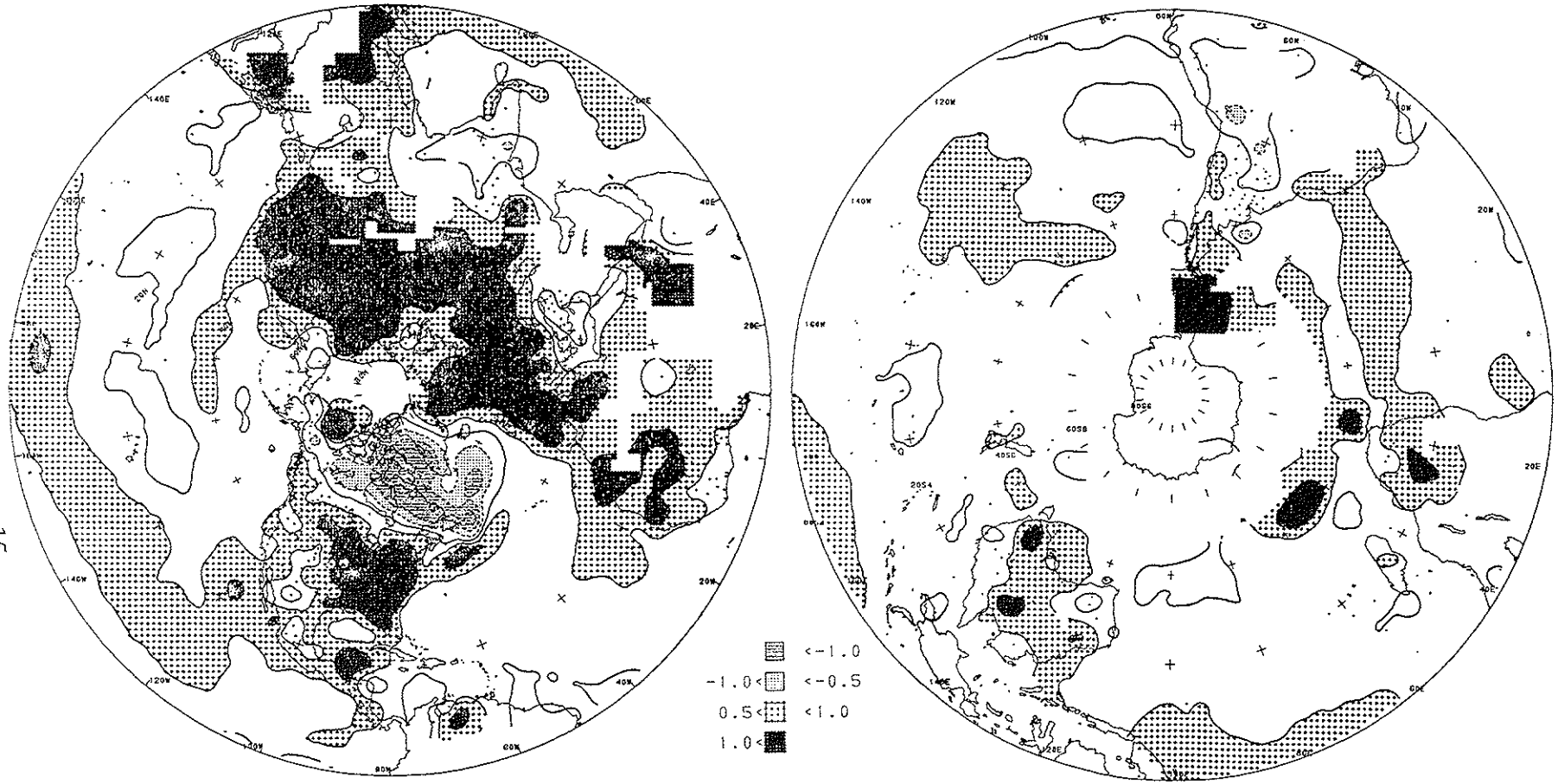

Fig. 7. Northern Hemisphere surface temperature anomaly for 1990. Analysis based on station data over land and sea surface temperature (SST) over the water. Anomalies for station data are from the 1951-80 base period, while SST anomalies are computed as departures from the COADS/ICE climatology (Reynolds, 1988). Contour interval is 0.5°C.

Fig. 8. Southern Hemisphere surface temperature anomaly for 1990. Analysis based on station data over land and sea surface temperature (SST) over the water. Anomalies for station data are from the 1951-80 base period, while SST anomalies are computed as departures from the COADS/ICE climatology (Reynolds, 1988). Contour interval is 0.5°C.

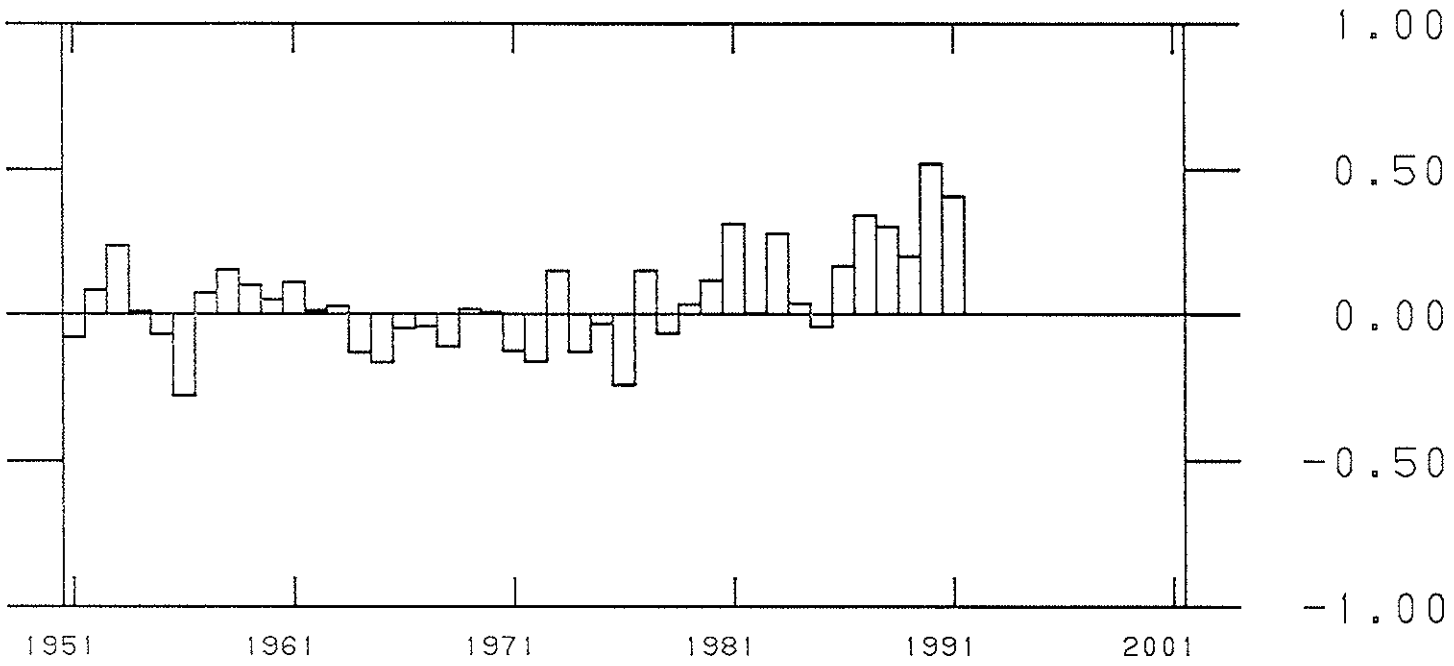

Fig. 9. Time series of estimated global surface temperature anomalies for the calendar year. Global temperature anomaly estimates are formed from area weighted averages of station anomalies over a 2^{o} latitude by 2^{o} longitude grid.

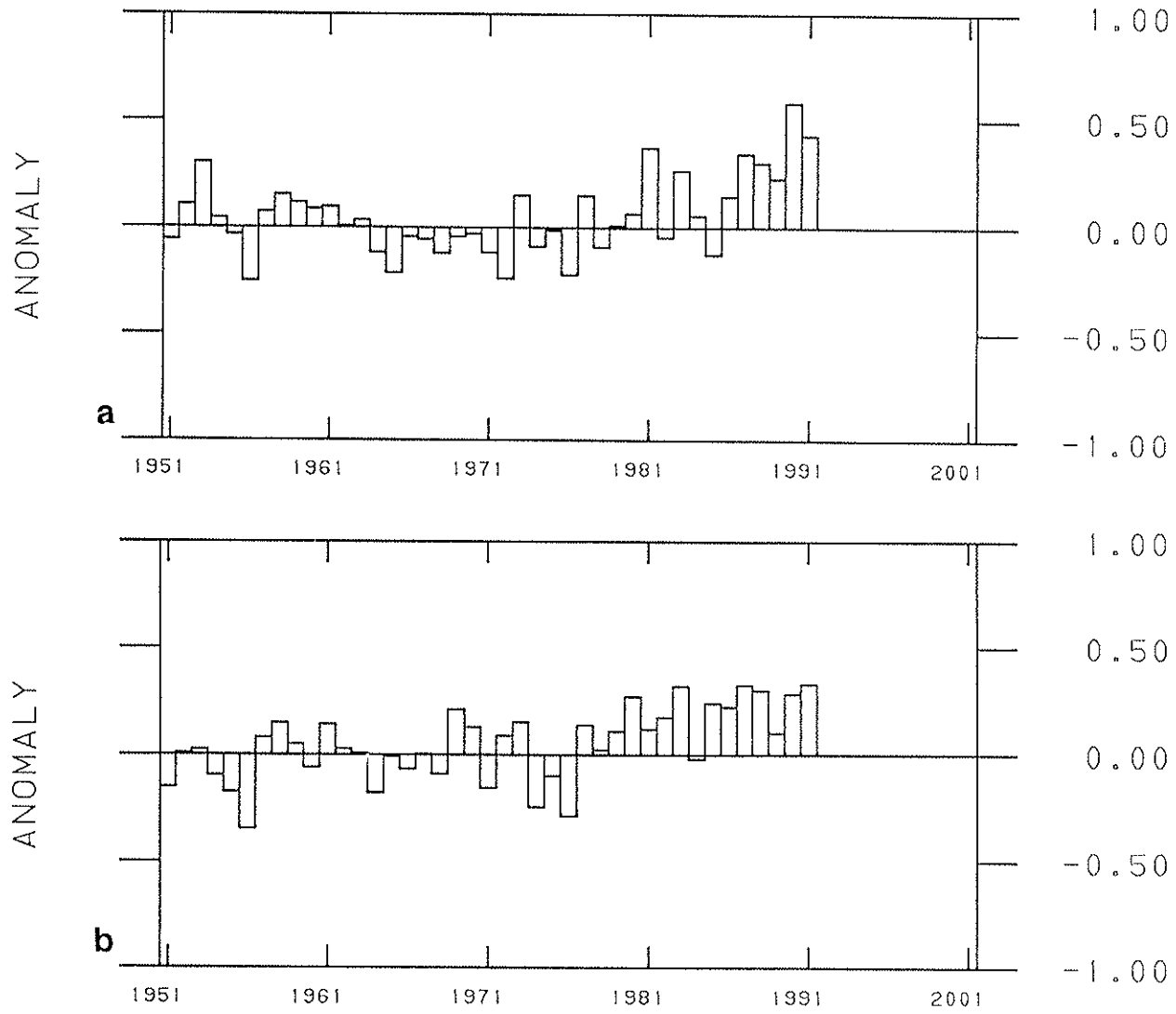

Fig. 10. Time series of estimated a) Northern Hemisphere and b) Southern Hemisphere surface temperature anomalies for the calendar year. Temperature anomaly estimates are formed from area weighted averages of station anomalies over 2^{o} latitude by 2^{o} longitude grids.

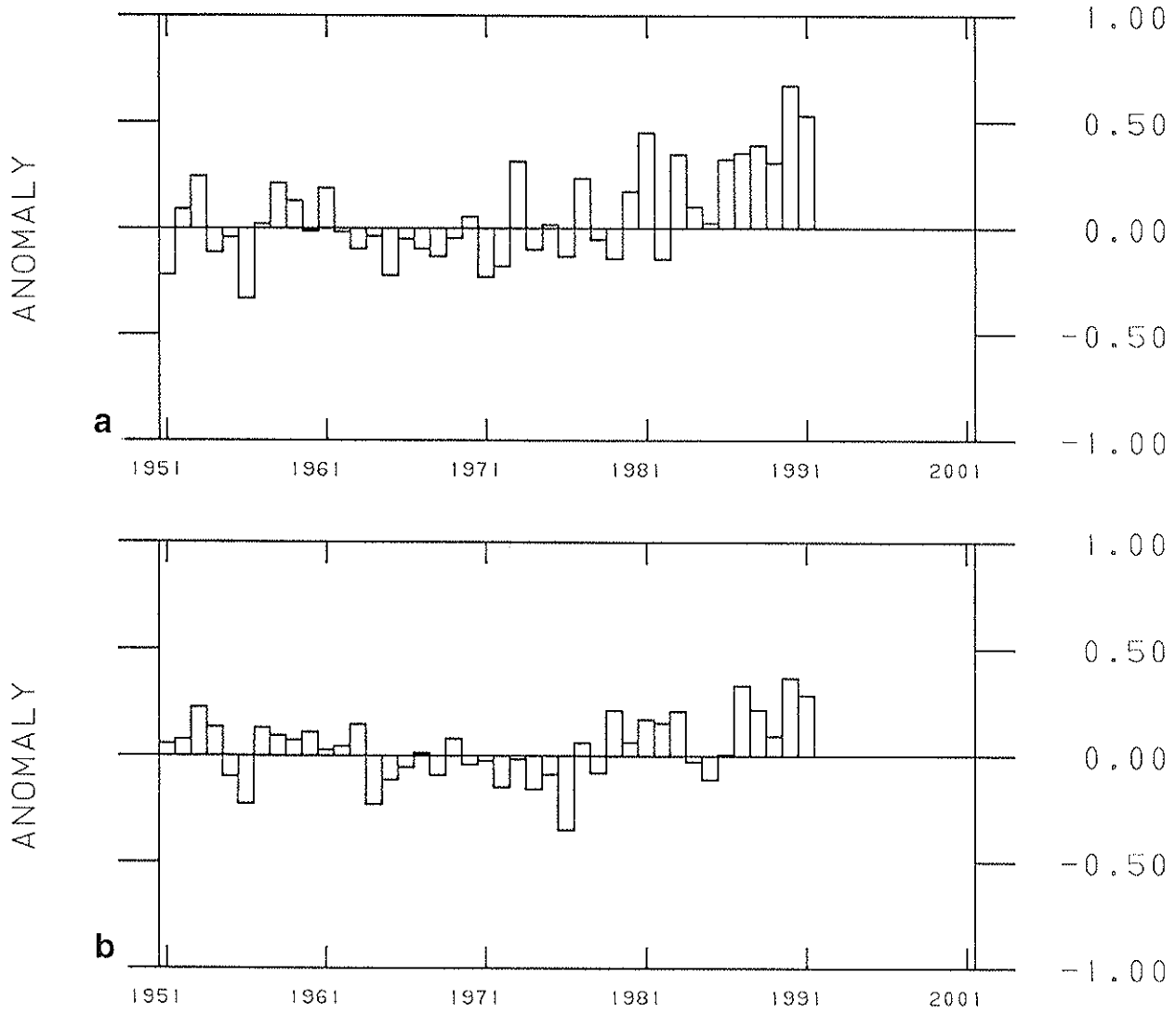

Fig. 11. Time series of estimated global surface temperature anomalies for a) January - June and for b) July - December. Global temperature anomaly estimates are formed from area weighted averages of station anomalies over a 2^{o} latitude by 2^{o} longitude grid.

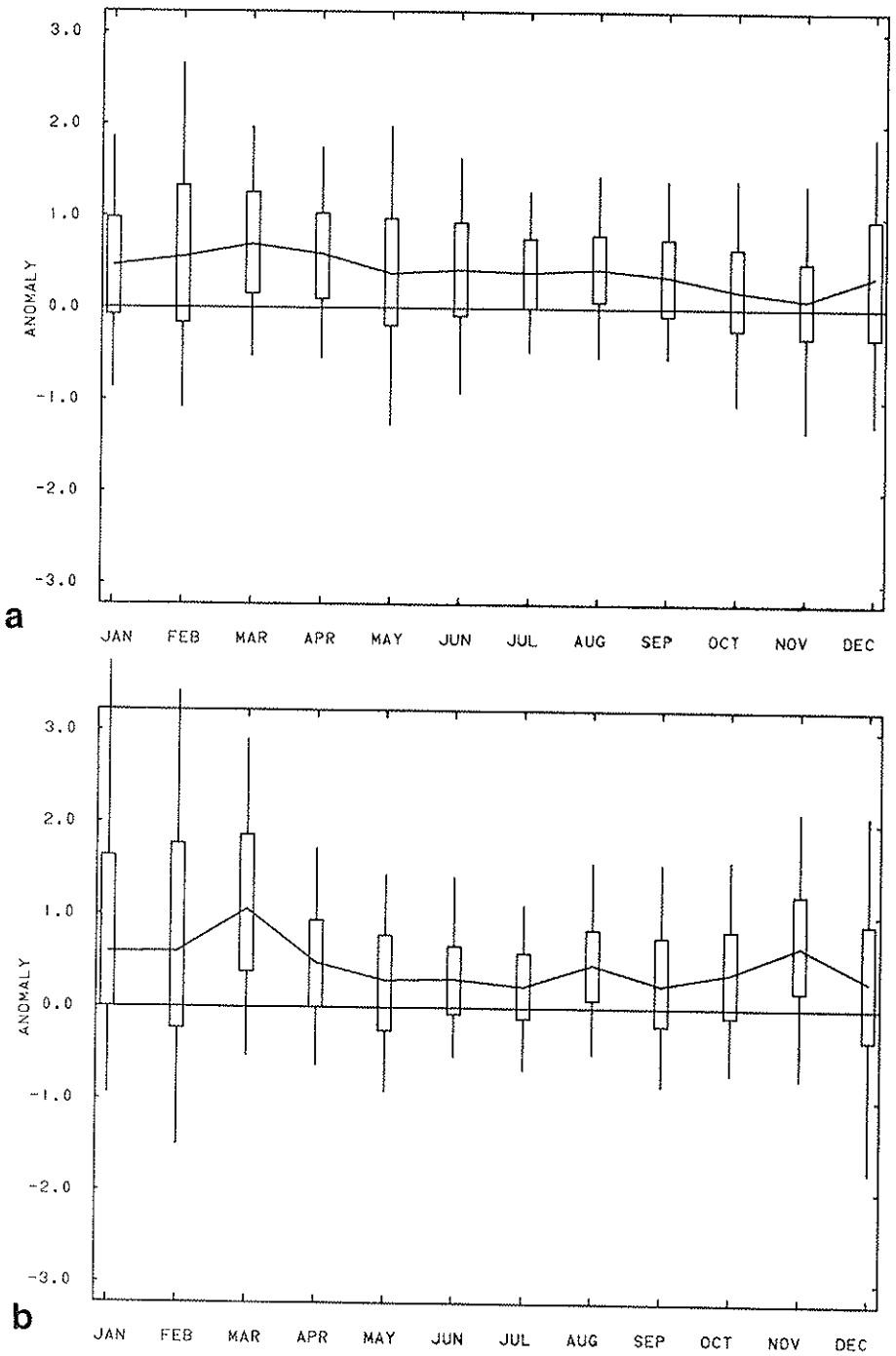

Fig. 12. Global monthly surface temperature index based on the average temperature anomalies in 2° latitude by 2° longitude areas over land for a) 1991 and for b) 1990. The solid line in each panel represents the 50%, or median, temperature anomaly for each month. Each "box" delineates the temperature anomalies at the 70th and 30th percentiles while the "whiskers" (lines) delineate the 90th and 10th percentile values. The anomalies are taken with respect to the 1951 to 1980 base period.

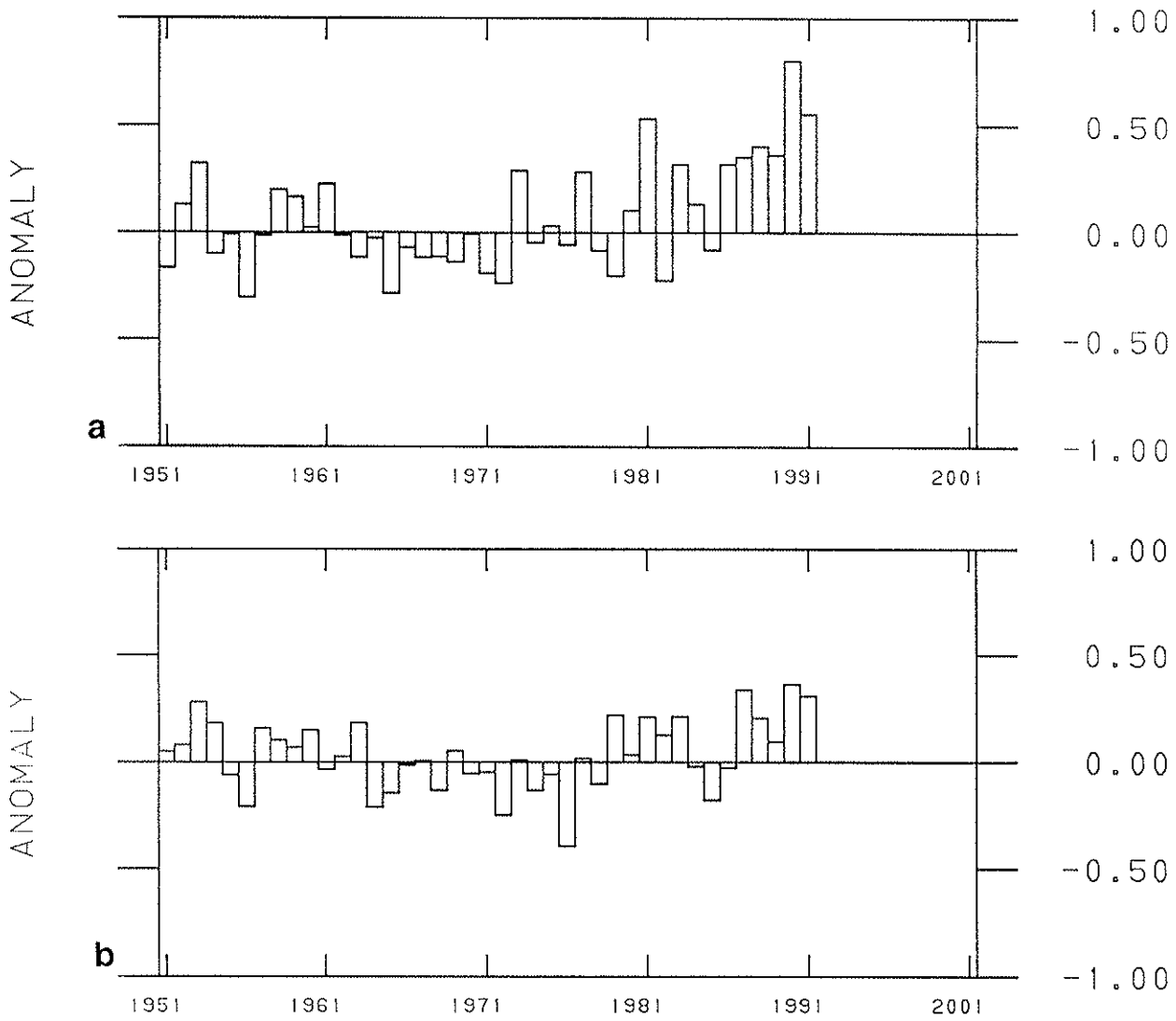

Fig. 13. Time series of estimated Northern Hemisphere surface temperature anomalies for a) January - June and for b) July - December. Global temperature anomaly estimates are formed from area weighted averages of station anomalies over a 2° latitude by 2° longitude grid.

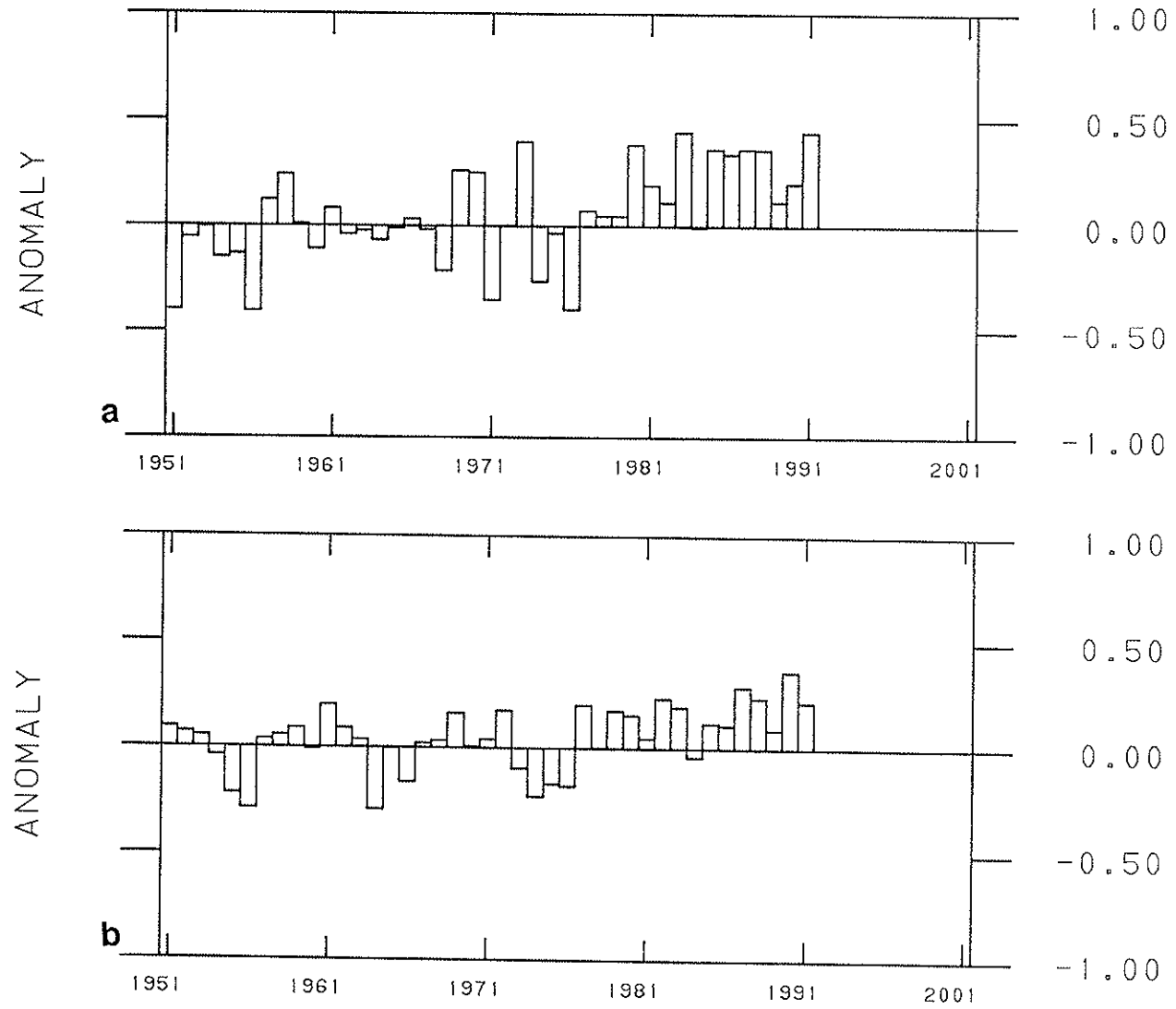

Fig. 14. Time series of estimated Southern Hemisphere surface temperature anomalies for a) January - June and for b) July - December. Global temperature anomaly estimates are formed from area weighted averages of station anomalies over a 2° latitude by 2° longitude grid.

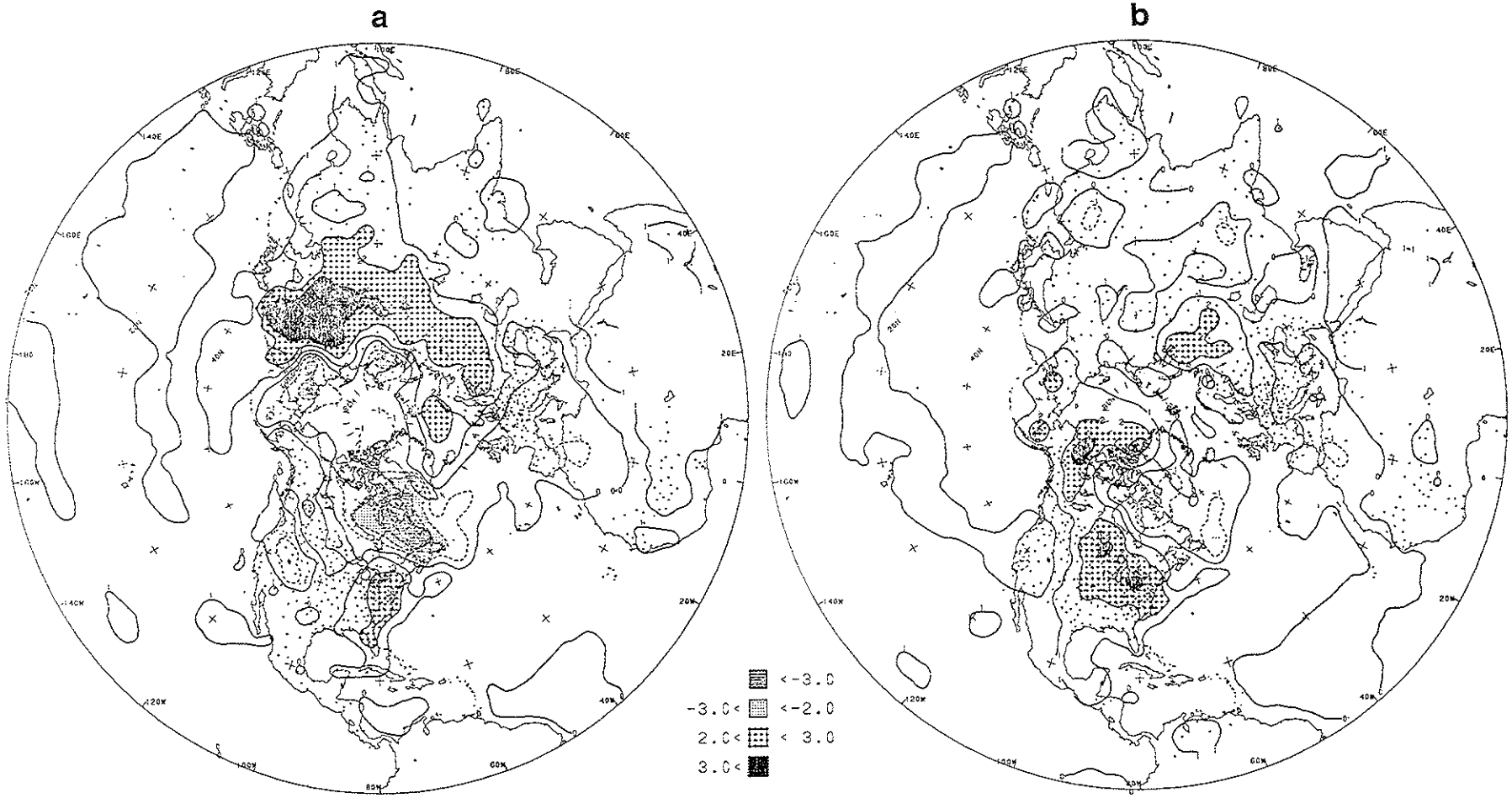

Fig. 15. Northern Hemisphere surface temperature anomalies for a) DJF 1990-91 and b) for MAM 1991. Analysis based on station data over land and sea surface temperature (SST) over the water. Anomalies for station data are from the 1951-1980 base period, while SST anomalies are computed as departures from the COADS/ICE climatology (Reynolds, 1988). Small plus signs indicate locations of data over land. Contour interval is 1.0°C, with negative anomalies dashed.

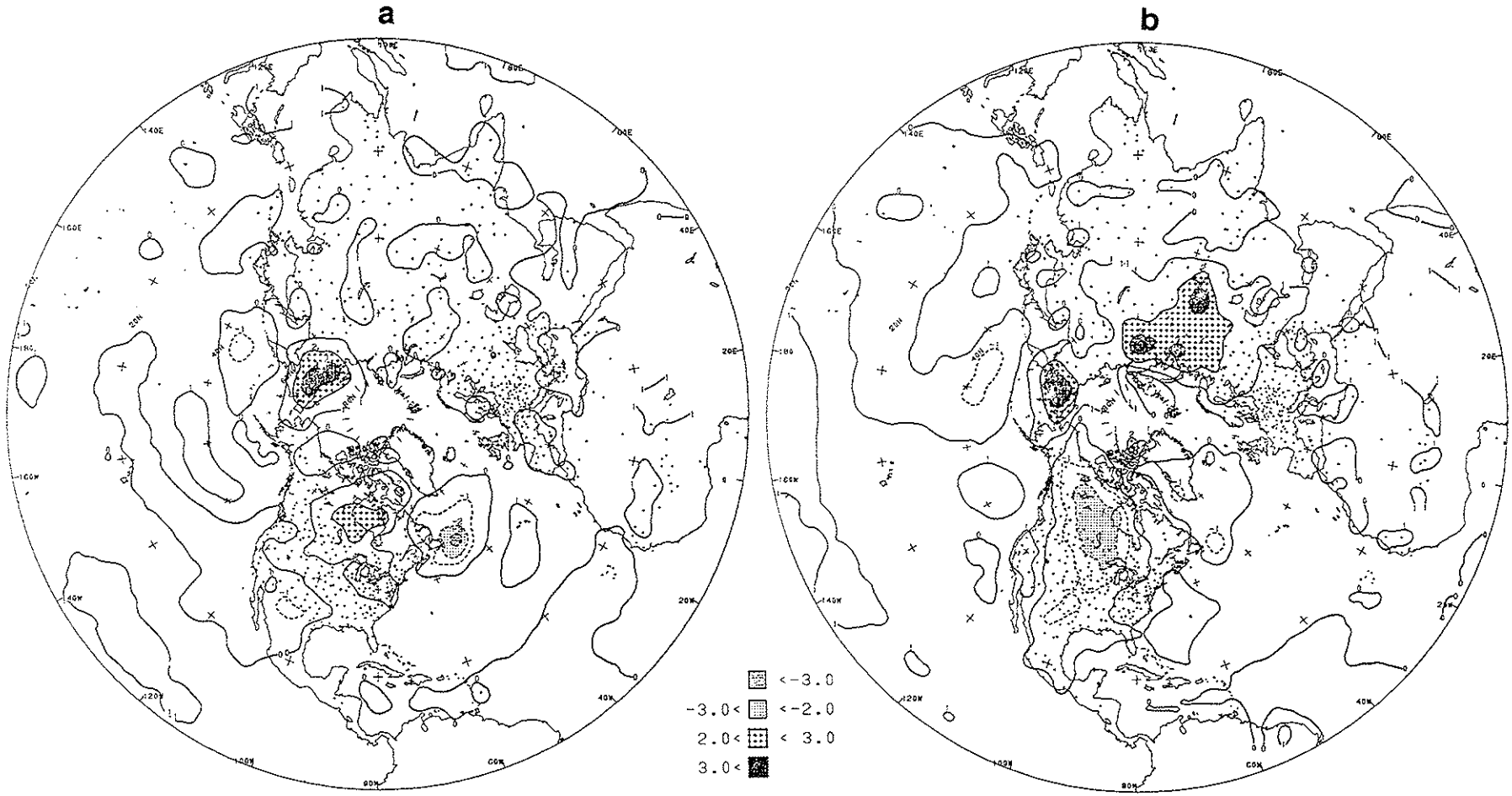

Fig. 16. Northern Hemisphere surface temperature anomaly for a) JJA and for SON 1991. Analysis based on station data over land and sea surface temperature (SST) over the water. Anomalies for station data are from the 1951-1980 base period, while SST anomalies are computed as departures from the COADS/ICE climatology (Reynolds, 1988). Small plus signs indicate locations of data over land. Contour interval is 1.0°C, with negative anomalies dashed.

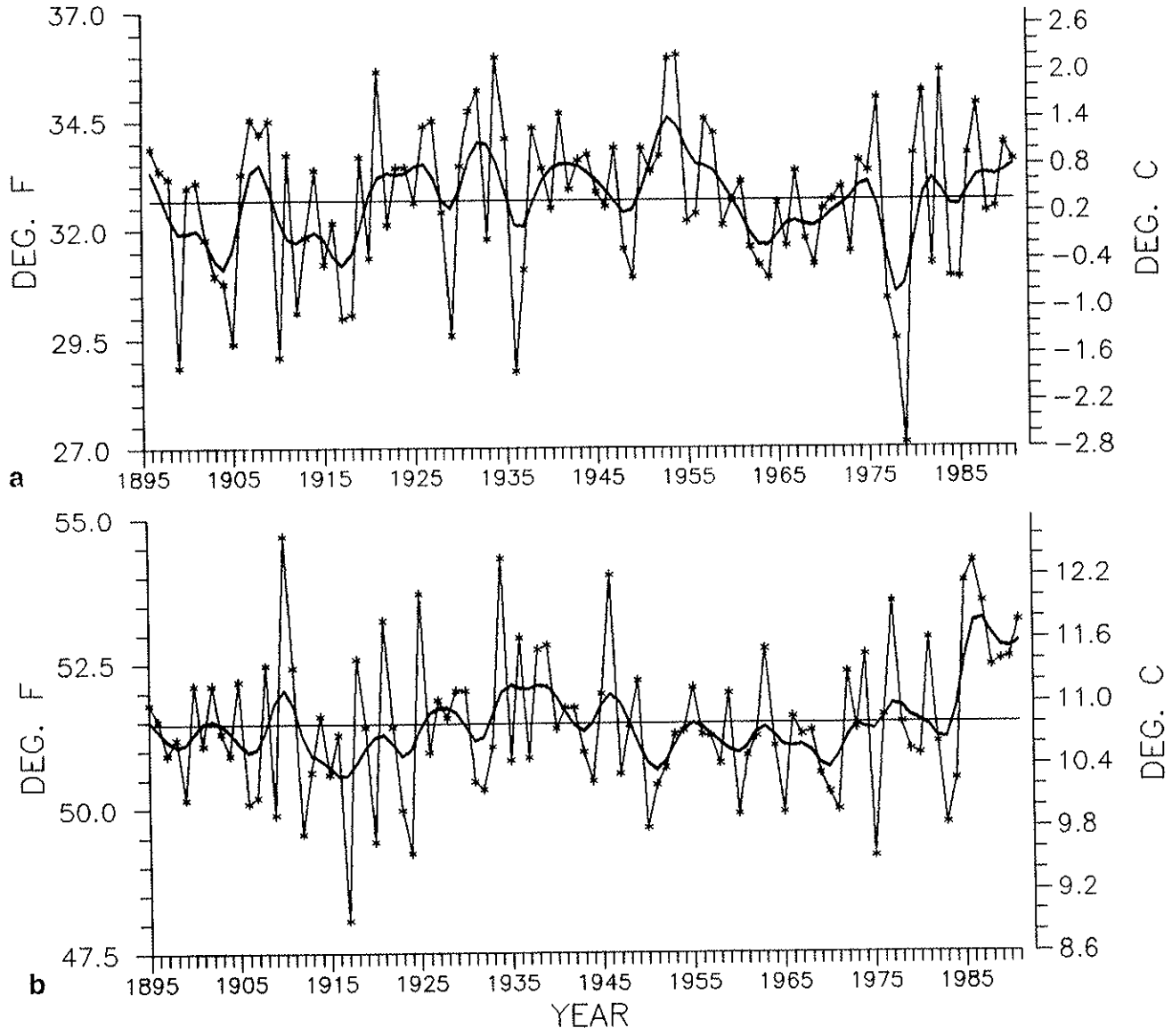

Fig. 17. Time series of temperature averaged over the contiguous United States and a binomially filtered curve for a) DJF 1990-91 and b) MAM 1991.

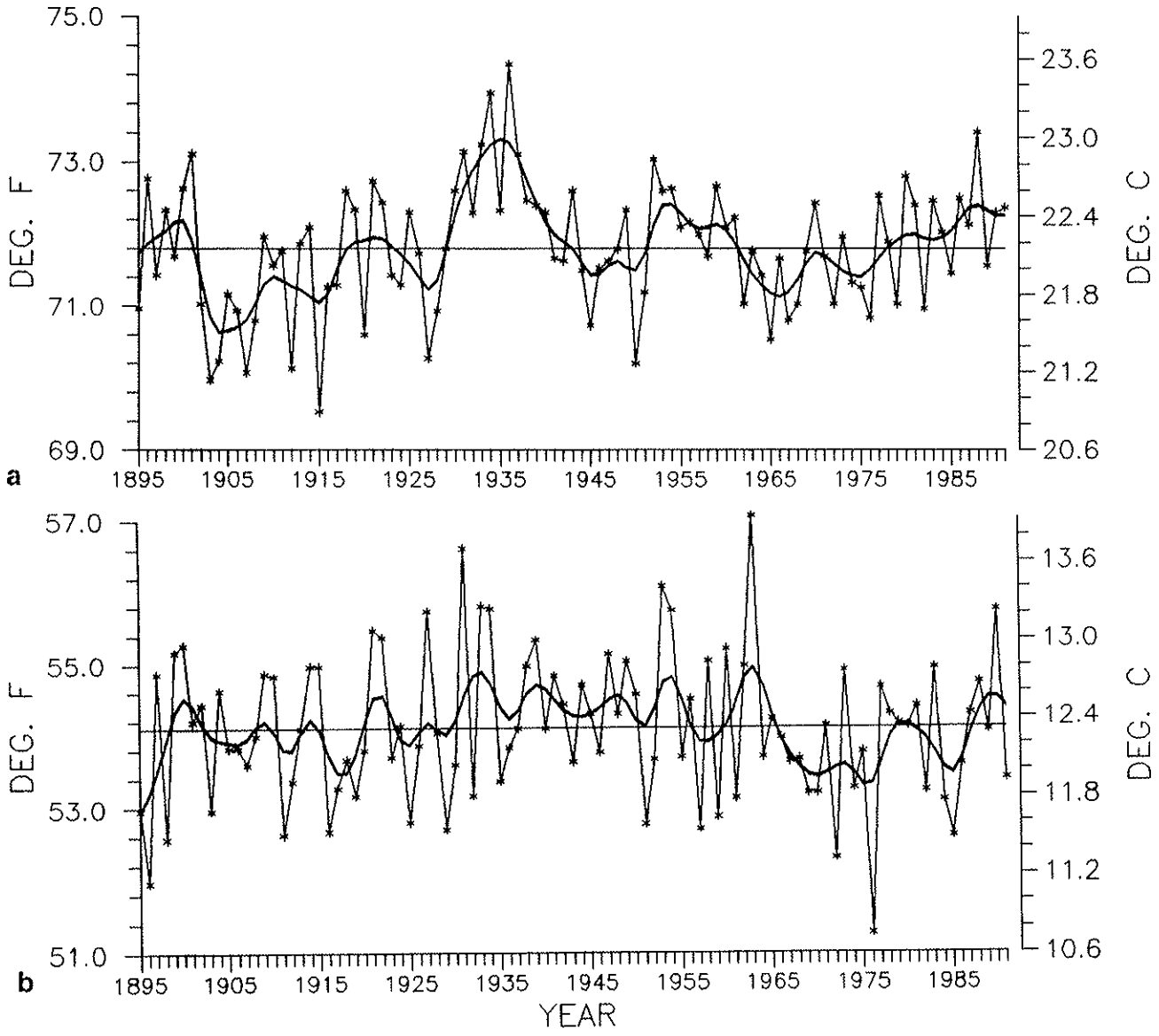

Fig. 18. Time series of temperature averaged over the contiguous United States and a binomially filtered curve for a) JJA and b) SON 1991.

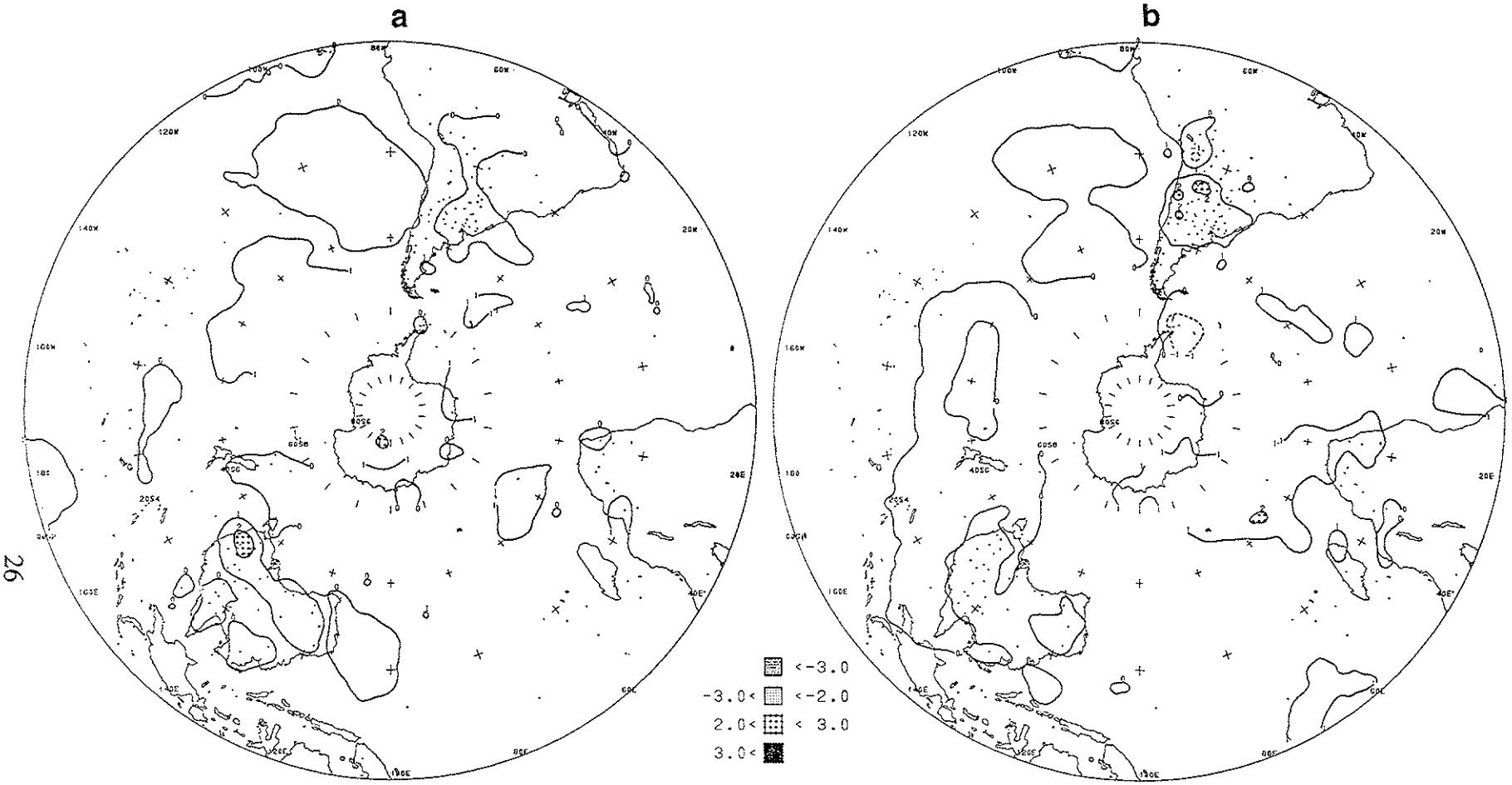

Fig. 19. Southern Hemisphere surface temperature anomalies for a) DJF 1990-91 and b) for MAM 1991. Analysis based on station data over land and sea surface temperature (SST) over the water. Anomalies for station data are from the 1951-1980 base period, while SST anomalies are computed as departures from the COADS/ICE climatology (Reynolds, 1988). Small plus signs indicate locations of data over land. Contour interval is 1.0°C, with negative anomalies dashed.

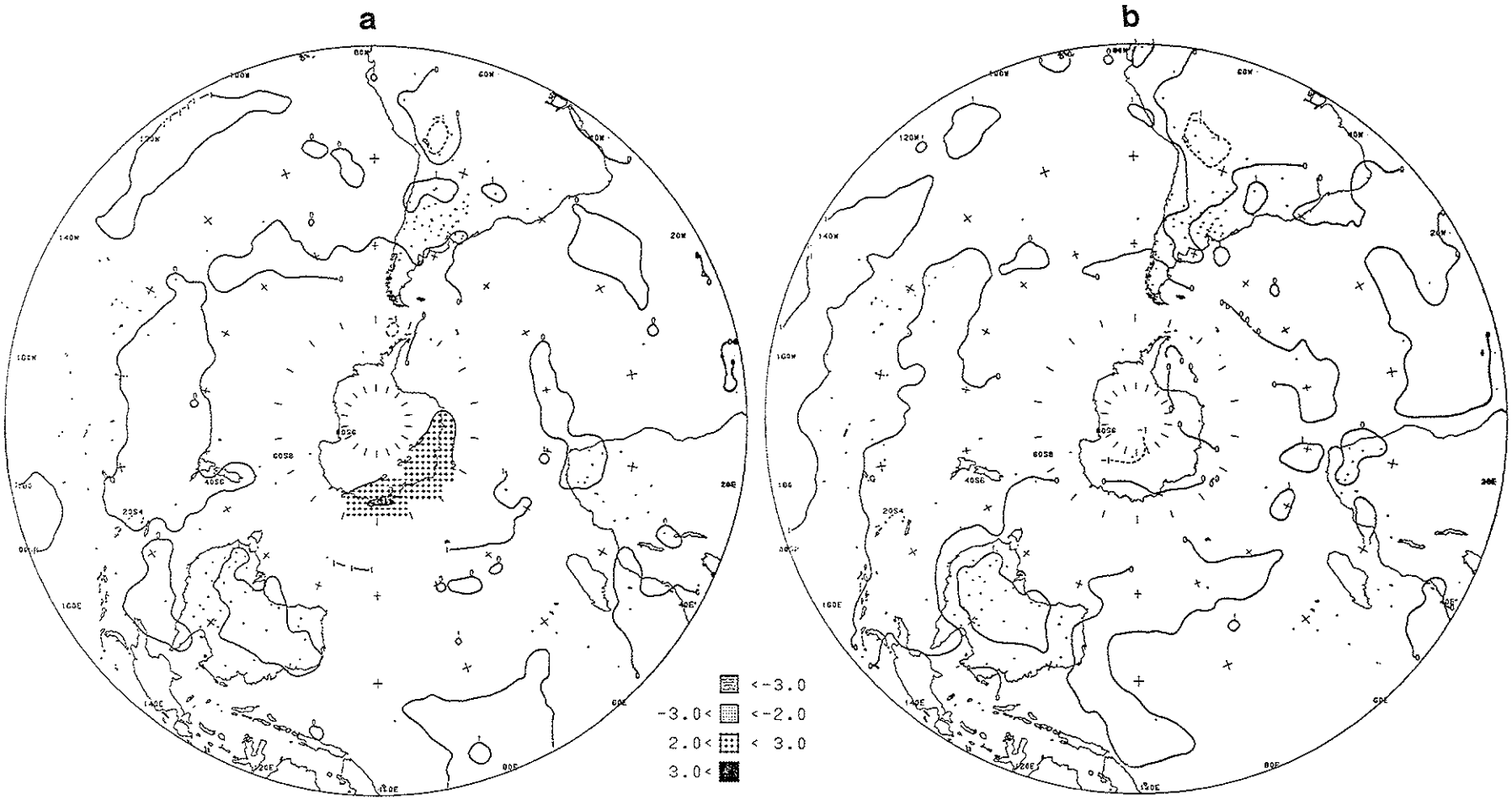

Fig. 20. Southern Hemisphere surface temperature anomaly for a) JJA and for SON 1991. Analysis based on station data over land and sea surface temperature (SST) over the water. Anomalies for station data are from the 1951-1980 base period, while SST anomalies are computed as departures from the COADS/ICE climatology (Reynolds, 1988). Small plus signs indicate locations of data over land. Contour interval is 1.0°C, with negative anomalies dashed.

PRECIPITATION

Global

The Northern Hemisphere (**Fig. 21a**) was relatively wet during 1991 across the central and southern regions of the United States, as well as across northern Asia. Drier than normal conditions were found over western Europe and dominated the tropical and sub-tropical regions of northwestern India, the African Sahel, and southeastern Asia. This pattern has similarities to that observed during 1990 (**Fig. 21b**), with notable exceptions over the southeastern United States and northern India.

Precipitation percentiles based on a gamma distribution during the winter (DJF) 1990-91 season (**Fig. 22a**) show very dry conditions over the west coast of the United States, which is a feature that has been observed since the mid-1980's. During the spring (MAM) season (**Fig. 22b**), very wet conditions developed across the southeastern United States, while heavy March rainfall resulted in greater than normal precipitation over California. Elsewhere, early season rains in the western Sahel resulted in a much wetter than normal spring, which is normally a dry season. Very dry pre-monsoon conditions characterized Indian springtime precipitation.

By the summer (JJA) season (**Fig. 23a**), wetter than normal conditions affected southern and central India, but dry conditions remained over the northwest part of the country throughout the season. Summer rainfall in the African Sahel was significantly below normal in the west, but close to normal in the central regions. The midwestern region of the United States experienced drier than normal conditions, following abnormal wetness in the preceding two seasons. Above normal precipitation persisted along the Gulf Coast, although JJA anomalies were not as large as during MAM. During the Fall (SON) season (**Fig. 23b**), wetter than normal conditions returned to the Midwest, while less than normal precipitation was observed over the East Coast. Drier than normal conditions over the Sahel and northwestern India implied an early end to their respective rainy seasons. A band of drier than normal conditions stretched from the Caspian Sea eastward to central China.

In the Southern Hemisphere during 1991 (**Fig. 24a**), precipitation percentiles indicate drier than normal conditions across the southern half of Australia with wetter than normal conditions in the northeast. Dry conditions also dominated the islands east of Australia. In contrast, Australia experienced drier than normal conditions across northern portions of the country and heavier than normal precipitation along eastern Australia and the islands just to the east during 1990 (**Fig. 24b**).

Seasonal maps for the Southern Hemisphere (**Figs. 25 - 26**)

give a better indication of the precipitation anomalies throughout 1991. In the southern summer (December 1990 - February 1991) (**Fig. 25a**), much above normal rainfall totals across the northern half of Australia contrasted with drier than normal conditions that affected northeastern Australia throughout the rest of the year. Very dry weather also covered the rest of Australia during the March - May season (**Fig. 25b**). Precipitation over southern Africa showed few extremes during the four seasons. Drier than normal conditions were found over northwestern South America during all four seasons.

Regional

Precipitation across the South-Central United States, including the states of Texas, Oklahoma, Kansas, Arkansas, Louisiana, and Mississippi, was much above normal during 1991 (**Fig. 27a**). This was the second consecutive year with much above normal precipitation for this area. By contrast, precipitation in California, Oregon, and Washington was below normal during the October - March period for the fifth straight year (**Fig. 27b**). Although California received heavy precipitation and short-term drought relief during March, amounts were not nearly enough to overcome the long-term precipitation deficits.

Precipitation over key regions during 1991 can be put in historical perspective through examination of precipitation indices. These indices are calculated by averaging the normalized precipitation values for stations in a region. The indices for the primary monsoon regions (**Fig. 28**) show that precipitation for the western Sahel and Southeast Asia was less than the 30 year mean, while amounts over northern Australia were greater than normal. India had its third straight year of near normal rainfall, although there was large variance across the country, with drier conditions across the north and wetter than normal conditions across the central and south. Southeast Asia had below normal rainfall for the tenth consecutive monsoon season. The above normal rainy season for northern Australia reflects large rainfall amounts during the December 1990 - February 1991 period. March and April turned very dry, reflecting an early end to their monsoon season. Very dry conditions in the Sahel continued the long running trend of dry rainy seasons that began in the early 1970s. Details on the Indian and Sahelian monsoons follow.

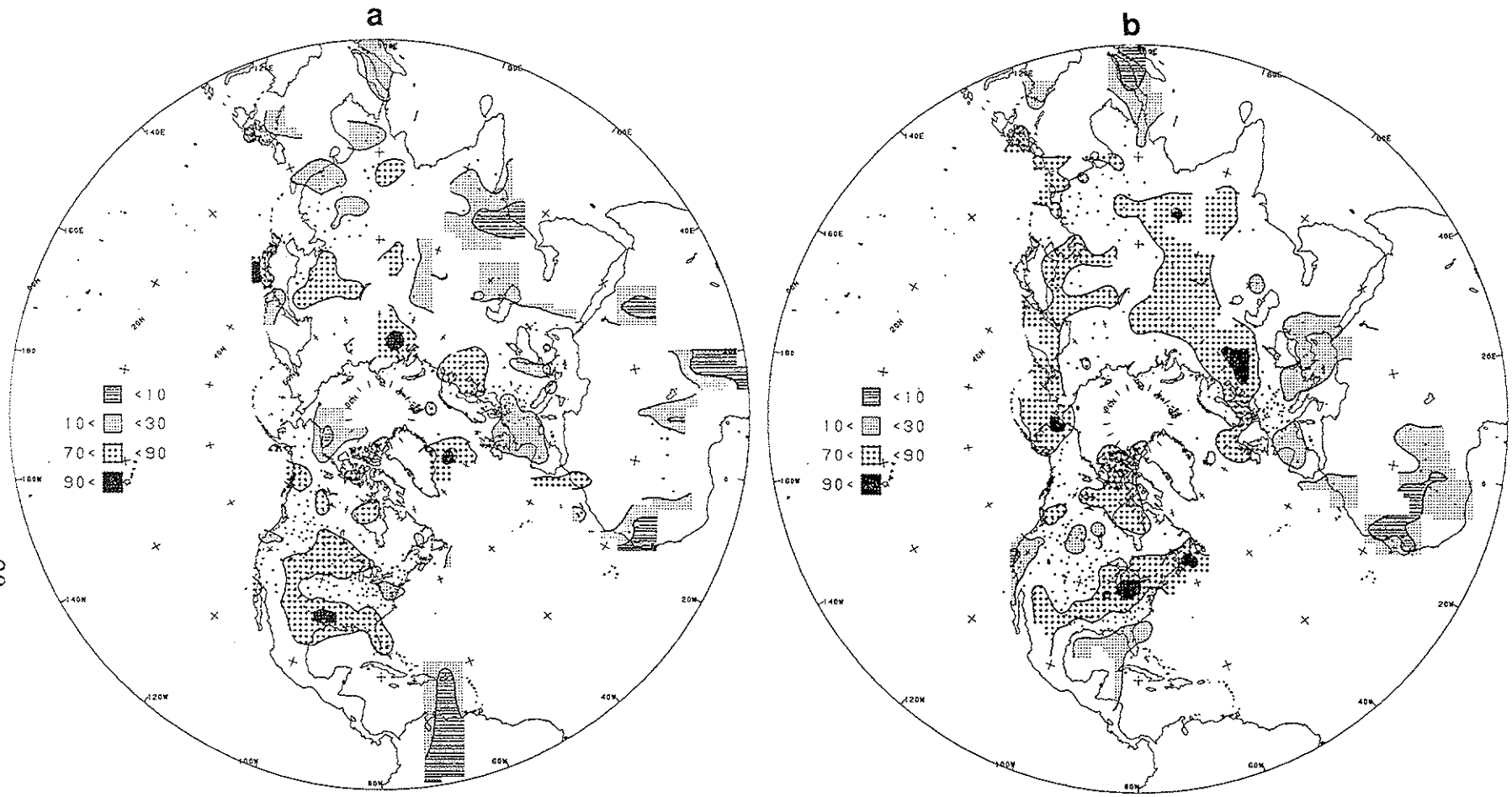

Fig. 21. Northern Hemisphere annual precipitation percentiles for a) 1991 and b) 1990 based on a Gamma distribution fit to the 1951-1980 base period. Station locations are denoted by small "+"; analysis not done in areas with insufficient data.

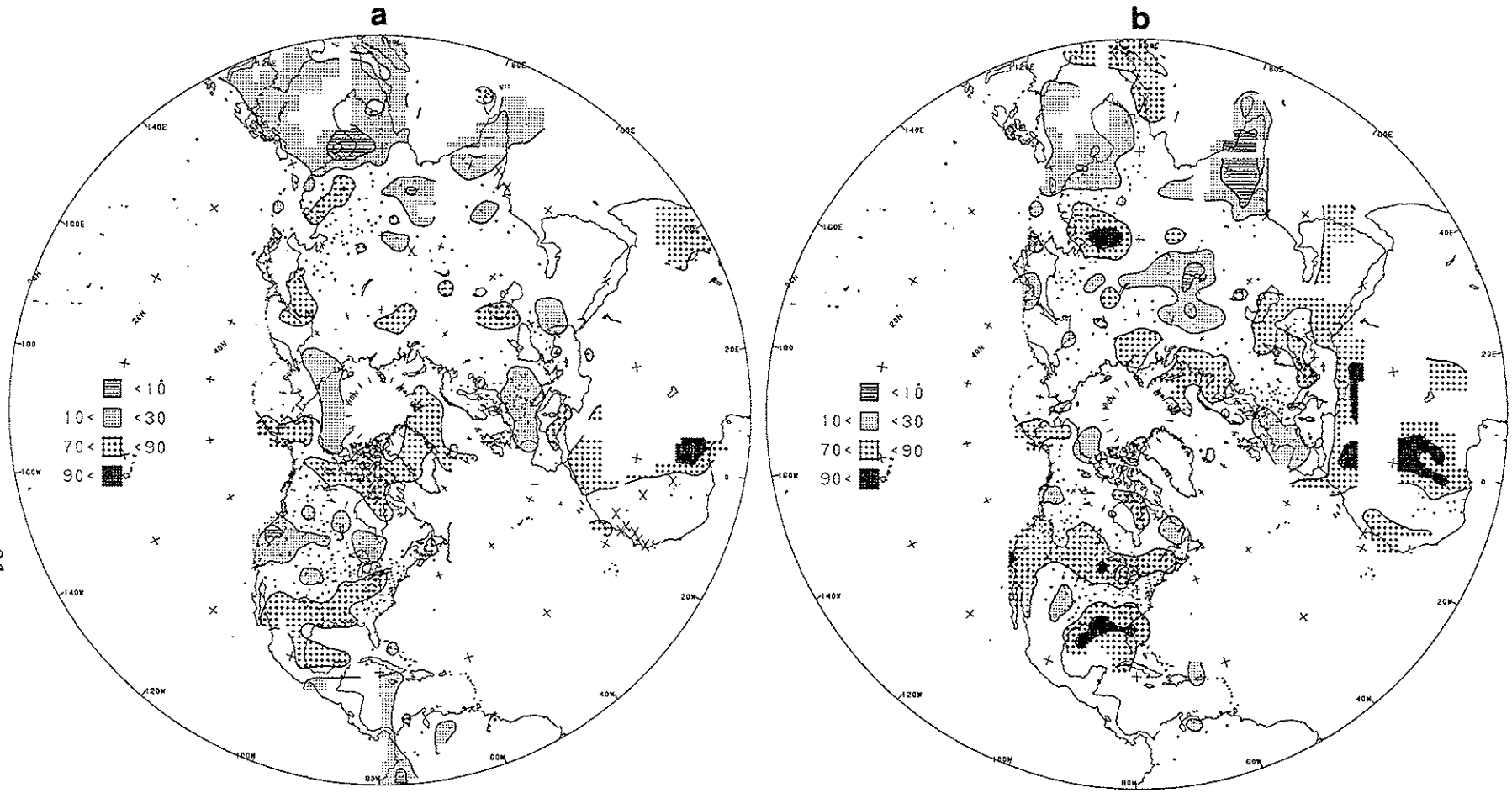

Fig. 22. Northern Hemisphere precipitation percentiles for a) DJF 1990-91 and for b) MAM 1991 based on a Gamma distribution fit to the 1951-1980 base period. Station locations are denoted by small "+"; analysis not done in areas with insufficient data.

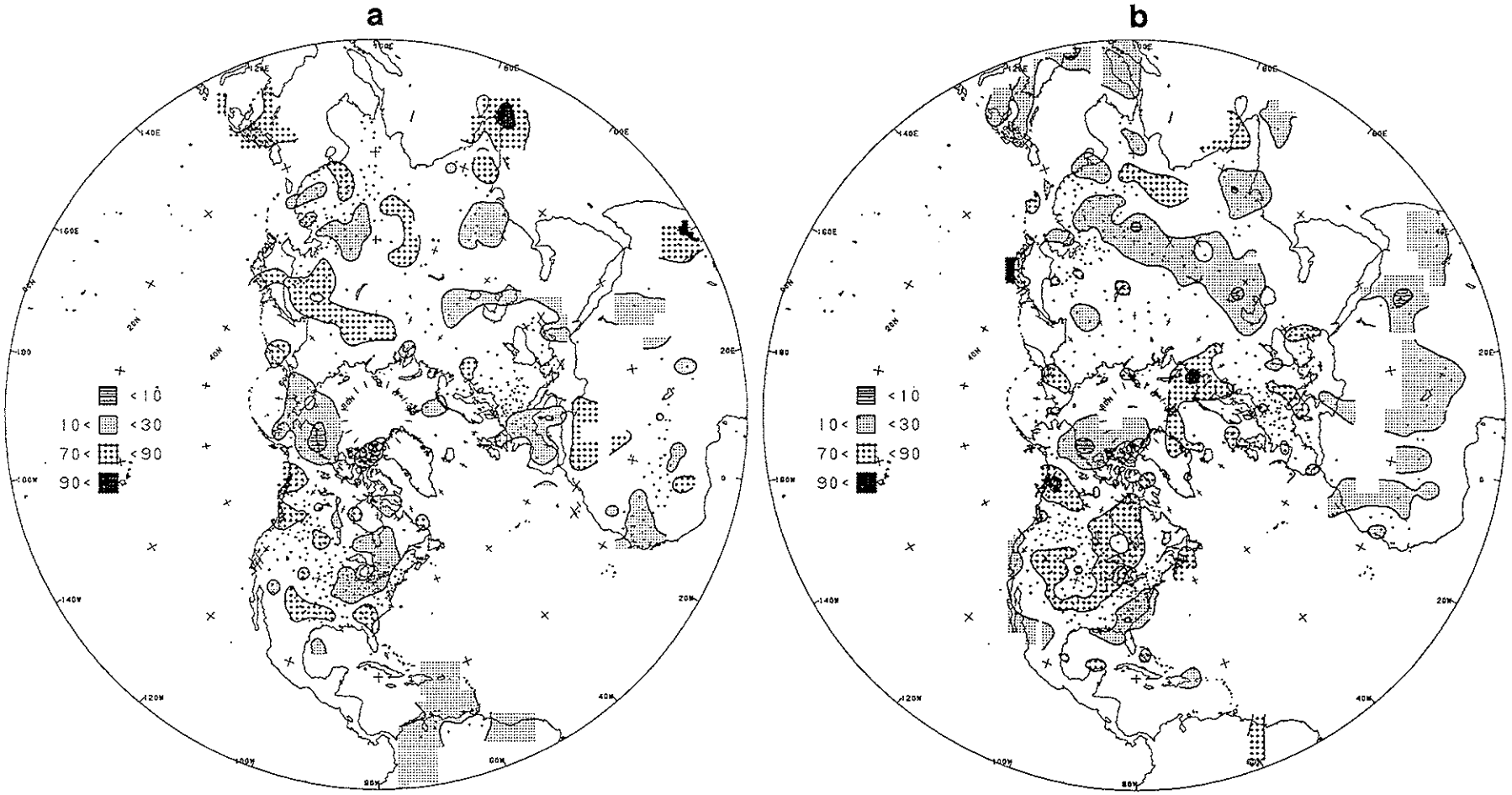

Fig. 23. Northern Hemisphere precipitation percentiles for a) JJA and for b) SON 1991 based on a Gamma distribution fit to the 1951-1980 base period. Station locations are denoted by small "+"; analysis not done in areas with insufficient data.

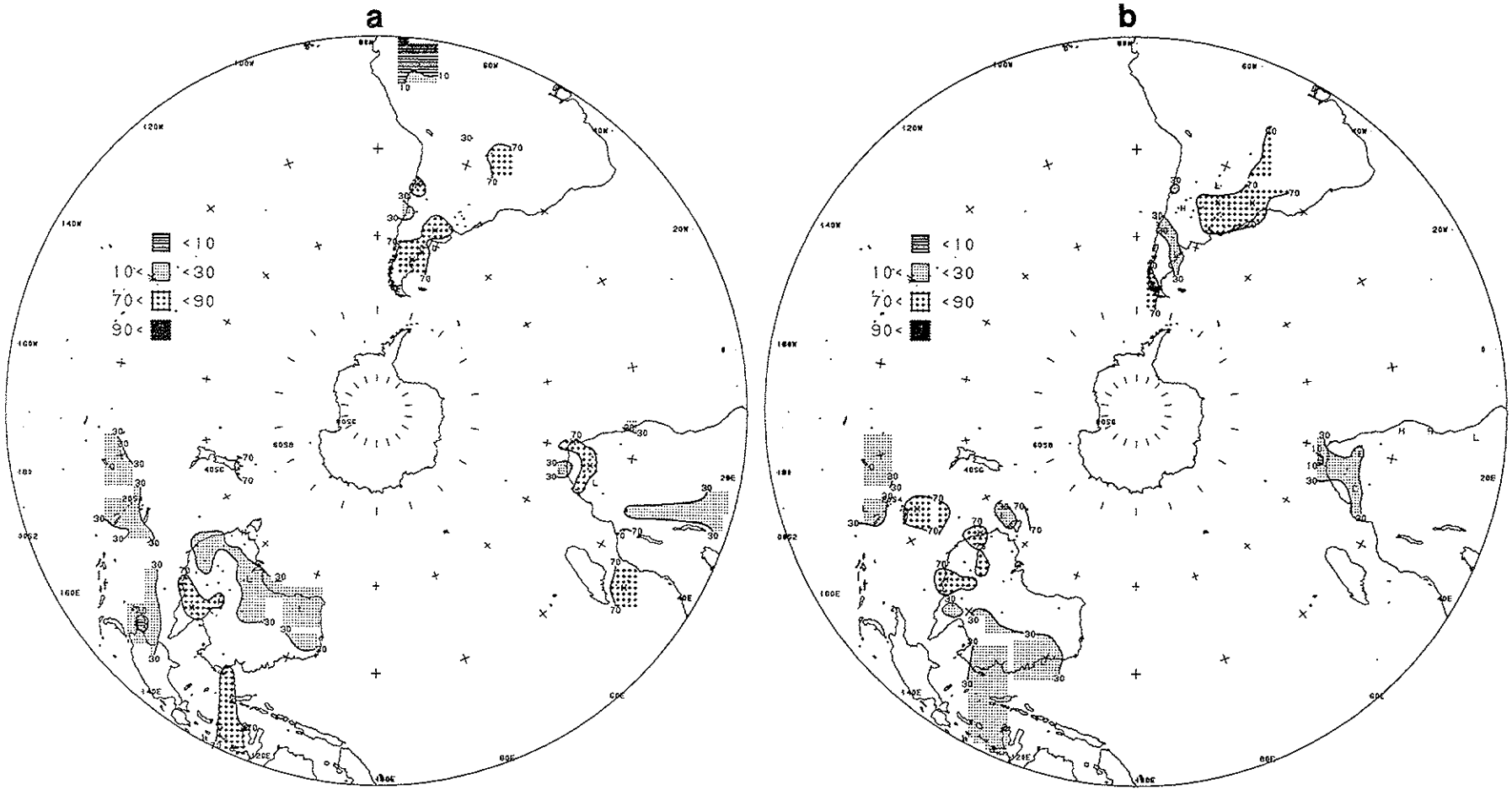

Fig. 24. Southern Hemisphere annual precipitation percentiles for a) 1991 and b) 1990 based on a Gamma distribution fit to the 1951-1980 base period. Station locations are denoted by small "+"; analysis not done in areas with insufficient data.

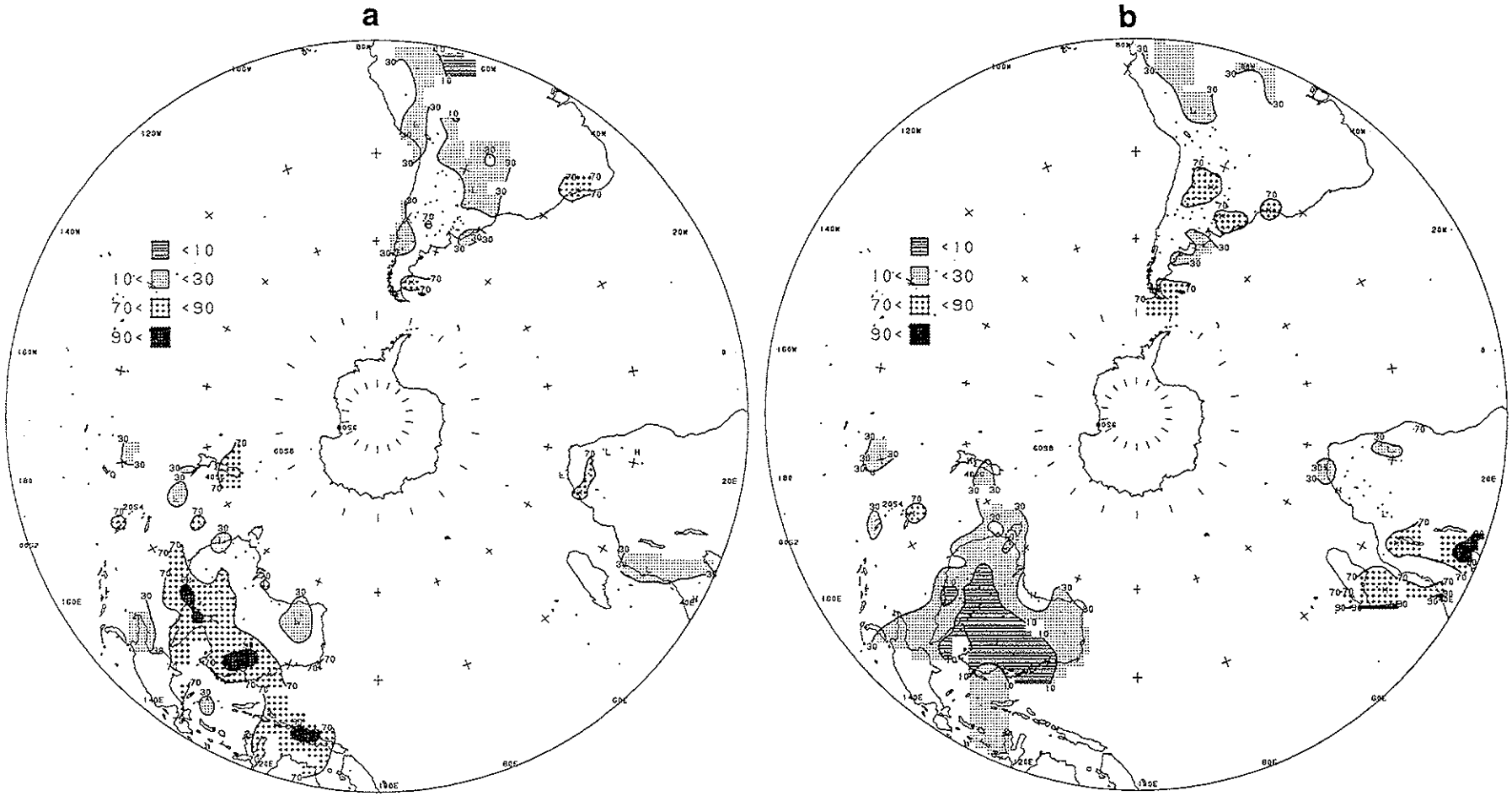

Fig. 25. Southern Hemisphere precipitation percentiles for a) DJF 1990-91 and for b) MAM 1991 based on a Gamma distribution fit to the 1951-1980 base period. Station locations are denoted by small "+"; analysis not done in areas with insufficient data.

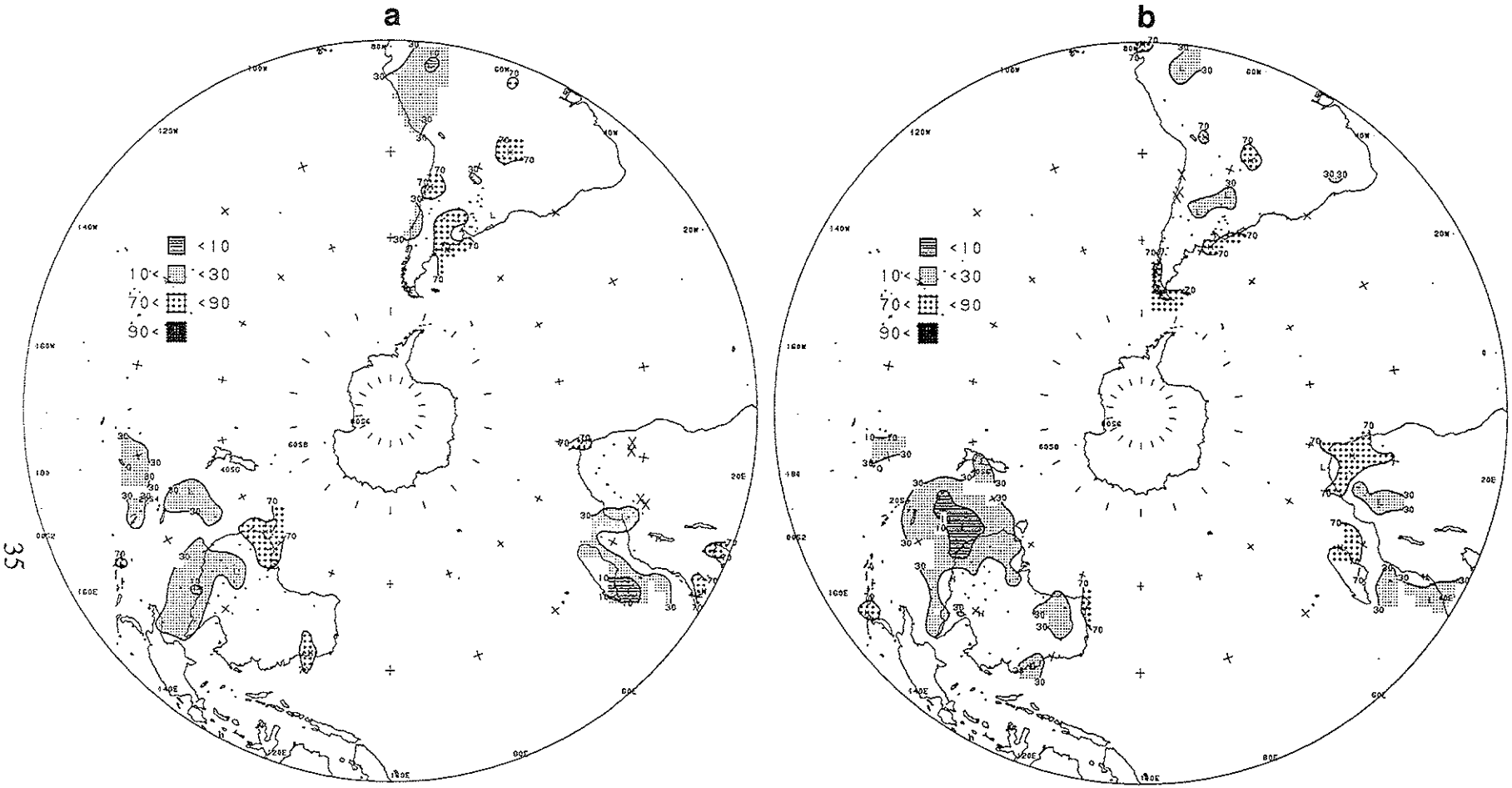

Fig. 26. Southern Hemisphere precipitation percentiles for a) JJA and for b) SON 1991 based on a Gamma distribution fit to the 1951-1980 base period. Station locations are denoted by small "+"; analysis not done in areas with insufficient data.

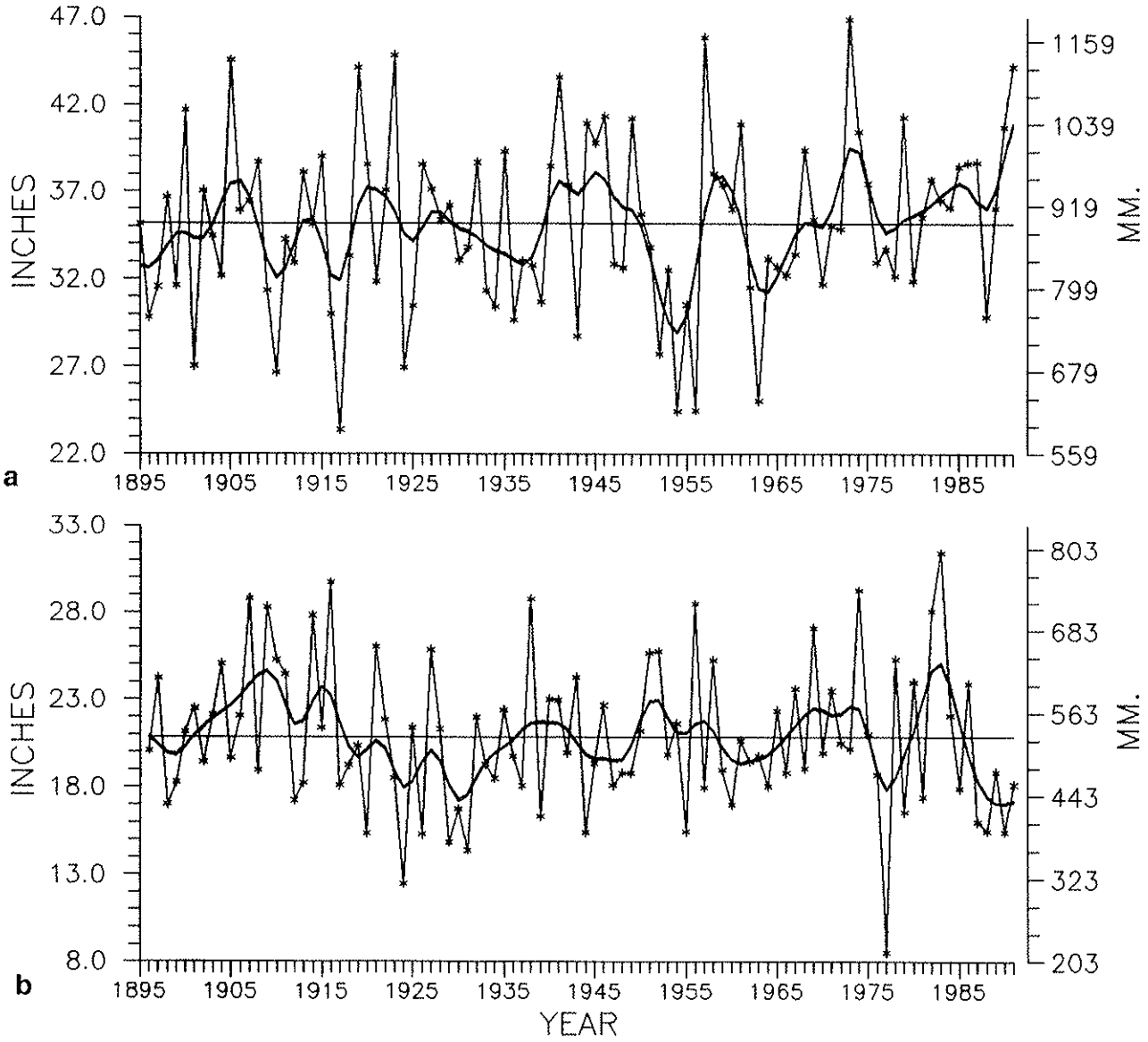

Fig. 27. a) Annual total precipitation for the South region of the United States from 1895 through 1991 and b) October-March total precipitation for the West region of the United States from 1895-96 through 1990-91. Asterisks are actual values; binomially filtered values are indicated by the solid line.

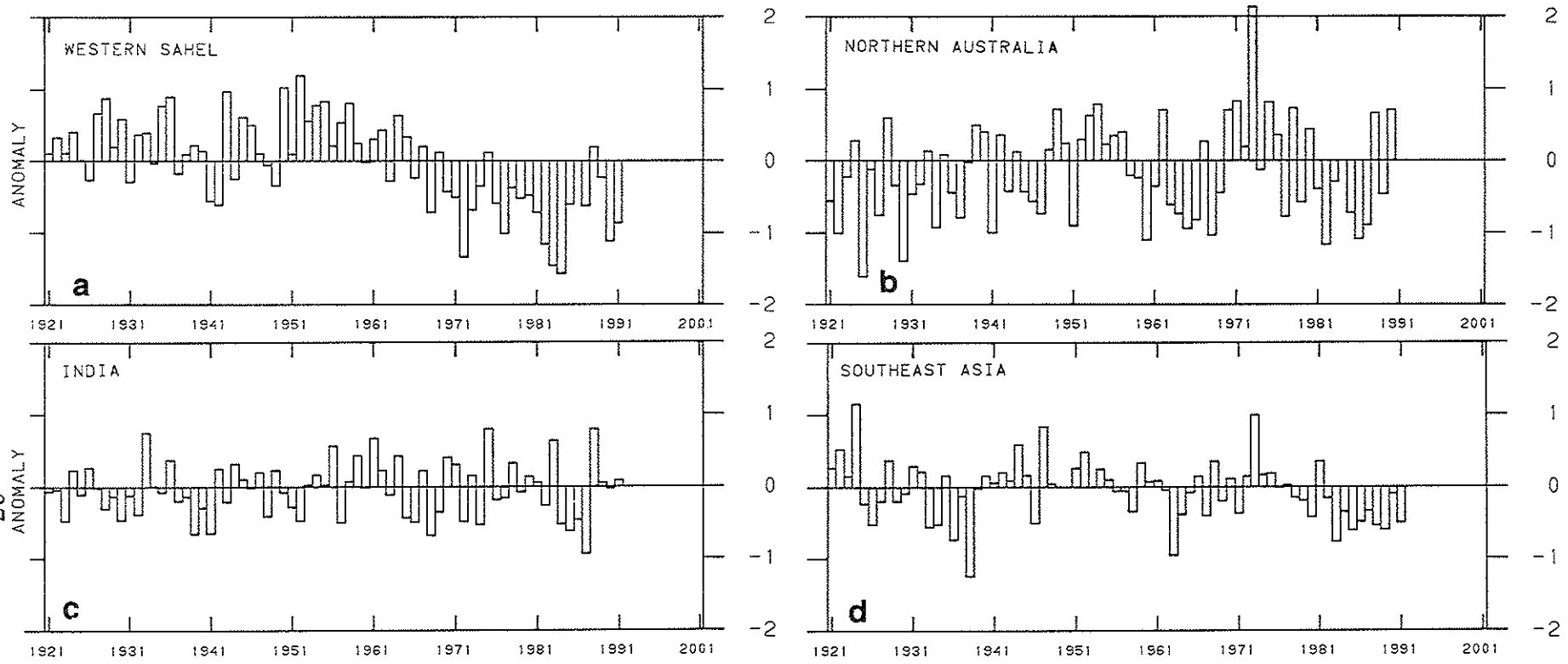

Fig. 28. Precipitation index (average gamma percentiles of station precipitation within the regions) time series for a) western Sahel, June - September; b) northern Australia, November - April; c) India, June - September; and d) southeastern Asia, April - September.

Indian Monsoon Season

Rains associated with the southwestern monsoon typically expand northwestward across the Indian subcontinent during the spring and summer months, reaching central Pakistan around mid-July (**Fig. 29a**). Approximately six weeks later, rainfall normally retreats from eastern Pakistan, reaching western India around mid-September before accelerating southeastward to the central peninsula by mid-October (**Fig. 29b**). The 1991 monsoon began in typical fashion, with abundant rains spreading across southern and eastern India and Bangladesh. However, the northwestward progression of the monsoon abruptly slowed around mid-June and never became fully established across extreme western India, central and southern Pakistan, and Nepal. Less than half of normal seasonal (May-September) rainfall was measured in those regions while only 50% to 85% of normal fell on much of central, northeast-central, and western India (**Fig. 30**).

A fairly typical retreat of monsoonal rains was observed during late September and most of October. According to the Indian Meteorological Department, the monsoon began its withdrawal from northwest India on September 18, and completely retreated from the country by October 18. There were, however, a few notable exceptions. Very heavy rains continued to soak Bangladesh and northeastern India after the "official" end of the monsoon season (Sep. 30). During September 22-October 19, 1991, 200-475 mm of rain deluged most of Assam state, adding another 50-300 mm onto the seasonal surplus that was measured during May 1-September 30. Then, from late October to late November, excessive precipitation drenched extreme southern India and Sri Lanka, including heavy mid-November rains (up to 550 mm) from Tropical Cyclone 04B which made landfall near Pondicherry.

The 1991 season was fairly typical in many respects. A wide array of rainfall totals were observed, ranging from under 100 mm in extreme western sections to nearly 3800 mm along portions of the southwestern coast (**Fig. 31**). Periodic flooding occurred in several areas, particularly in Bangladesh. In India, the country's Meteorological Department reported varying amounts of rain and flood damage in the states of Assam, Bihar, Kerala, Maharashtra, Orissa, West Bengal, and Uttar Pradesh, affecting about 23 million people. The Department also stated that 28 of 35 Indian sub-divisions, which constitutes about 75% of the Indian landmass, received near normal (more than 80% of average) to excess June-September rainfall.

It should be noted that the monsoonal rains from Nepal westward across central and western India and Pakistan may have been affected by the development of a warm (ENSO) episode in the equatorial Pacific Ocean. The development of an ENSO usually correlates with an abnormally weak (dry) monsoon season from Nepal and western Orissa westward into Pakistan, along with atypical October-December wetness in southern India and Sri Lanka (Ropelewski and Halpert 1987).

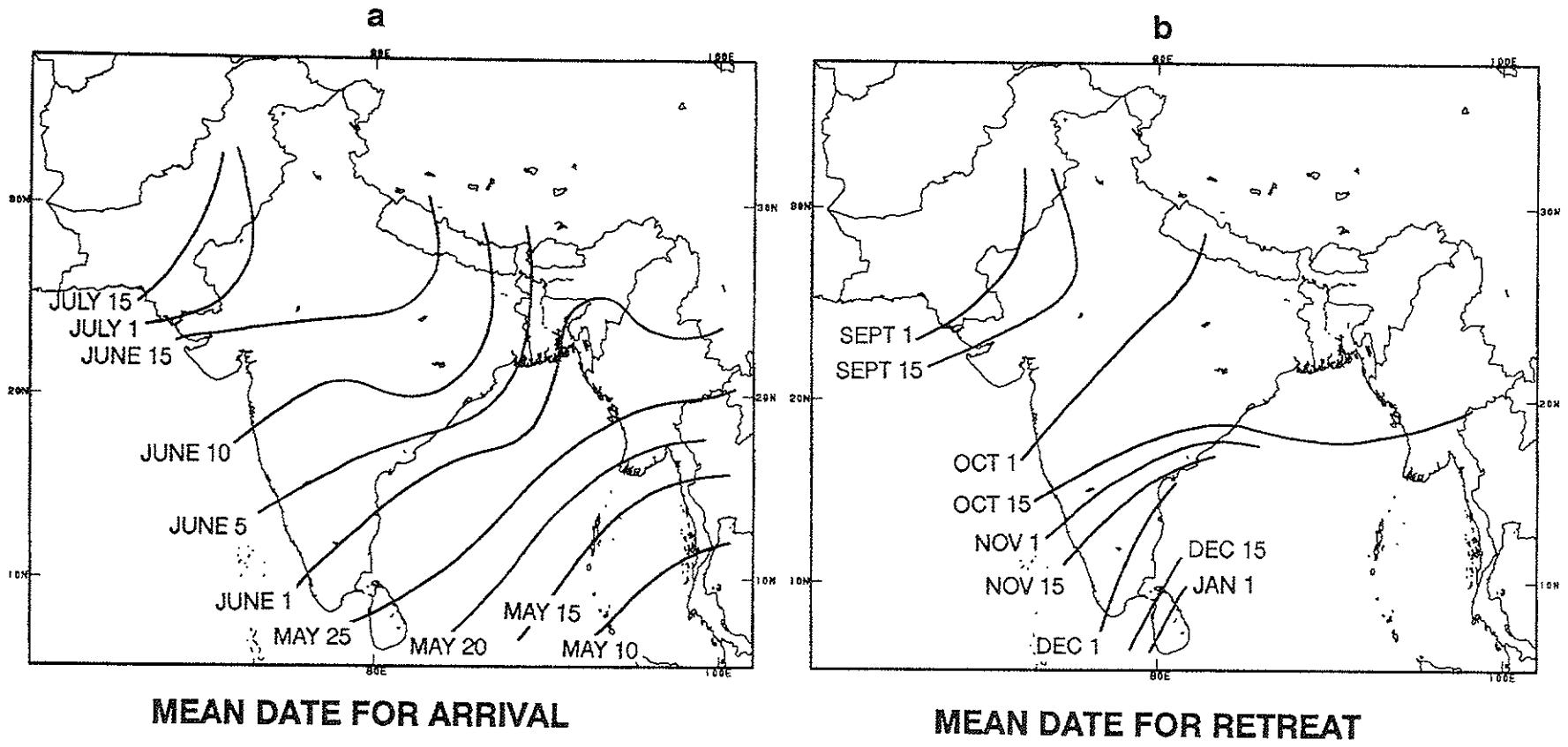

Fig. 29. a) Mean dates of the southwest monsoon's arrival and b) Mean dates of the southwest monsoon's retreat.

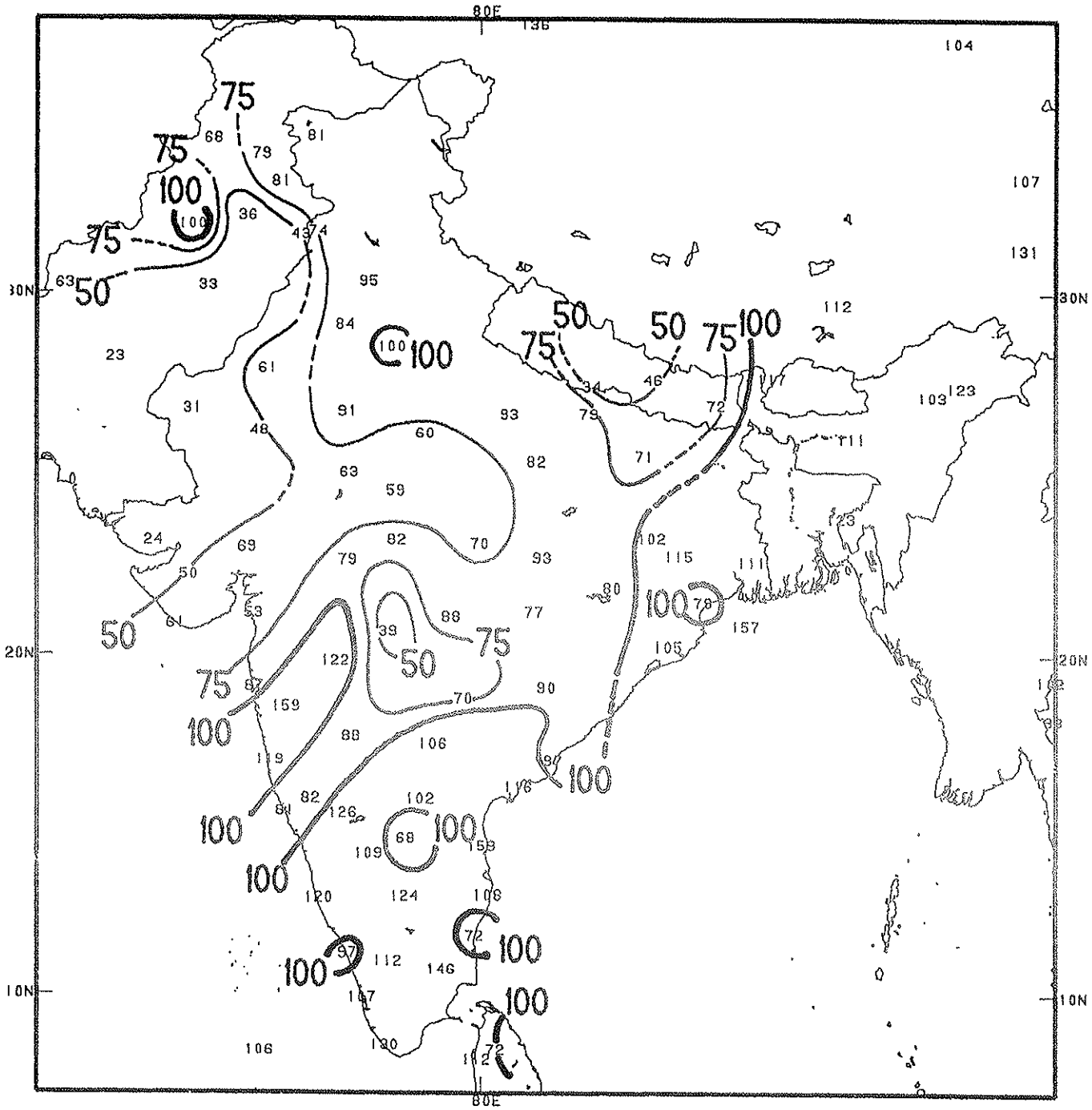

Fig. 30. Percent of normal precipitation during May 1 - September 30, 1991. Isopleths drawn for 50%, 75%, and 100% (thick line).

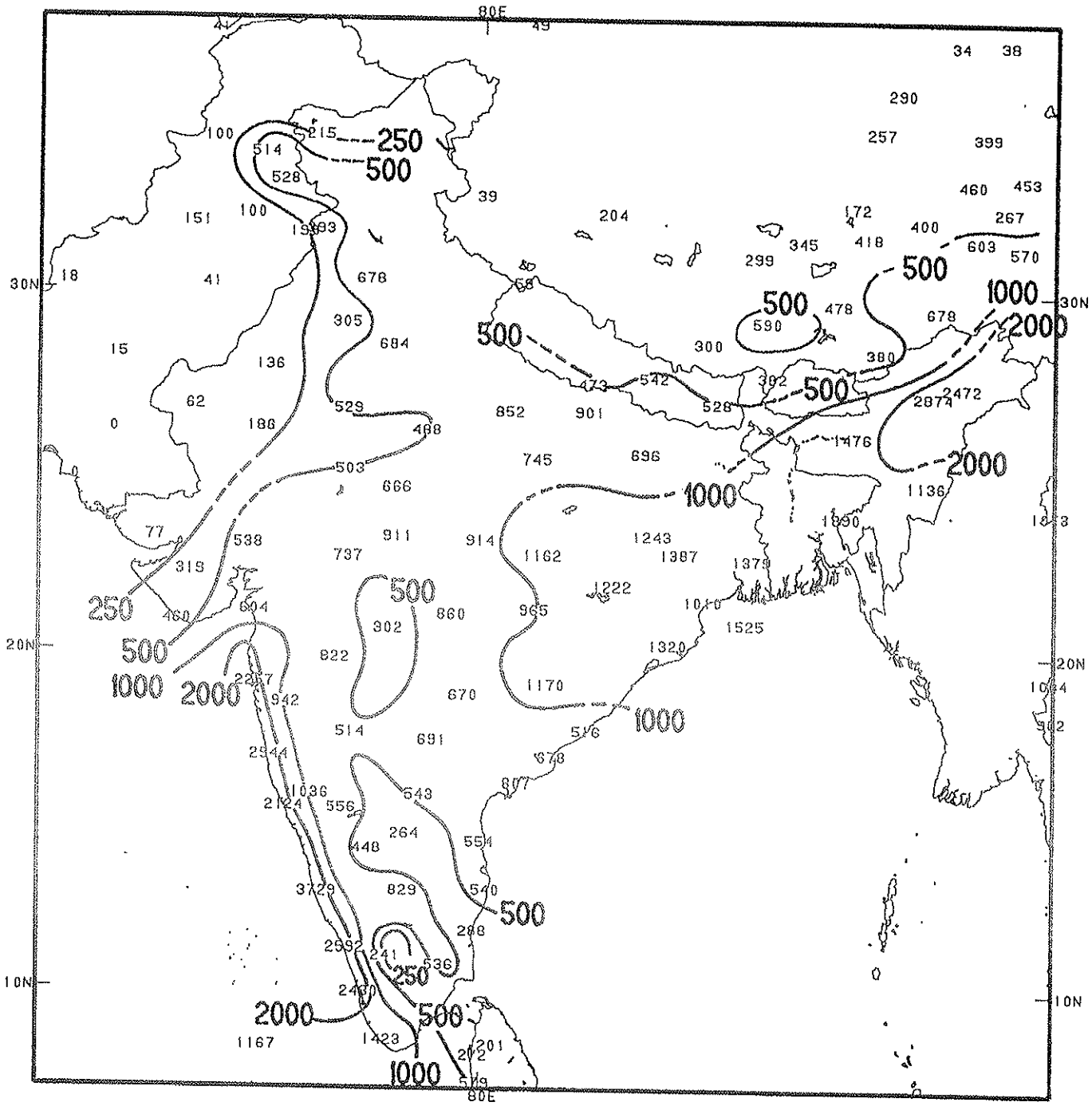

Fig. 31. Total precipitation during May 1 - September 30, 1991. Isohyets drawn for 250, 500, 1000, and 2000 mm.

AFRICAN SAHEL RAINY SEASON

A standardized precipitation index, using June-September rainfall totals from up to 20 locations in the western Sahel, indicated an atypically dry 1991 season (**Fig. 28a**). This index, however, does not take into account the timeliness of the rains. The 1991 season threatened to bring adversely low rainfall totals to a few portions of the Sahel and, simultaneously, to deluge other sections. Fortunately, timely weather changes seemed to occur before these trends resulted in serious agricultural or hydrological impacts.

The 1991 wet season got off to an abnormally early and wet start across parts of Niger, Chad, and the Sudan south of 11°N in May. These locations went on to record below normal amounts during June and fairly typical totals during the rest of the season, limiting significant seasonal surpluses to portions of south-central and southwestern Niger, extreme southern Burkina Faso, and adjacent Mali, where heavy rains were measured sporadically during July and August. In addition, scattered downpours generated isolated flooding in northern Ghana, southern Burkina Faso, and the Sudan during August, but subsequently drier conditions allowed these regions to quickly recover.

In contrast, very dry conditions affected southwestern Mali, Senegal, and southern Mauritania until mid-July, when seasonal rains finally commenced. The last half of July and most of August brought above normal rainfall to the region, and unusually heavy late-season rains continued through September and into October. The wet season as a whole brought only 40%-60% of normal rainfall to northern and western Senegal, with totals somewhat closer to normal measured farther north and east (**Fig. 32a**). Crop development got off to a very late start because of the dryness, but heavy September rains and significant October totals minimized agricultural impacts despite the very low totals recorded in parts of Senegal. Farther east, much of the Sudan north of 11°N also experienced an abnormally dry 1991 rainy season, despite spotty flooding slightly south of this region, while eastern Ethiopia and Djibouti received below normal rainfall during May-September 1991 (**Fig. 33**), although the summer wet season is secondary to a typically rainy late winter and early autumn.

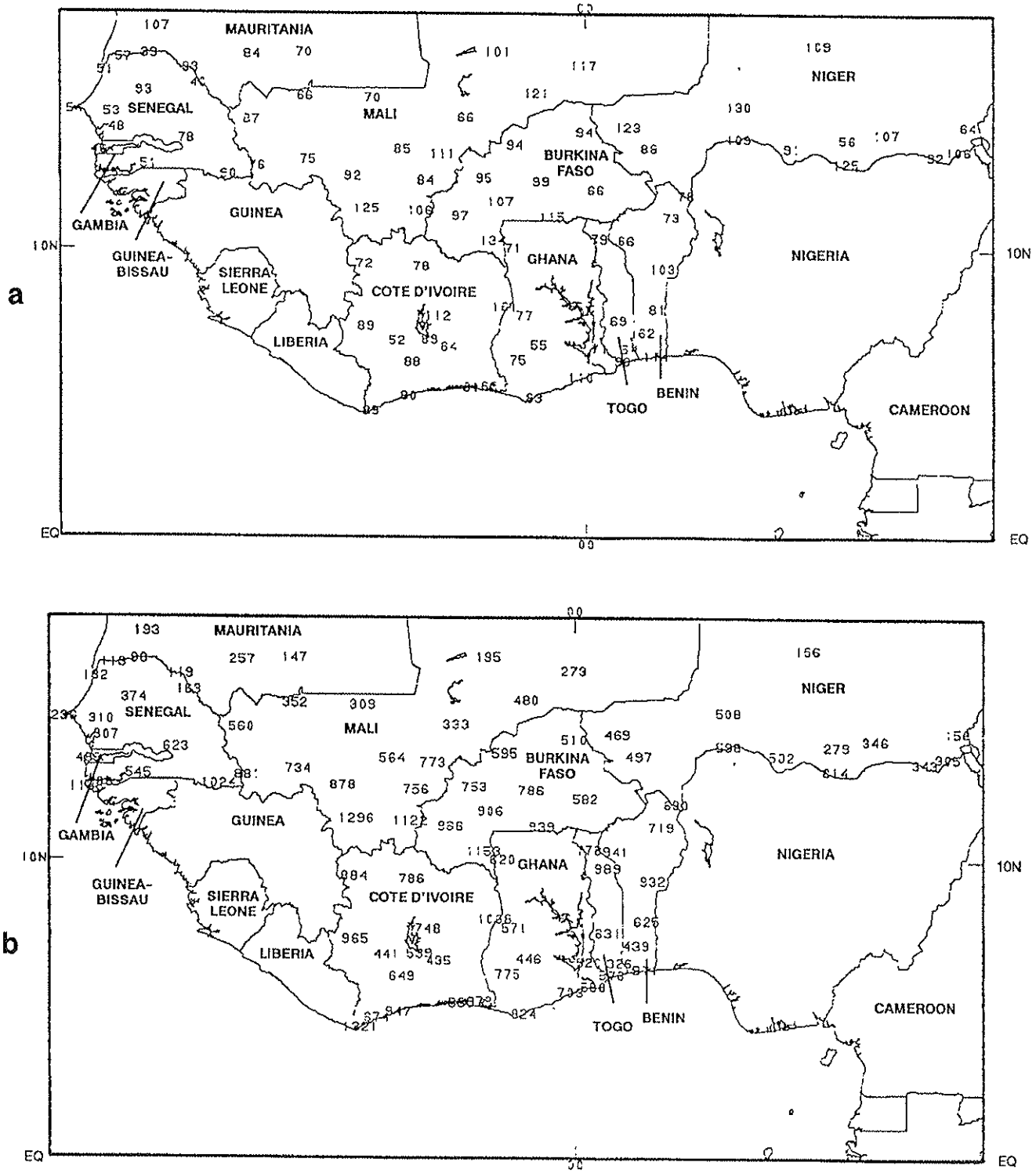

Fig. 32. a) West African Sahel percent of normal precipitation during May 1 - September 30, 1991 and b) West African Sahel total precipitation (mm) during May 1 - September 30, 1991.

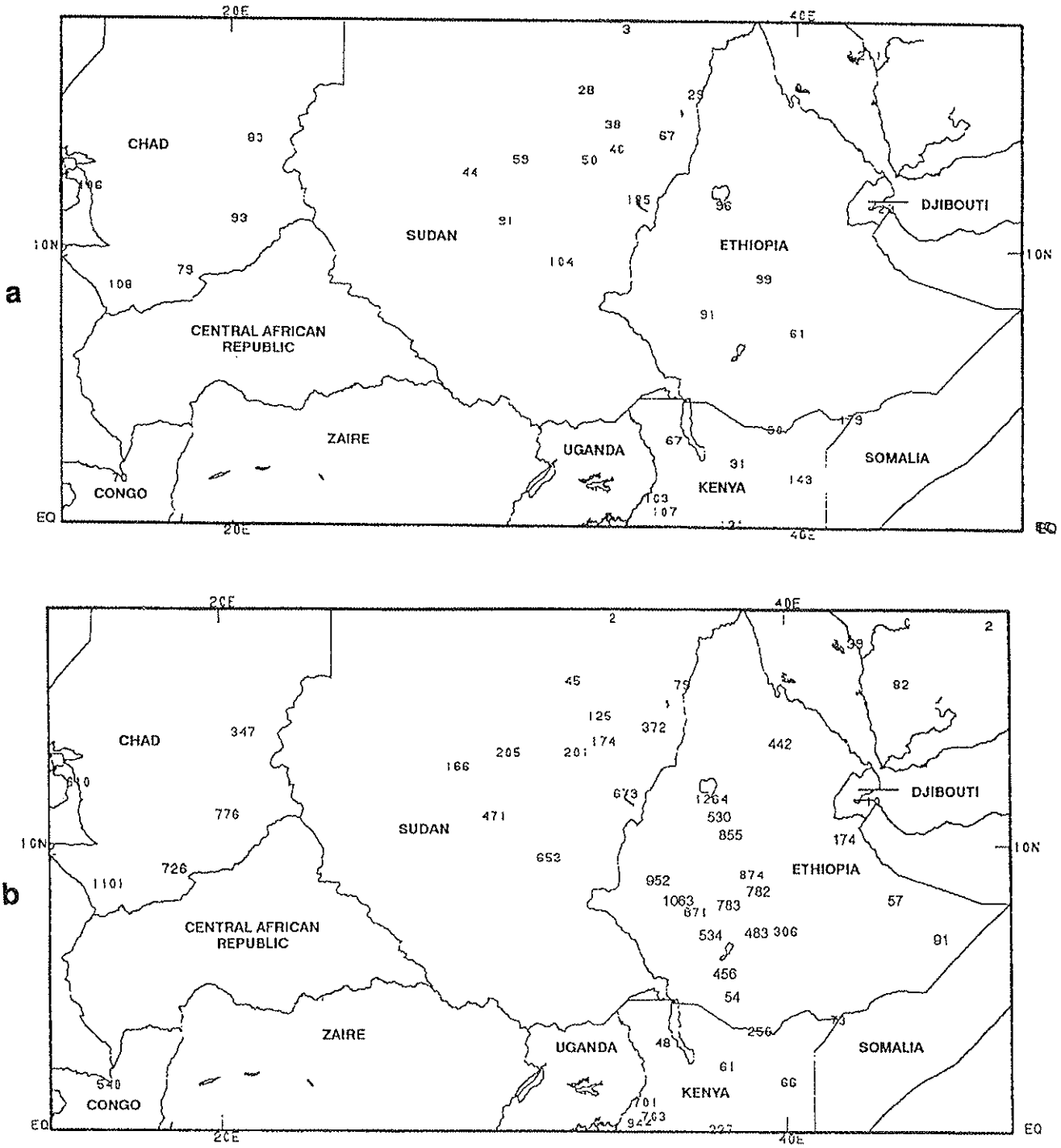

Fig. 33. a) East African Sahel percent of normal precipitation during May 1 - September 30, 1991 and b) East African Sahel total precipitation (mm) during May 1-September 30, 1991.

Satellite Rainfall Estimates

Tropical rainfall anomalies, as estimated from geostationary and polar orbiting infrared radiance data, are shown in **Figs. 34-35.** These estimates are produced at the Climate Analysis Center for the Global Precipitation Climatology Project (Janowiak and Arkin 1991) using a technique developed by Arkin and Meisner (1987). Their method uses cloud-top temperature information to estimate rainfall from convective systems over relatively large (2.5^{o} lat/lon) regions. Since the method uses only temperature to infer rainfall, regions of highly persistent cirrus are erroneously depicted as a precipitating cloud. Similarly, extremely cold surface temperatures (such as over the Tibetan Plateau during northern winter) may erroneously indicate rainfall, therefore, estimates are only shown south of 20^{o}N.

Estimated rainfall anomalies indicate drier than normal conditions over much of the Indonesia region (2 to 8 mm/day deficit) during the year, particularly for the period June - November 1991. In contrast, an enhanced Pacific ITCZ (2 to 6 mm/day excess) is apparent during all seasons except December 1990 - February 1991. These rainfall anomaly patterns are consistent with the warm (ENSO) episode conditions which were developing in the tropical Pacific during mid-late 1991. Elsewhere, anomalies are generally confined to small areas or are smaller than 2 mm/day.

Due to the short base period being used, it is possible that the magnitudes of some of these anomalies are an artifact of inadequate sampling. For example, during the 1986-90 period, the equatorial mid-Pacific was affected by both phases of the ENSO cycle (warm during 1986-87, cold during 1988-89) which caused significant departures from normal conditions. Obviously, the 5-year "normal" for this region is computed over a period in which the rainfall was highly "non-normal". By the same token, the anomalously high rainfall during the warm episode conditions was offset by drier than normal conditions during the cold phase of the Southern Oscillation, perhaps yielding a reasonable climatology near the date line and equator.

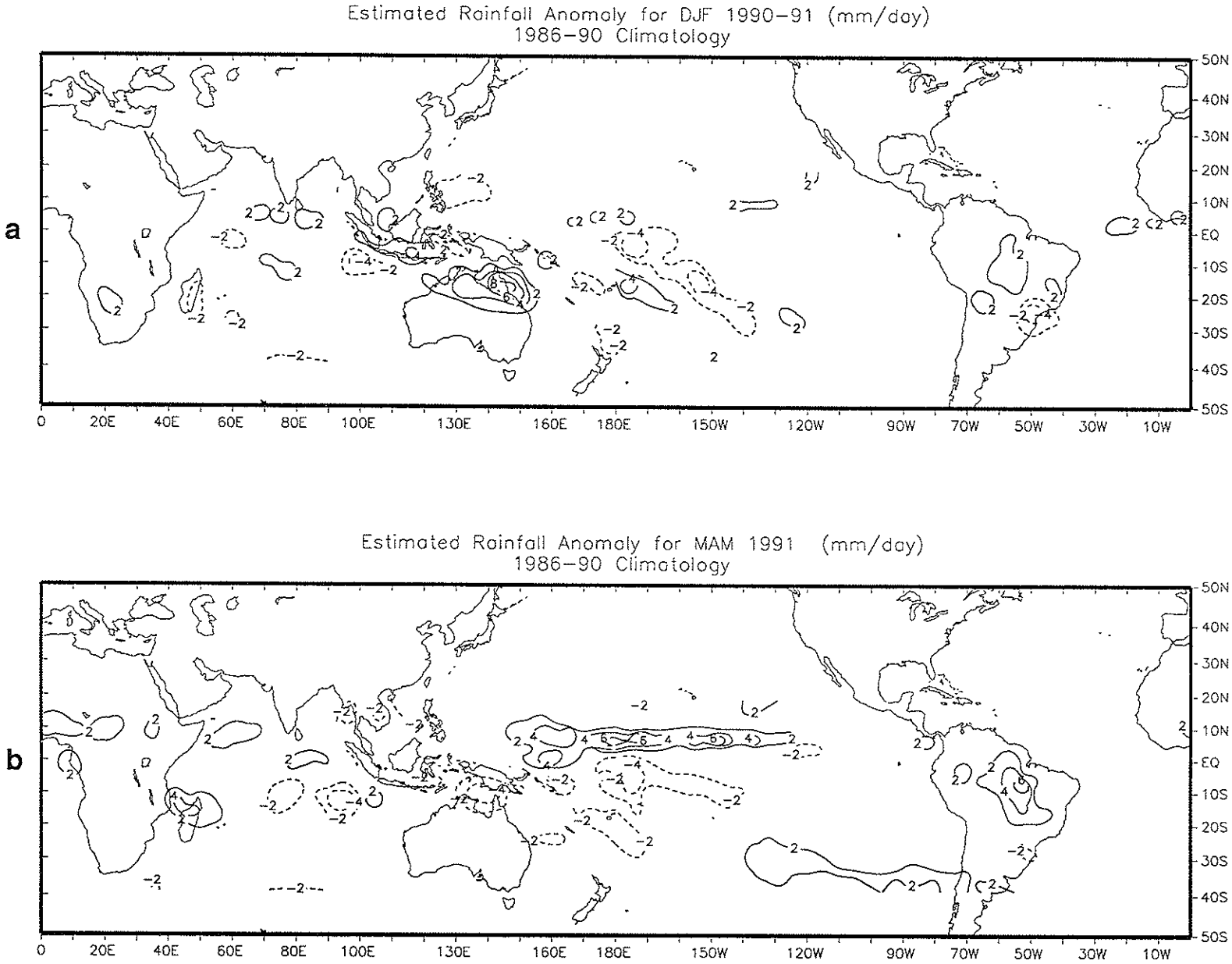

Fig. 34. Estimated rainfall anomalies (mm/day) for a) DJF 1990-91, and for b) MAM 1991. Base period is 1986-90. Solid (dashed) lines indicate greater (less) than normal rainfall.

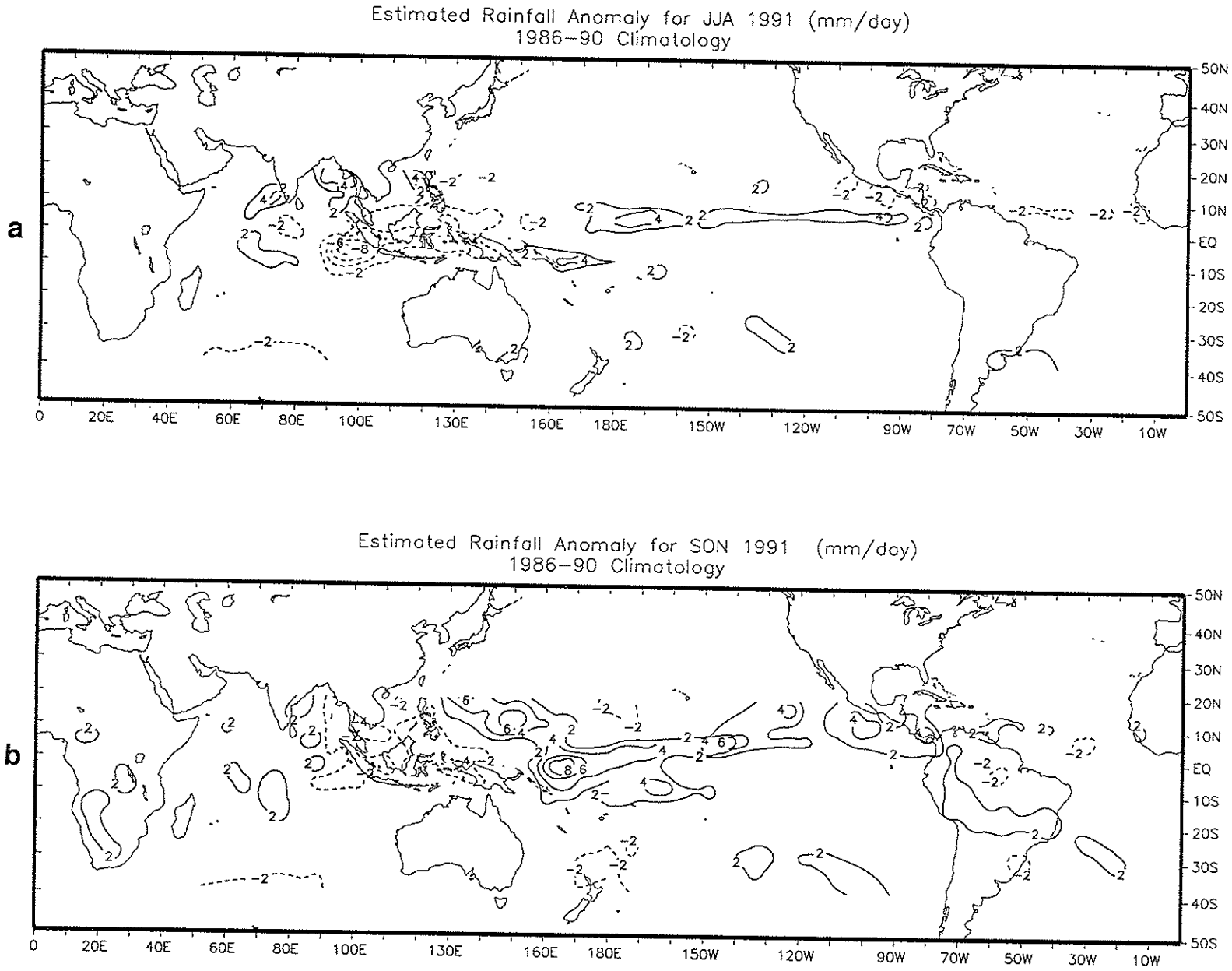

Fig. 35. Estimated rainfall anomalies (mm/day) for a) JJA 1991, and for b) SON 1991. Base period is 1986-90. Solid (dashed) lines indicate greater (less) than normal rainfall.

CRYOSPHERE

Snow cover was considerably below average for the December 1990 to May 1991 period (**Fig. 36a**). The snow cover deficit in North America was roughly coincident with areas of largest positive temperature anomalies during the same season (**Fig. 36b**). Only the far western United States experienced both below normal temperatures and snow cover. The low amount of snow cover is another manifestation of the multi-year drought in this region.

The relationship between Eurasian snow cover and temperature for the December 1990 to May 1991 period was considerably more complex. Overall, the Eurasian snow cover was also below the 1973 to 1992 mean. However, a patchy band of above average snow cover stretched from the Aral Sea eastward to the Korean peninsula (**Fig 36a**).

Sea ice charts have been prepared weekly by the Navy/NOAA Joint Ice Center since 1973. These charts depict the ice edge and concentration derived from subjective analyses of satellite data. In recent years, visual data has been augmented by microwave estimates of sea ice. The charts have been digitized for analyses starting in 1973. The largest variability in global sea ice occurred early in the record, when global sea ice area decreased (mostly driven by the Antarctic) during the 1973 to 1980 period. Since then sea ice area has shown considerable interannual variability, but no consistent multi-year trends. Global sea ice area was considerably lower than average from 1990 through mid-1991 (**Fig. 37**). These area deficits mainly reflect less than normal sea ice extent in the Arctic.

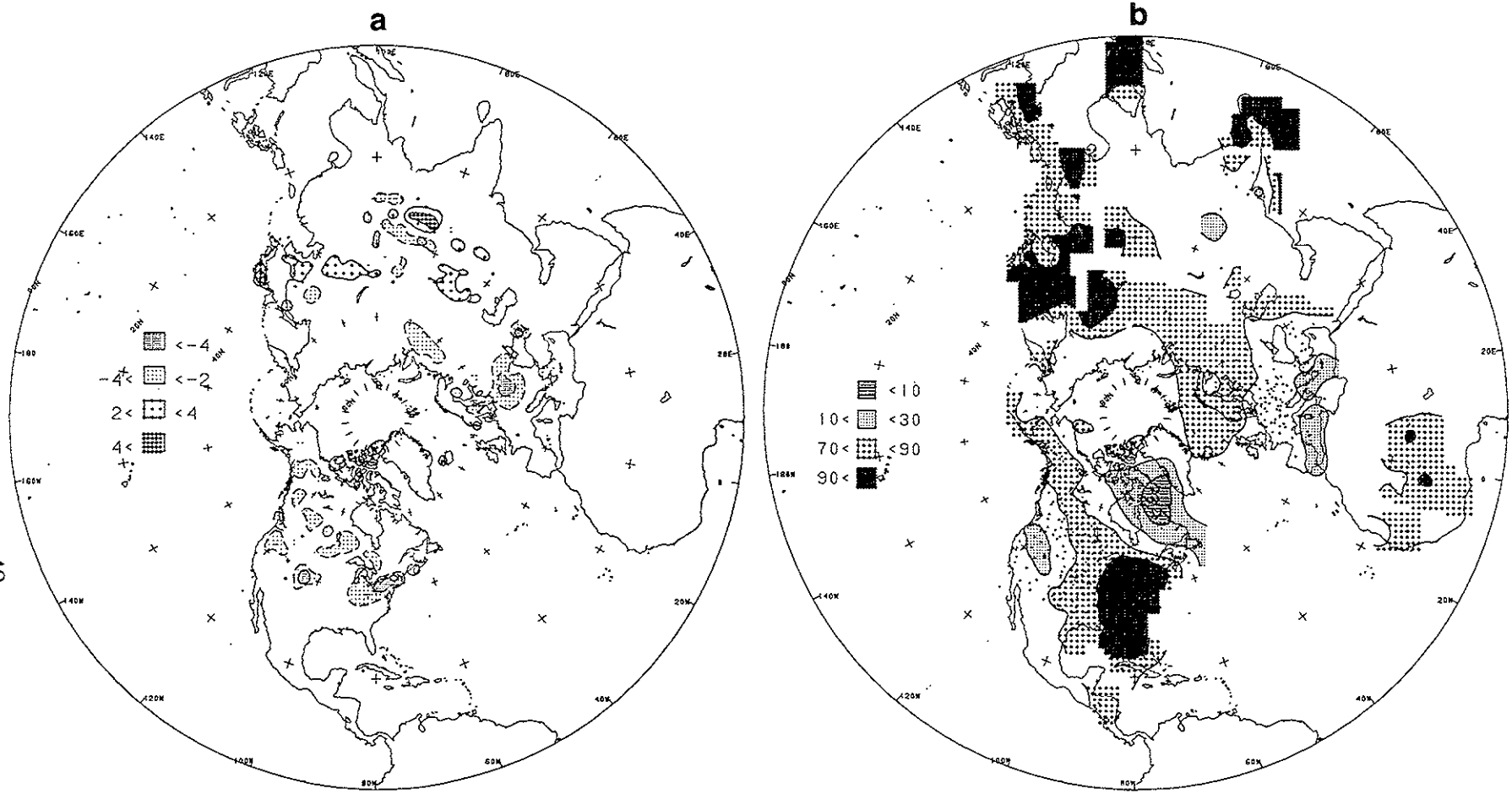

Fig. 36. a) Snow cover anomaly expressed as a deficit or excess of the number of weeks with snow cover compared to the 1973 to 1992 average and b) temperature anomaly expressed as percentiles of a normal distribution compared to the 1951-1980 base period for the December 1990 through May 1991 period.

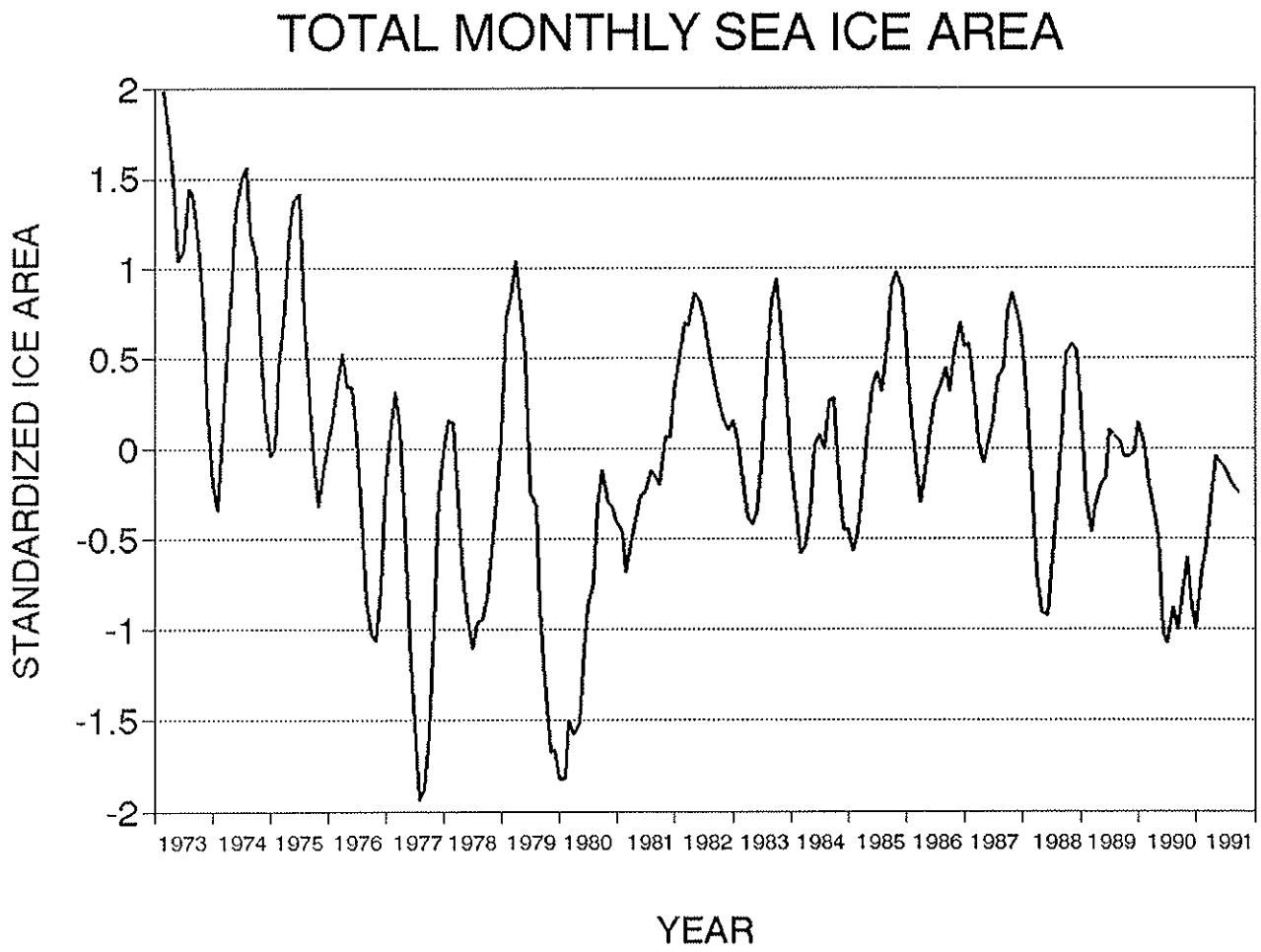

Fig. 37. Five month running mean of the standardized global (Arctic and Antarctic) sea ice area anomalies computed from the 1973 - 1991 base period.

TROPOSPHERIC AND STRATOSPHERIC ANALYSIS

Tropospheric Temperatures

A time series of global lower tropospheric (1000-400 mb) temperature anomalies, derived from Microwave Sounding Unit (MSU) satellite observations, shows a decrease of about 0.5°C since June 1991 (**Fig. 38**). These data are derived from 2.5° latitude by 2.5° longitude resolution zonal mean anomalies for "channel 2R" between 82.5°N and 82.5°S (Spencer and Christy, 1990), with the anomalies computed from a mean based on the entire record. The December anomaly is the lowest anomaly since early 1989 and is probably related to the volcanic eruption of Mt. Pinatubo in June. This cooling is also apparent in the time series plots for both the Northern Hemisphere and the Southern Hemisphere .

The time series of tropospheric mean temperature derived from radiosonde data (**Fig. 39**) shows that 1991 was 0.06°C cooler than the value recorded for 1990. This temperature decrease was entirely due to a cooler September - November period during 1991. The time series is consistent with the lower tropospheric temperatures obtained from the MSU (**Fig. 38**), although the decrease between 1990 and 1991 in the radiosonde data was not as large. The temperature time series derived from radiosonde data would probably have decreased more except for the warming influence of the developing ENSO episode.

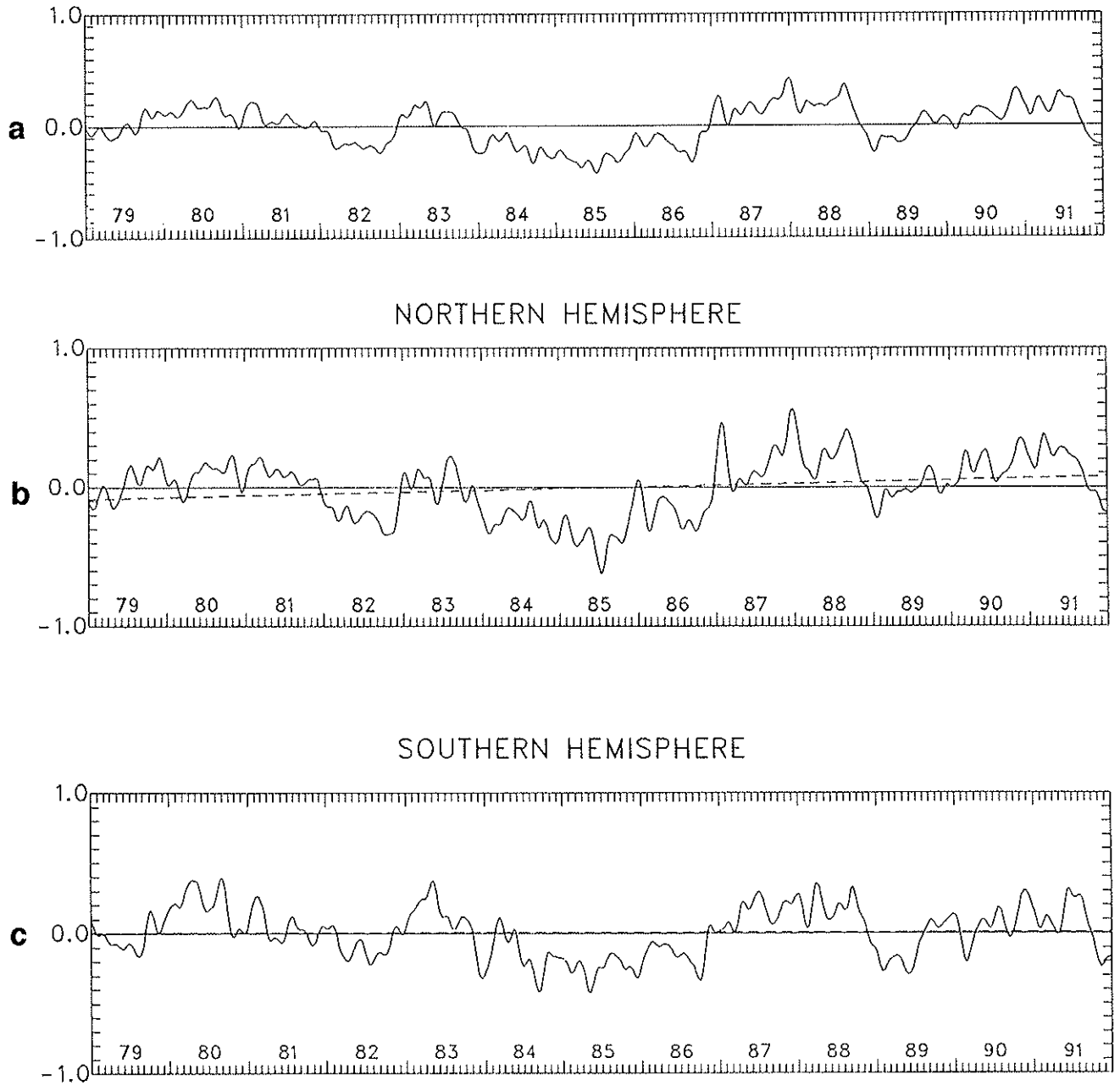

Fig. 38. Time series of a) global, b) Northern Hemisphere and c) Southern Hemisphere lower tropospheric temperature anomalies derived from satellite Microwave Sounding Unit (MSU) observations.

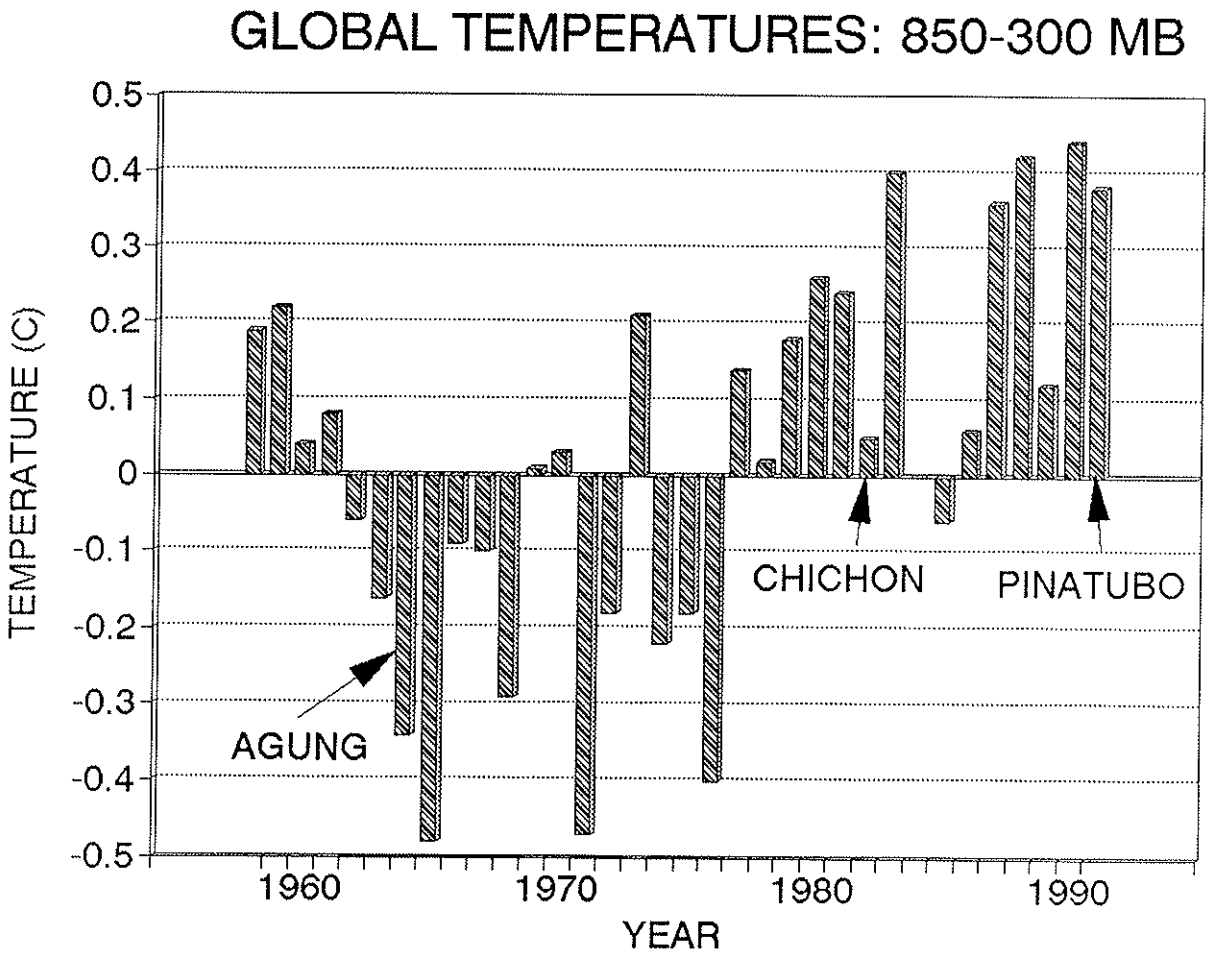

Fig. 39. Time series of global tropospheric (850 - 300 mb) temperature anomalies derived from radiosonde data, data supplied by Jim Angell.

Stratospheric Temperatures/Ozone

Temperatures in the lower stratosphere, based on the CAC global stratospheric analyses derived from NOAA 11 TOVS data and rawinsonde information, have shown a marked increase after the eruptions of Mount Pinatubo, Philippines. **Figure 40** shows the progression of the 30 mb (approx. 24 km) zonally averaged temperature at 10°S for 1991 (solid line) relative to the 1978-1991 average (dotted line). The January to June 1991 tropical 30 mb temperatures were approximately 2°C below the long-term average. After the Pinatubo eruptions, temperatures increased dramatically, reaching approximately 2°C above average by the end of September.

Another measure of lower stratospheric temperatures, channel 4 of the MSU, also indicated an increase in near global (82.5°S and 82.5°S) temperatures between July and September 1991 (**Fig. 41a**). The temperature anomalies decreased between September and the first part of December, but then began increasing through the end of the year in the Northern Hemisphere (**Fig. 41b**). Maximum stratospheric temperature anomalies during 1991 in both hemispheres reached values near those observed during 1982-83 after the El Chichon eruption.

Lower stratospheric temperature anomalies, averaged for the entire year, were above normal in all regions except for the southeast Pacific Ocean (**Fig. 42**). These negative temperature anomalies coincided with a persistent tropospheric blocking pattern that dominated this portion of the Southern Hemisphere from April through June. Positive temperature anomalies were generally less than 0.25°C over the tropics, with the largest anomalies occurring over the Mediterranean and India in the Northern Hemisphere and over the southern Indian Ocean in the Southern Hemisphere.

Temperature conditions in the Antarctic lower stratosphere are of special interest in connection with the "ozone hole". **Figure 43** shows that the 50 mb zonal temperatures at 80°S during 1991 were near the long-term average for most of the year, with positive anomalies from October to mid-December.

Figure 44 shows monthly average polar total ozone values over the Antarctic region from TOVS. The 70°S to 90°S TOVS total ozone values for 1991 included periods when some daily values were the lowest observed in the record. Overall, the minimum monthly-averaged values for the past several years have been similar, after the very steep decreases of the 1980's.

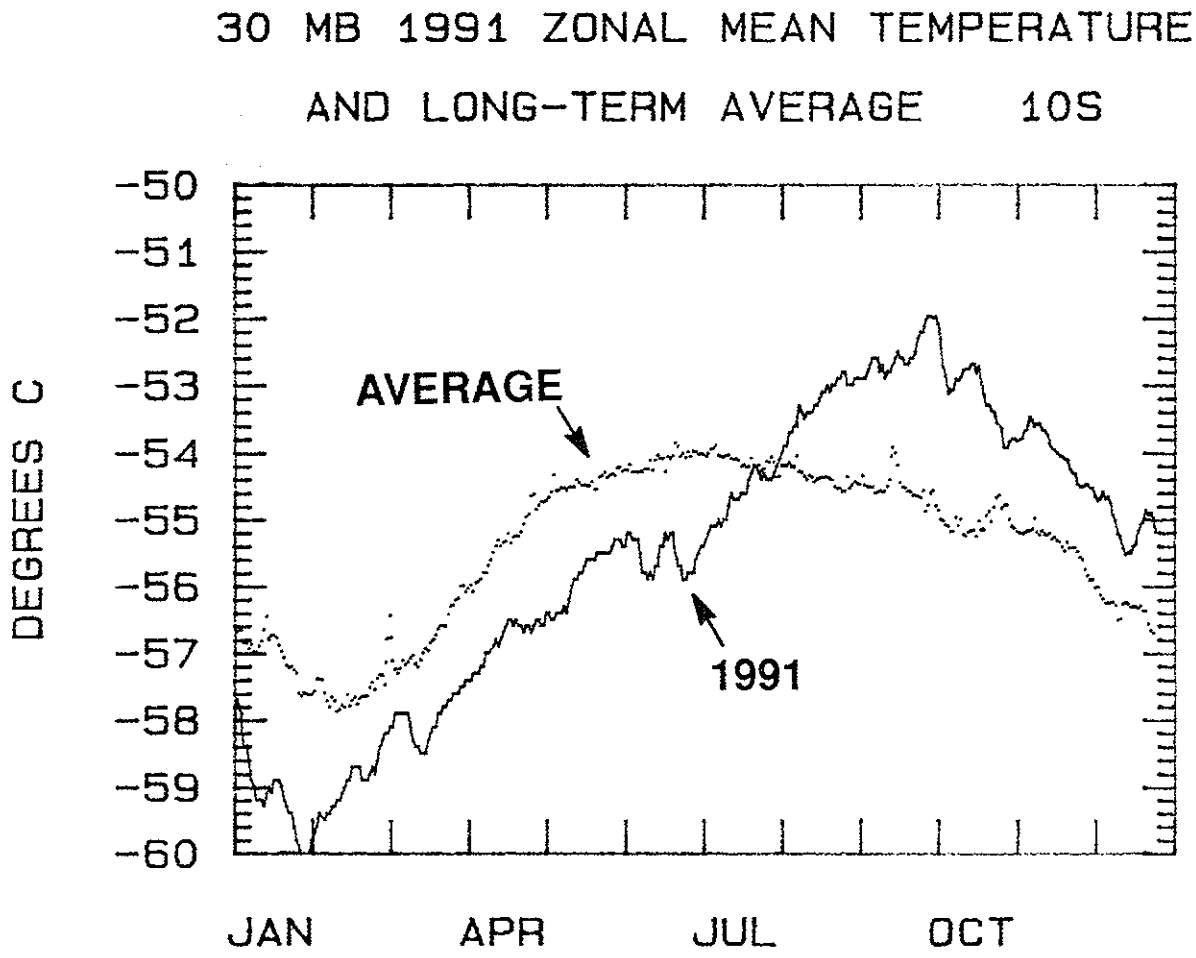

Fig. 40. Daily zonal average 10°S 30 mb (approx. 24 km) temperatures for 1991 (solid line) relative to the 1978-1991 average (dashed line).

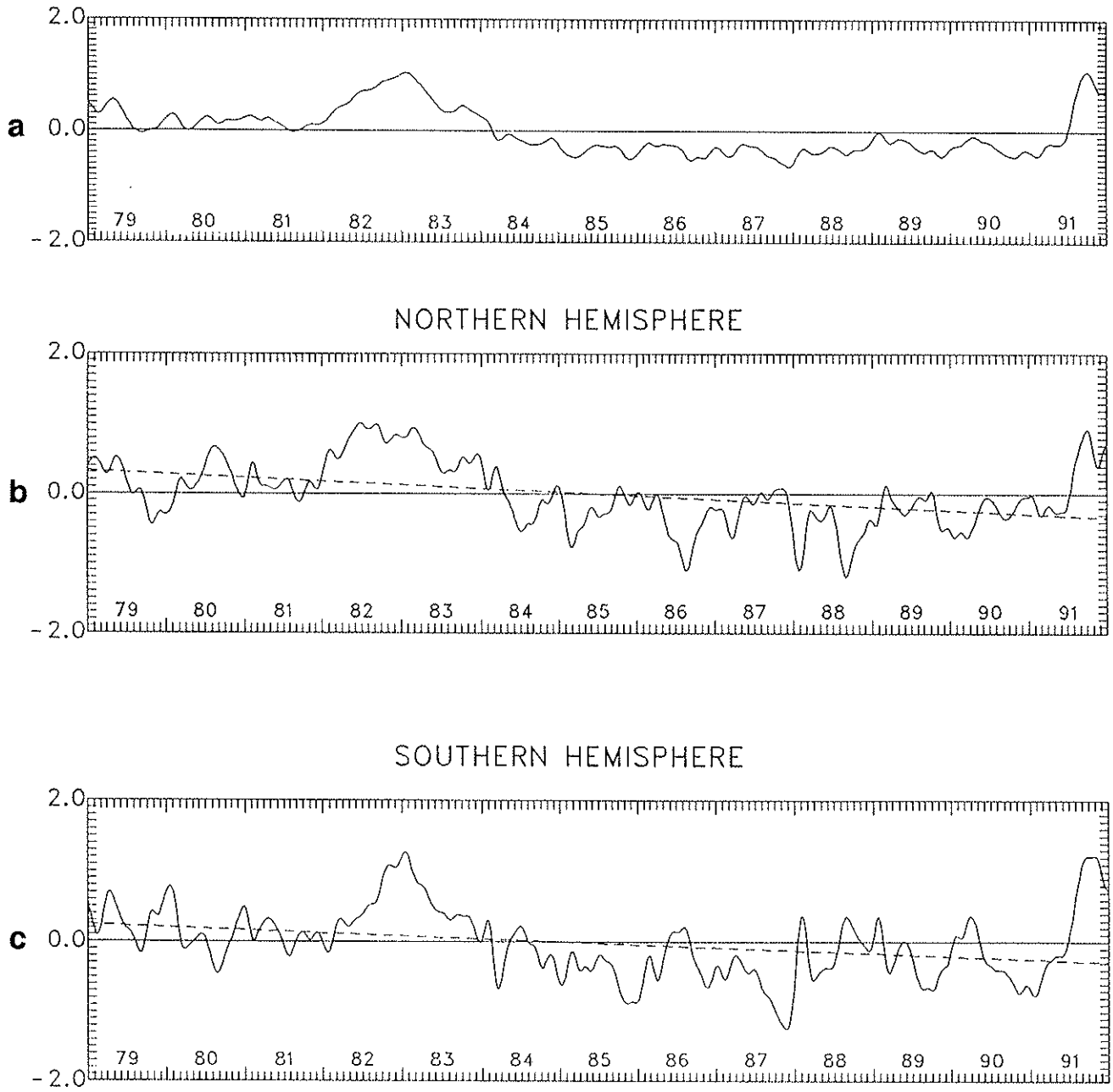

Fig. 41. Time series of a) global, b) Northern Hemisphere and c) Southern Hemisphere lower stratospheric temperature anomalies derived from satellite Microwave Sounding Unit (MSU) observations.

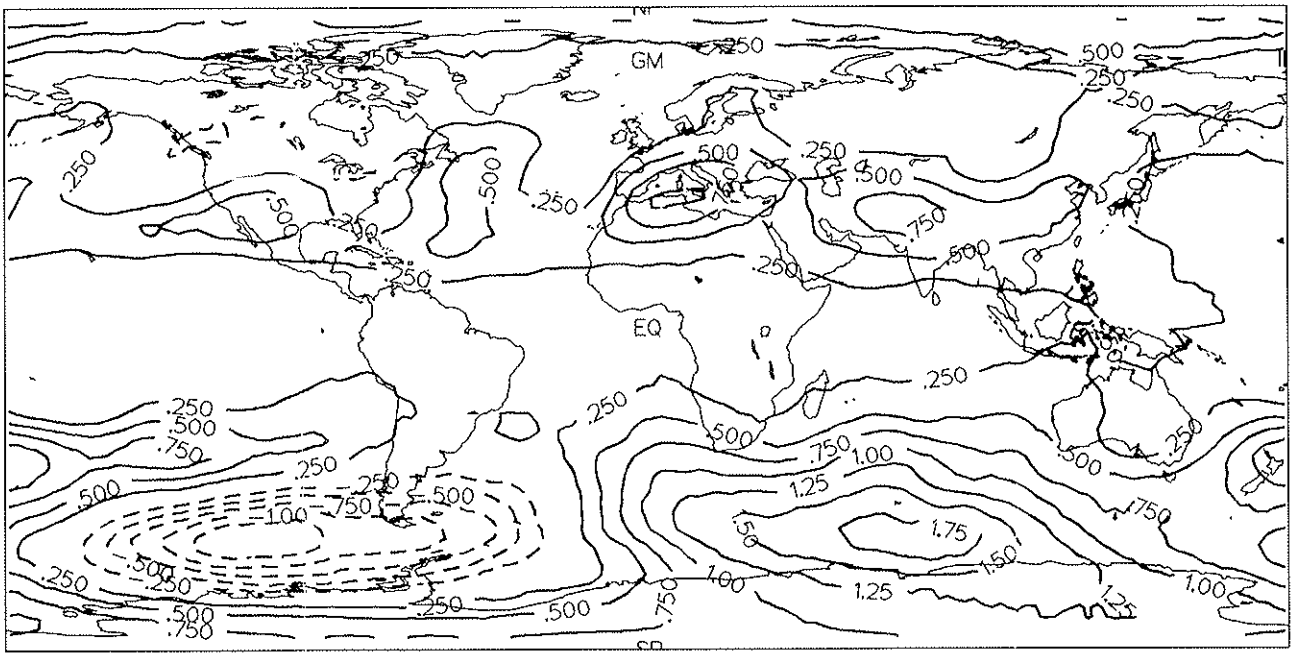

Fig. 42. Lower stratospheric temperature anomalies for 1991 computed from the 1979-1991 base period. Contour interval is 0.25°C, negative anomalies are dashed.

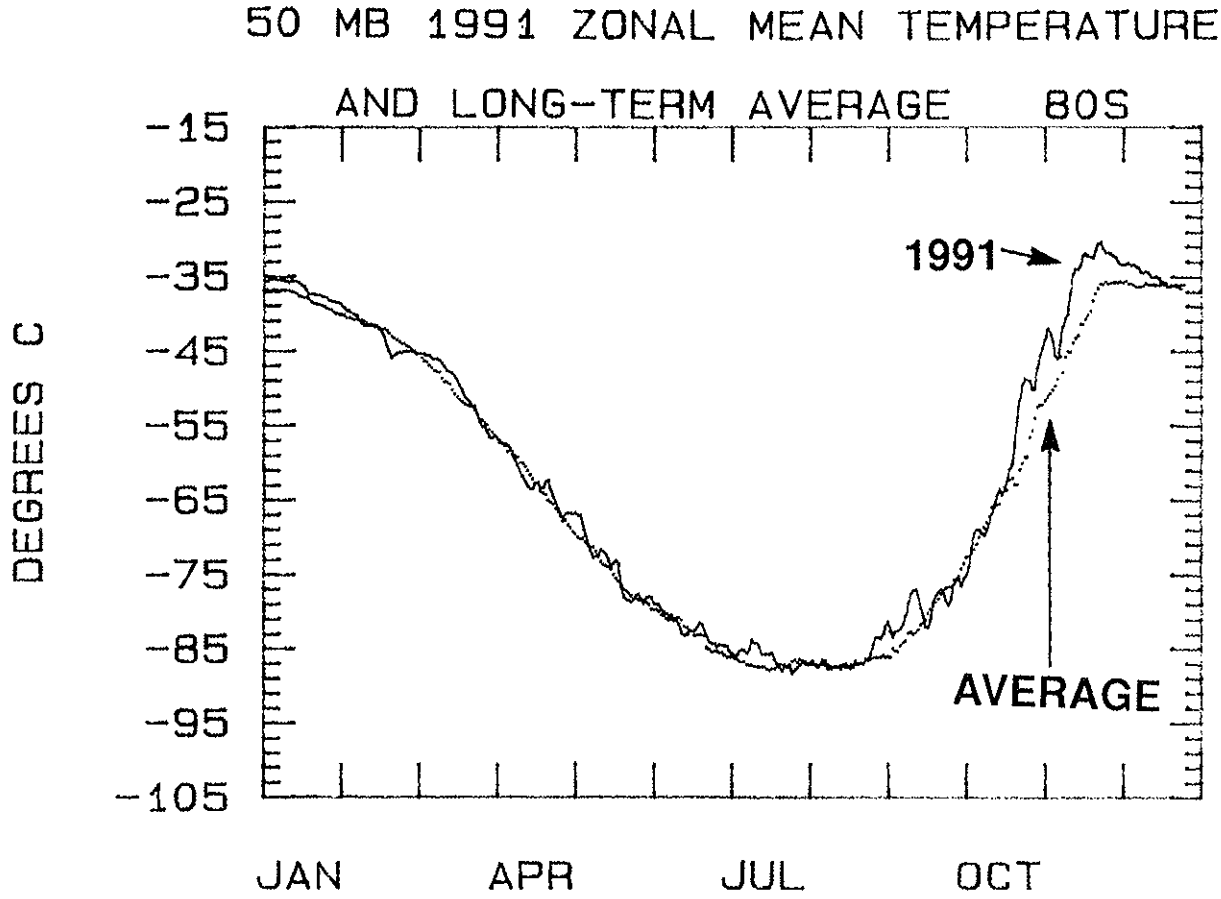

Fig. 43. Daily zonal average 80°S 50 mb (approx. 20 KM) temperatures for 1991 (solid line) relative to the 1978-1991 average (dashed line).

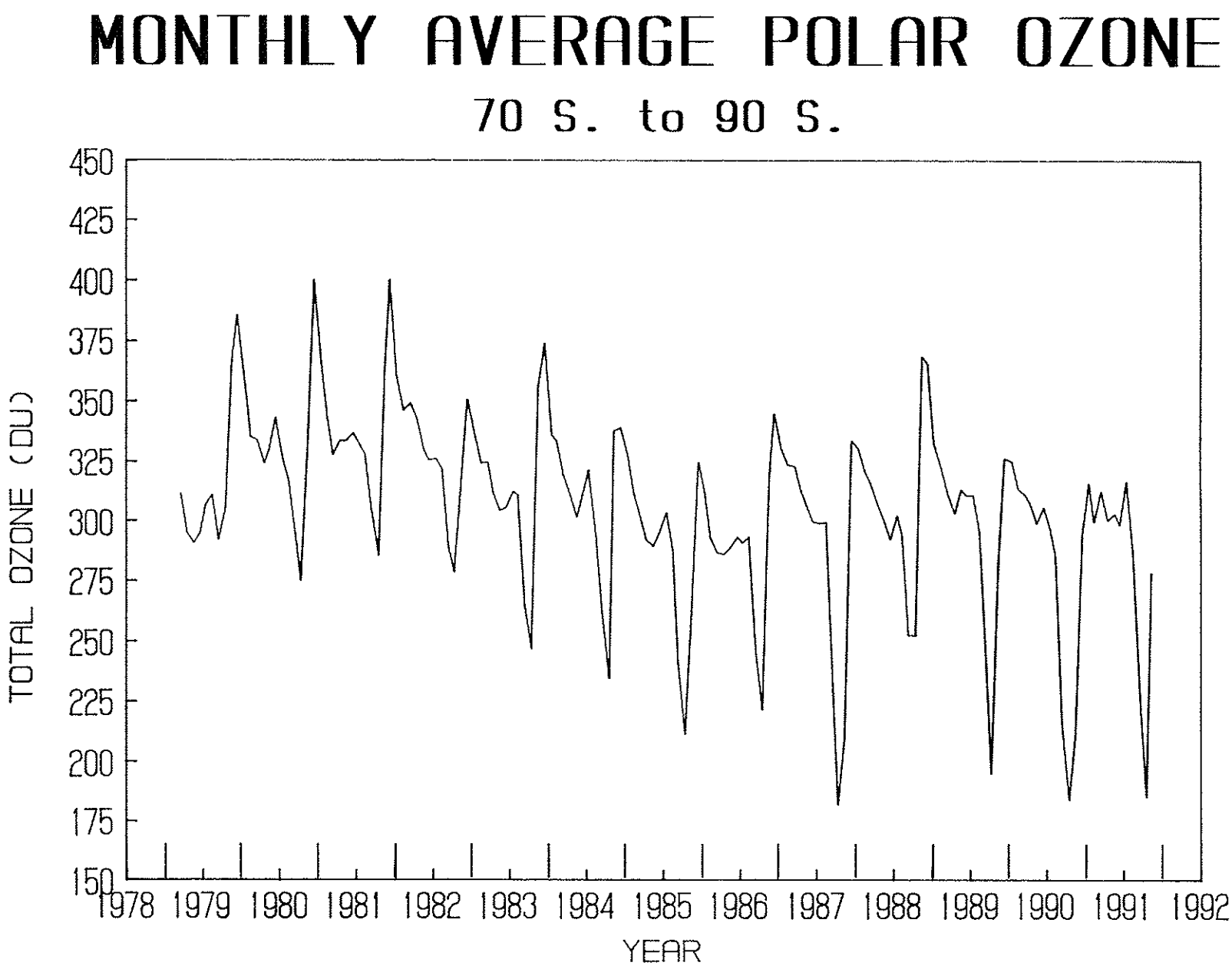

Fig. 44. TOVS monthly average total ozone, 70°S-90°S, from 1978 to 1991.

Aerosol Optical Thickness

NOAA/NESDIS has developed an aerosol optical thickness parameter from analysis of reflected solar radiation measurements from the Advanced Very High Resolution Radiometer on the NOAA Polar Orbiting Environmental Satellites (Rao, et al., 1989, Stowe, 1991). The intensity of the reflected radiation for cloud-free observations is converted into a measure of the amount of aerosol particles in a vertical column of the atmosphere, termed the aerosol optical thickness (AOT). This analysis is only done over ocean areas, as land area reflectivity is too large and variable to be used with the current retrieval algorithm. It is also limited to regions where the solar elevation angle is sufficiently large (greater than 20 degrees), and the satellite viewing angle is away from regions of direct solar reflection (specular reflection).

These observations are composited over a seven-day period, analyzed and contour plotted on charts. Monthly charts are available from July 1989. They typically have shown the occurrence of dust from the African, Saudi Arabian, and Asian deserts, smoke from forest fires and agricultural burning, and haze from industrialized regions, usually exhibited by AOT values in excess of 0.2. In the absence of these tropospheric events, values are typically below 0.1. However, with the eruption of the Mt. Pinatubo volcano in the Philippines on June 15, 1991, these charts have been dominated by an enhanced AOT signal caused by reflection from the stratospheric aerosol layer it generated (Stowe, et al. 1992).

This past year's record of aerosol information, including the evolution of the Mt. Pinatubo and Mt. Hudson volcanic aerosol layers, is detailed in **Figs. 45-48.** Prior to the eruption, **Fig. 45** (January through March) shows AOT values generally below 0.1, with the exception of the tropical Atlantic Ocean. AOT values progressively increase from January to March 1991 in the Western tropical and mid-latitude northern Pacific Ocean. These regions of elevated tropospheric aerosol particle concentrations have been ascribed to wind-blown dust from the Saharan and Gobi deserts, respectively.

High levels of tropospheric aerosol continued to be associated with wind-blown dust for the April through June 1991 period (**Fig. 46**), but to a somewhat larger extent from the Saharan desert, while diminishing from the Gobi desert. AOT increases above the 0.1 level in the eastern mid-latitude and tropical North Pacific Ocean are possibly associated with dust from either Asia or Africa. The effects of smoke from agricultural burning are evident around Central America. In June, there is some indication of elevated AOT values off the East Coast of the U. S., the result of increased haze from industrial and automobile emissions in stagnant summertime air-masses. Even though the Mt. Pinatubo eruption occurred in mid-June, the only evidence of anomalous aerosol content from it is

in the region north and west of the Philippines, but this change would be hard to diagnose without prior knowledge of the eruption.

However, the map for July (**Fig. 47**) clearly shows an increased backscatter throughout the tropics from about 18°S to 25°N from the stratospheric aerosol layer produced by this eruption. AOT values are well in excess of 0.2 through much of this region. The effects of the volcanic aerosols are less evident in regions already impacted by high concentrations of tropospheric aerosols.

The August chart shows the Mt. Pinatubo layer expanding north and south, from about 20S to 30N, with some patches at higher latitudes which may be associated with dispersion of aerosol from the tropics, but also may be the result of local sources of tropospheric aerosol.

The chart for September shows the tropical stratospheric layer in about the same location, with slightly lower AOT values possibly indicative of dispersion. Most notable is the increase in AOT in the southern extratropics. This is probably the result of changes in stratospheric wind circulation concomitant with the change in seasons, transporting the Mt. Pinatubo aerosol to higher latitudes. However, it is also partially the result of added aerosol particles from the mid-August eruption of the Mt. Hudson volcano in Chile. The patches of elevated levels in the mid northern Pacific and Atlantic Oceans may also be related to Mt. Pinatubo. Other more sensitive satellite and aircraft measurements have indicated that the aerosol was distributed globally by the end of August, but at levels below an AOT of 0.1, the smallest level detectable from these charts.

Figure 48 shows the continuing dispersion of the tropical aerosol layer from Mt. Pinatubo and the formation of a secondary band of elevated AOT circling the Antarctic Continent between 40°S and 60°S. This latter band, made up of aerosol from both Mt. Pinatubo and Mt. Hudson, has an area integrated aerosol optical depth (proportional to aerosol total mass) that is about a tenth the size of the Mt. Pinatubo tropical band at its peak. The aerosol particles from the tropical band of Pinatubo did not disperse into the Northern Hemisphere as effectively as they have in the Southern Hemisphere. Thus, the Pinatubo eruption appears to have a different character from the El Chichon eruption of 1982, where much of the aerosol was distributed throughout the Northern Hemisphere by December of that year. This difference may be related to the fact that most of the El Chichon aerosol was confined to a latitude band between 5°N and 25°N several months after its eruption, while the Pinatubo aerosol layer covered a much larger latitude band, and had its highest concentrations just south of the equator.

Monthly zonal mean values of AOT in the band 30°N-20°S are illustrated in **Fig. 49** for the period June 27 through December

1991. Measurements in the 40°S-60°S band are unavailable for June - August due to insufficient solar illumination. The tropical Pacific band shows a rapid rise in AOT from June to August followed by a continuous decline. The 40°S-60°S band shows some indication of decreasing AOT in December. In pre-eruption conditions, AOTs in both bands had typical values of less than 0.07.

It is estimated that Mt. Pinatubo generated stratospheric AOT values about 1.6 to 1.8 times larger than those from El Chichon for the 20°S - 30°N latitude band. This ratio was computed from nearly identical analyses of the error in AVHRR derived sea surface temperature (DSST) caused by aerosols from the two eruptions. The time series of monthly zonal mean AOT in the stratosphere (tropospheric back-ground AOT removed) for the two volcanoes, starting with the month prior to each eruption and ending with December are compared in **Fig. 50**. Two reflectance derived estimates (curves C and D) are included for comparison. The magnitude of Pinatubo's AOT relative to El Chichon's is clearly seen. The time series suggests that the thinning of the AOT began in September for each eruption. This further suggests similar changes in stratospheric wind circulation in September of both years (1982 and 1991), prompting the dissipation of the tropical layer.

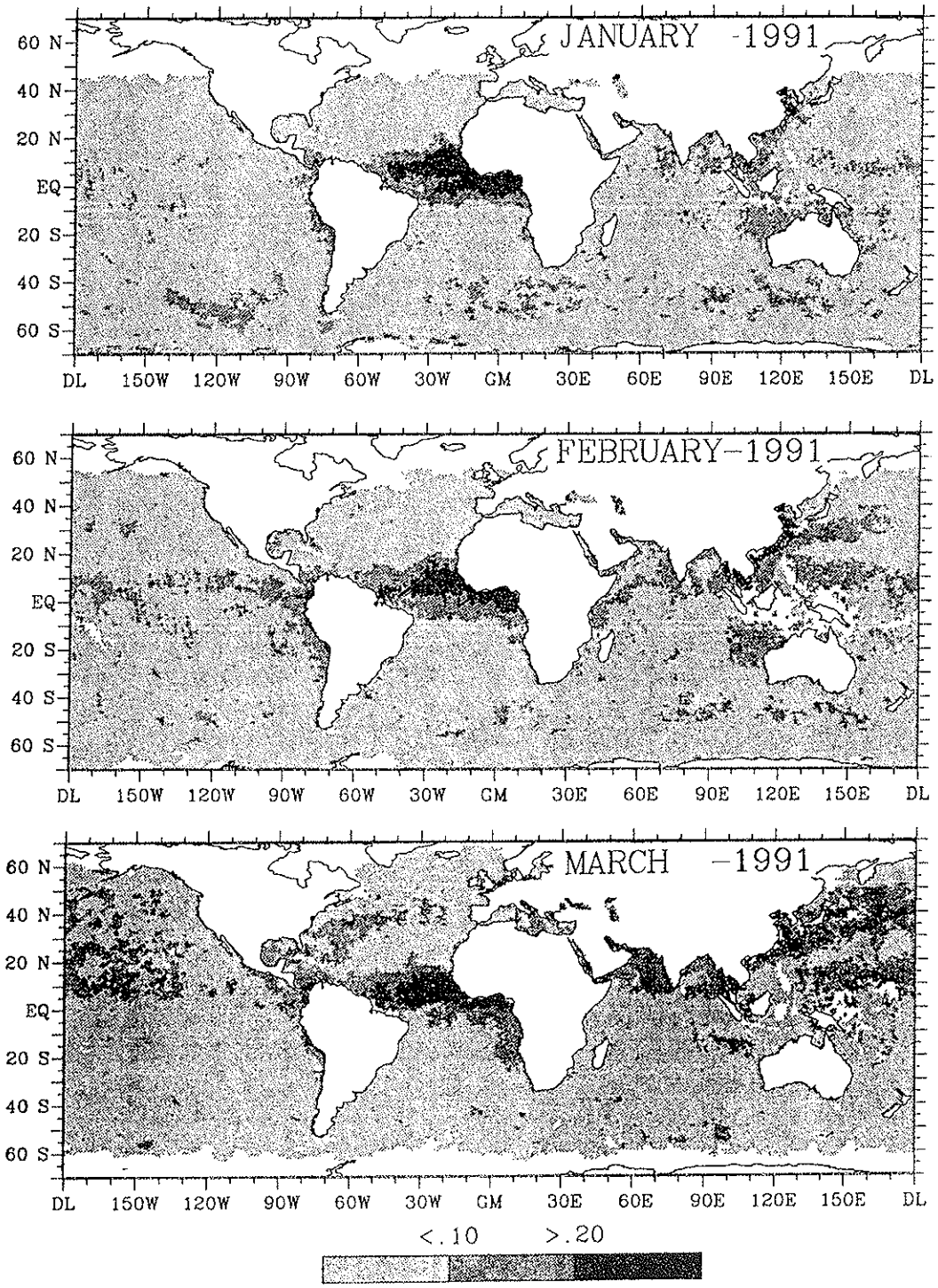

Fig. 45. Monthly mean aerosol optical thickness at a wavelength of 0.5 micrometers as derived from the AVHRR instrument on the NOAA-11 satellite for January through March of 1991. White represents no measurements possible, either due to poor solar illumination, persistent cloud cover, or land areas.

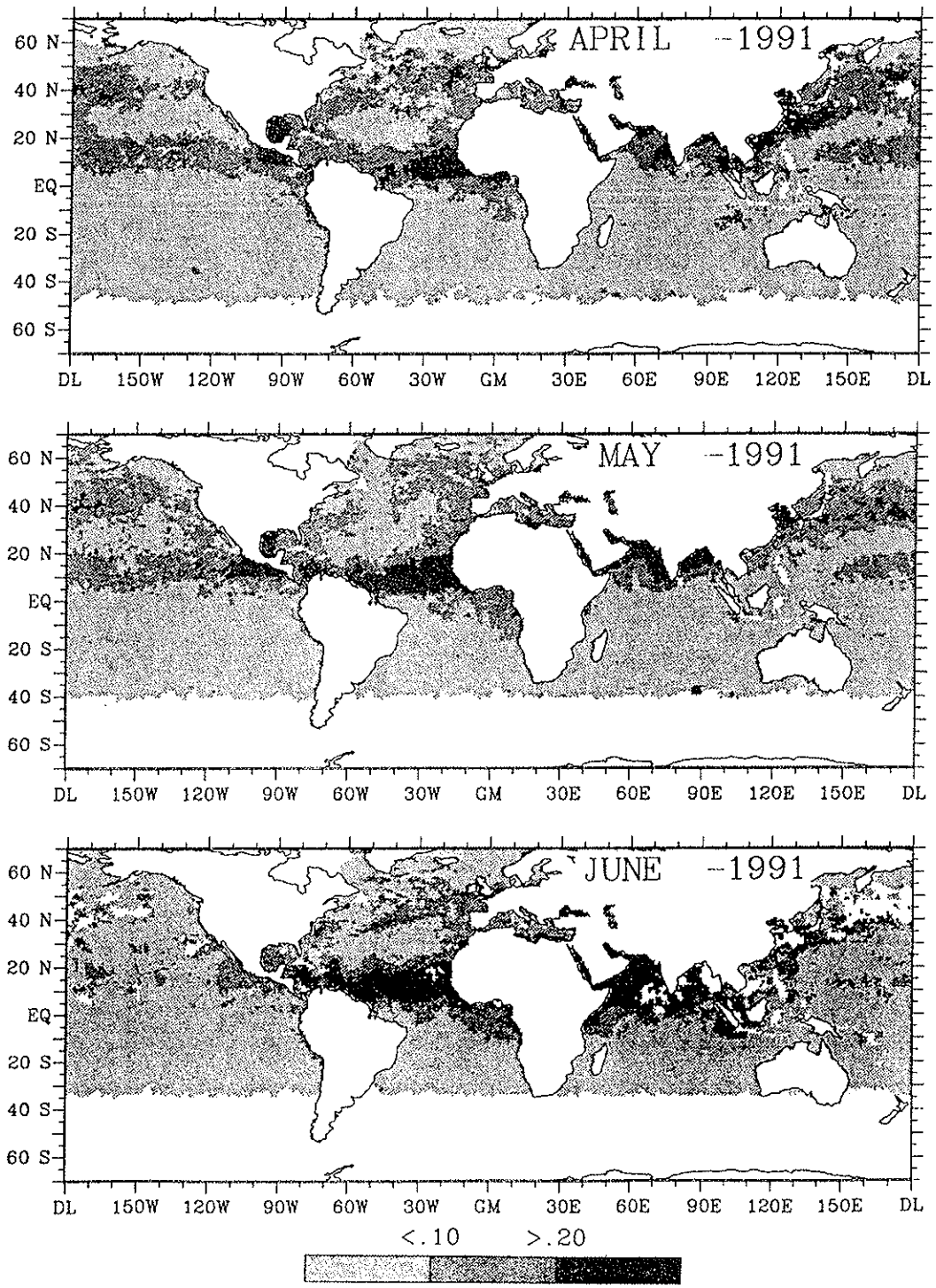

Fig. 46. Monthly mean aerosol optical thickness at a wavelength of 0.5 micrometers as derived from the AVHRR instrument on the NOAA-11 satellite for April through June of 1991. White represents no measurements possible, either due to poor solar illumination, persistent cloud cover, or land areas.

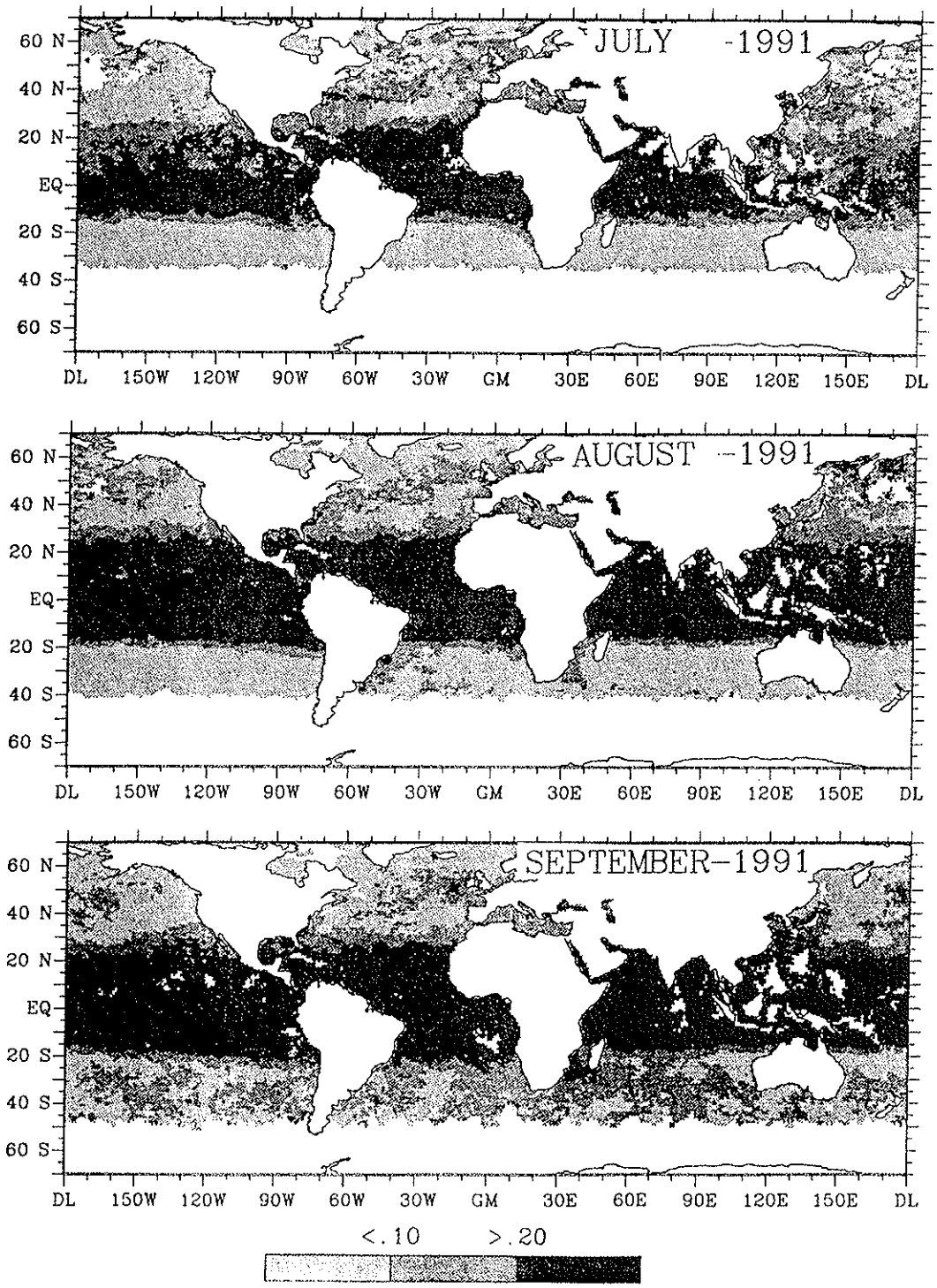

Fig. 47. Monthly mean aerosol optical thickness at a wavelength of 0.5 micrometers as derived from the AVHRR instrument on the NOAA-11 satellite for July through September of 1991. White represents no measurements possible, either due to poor solar illumination, persistent cloud cover, or land areas.

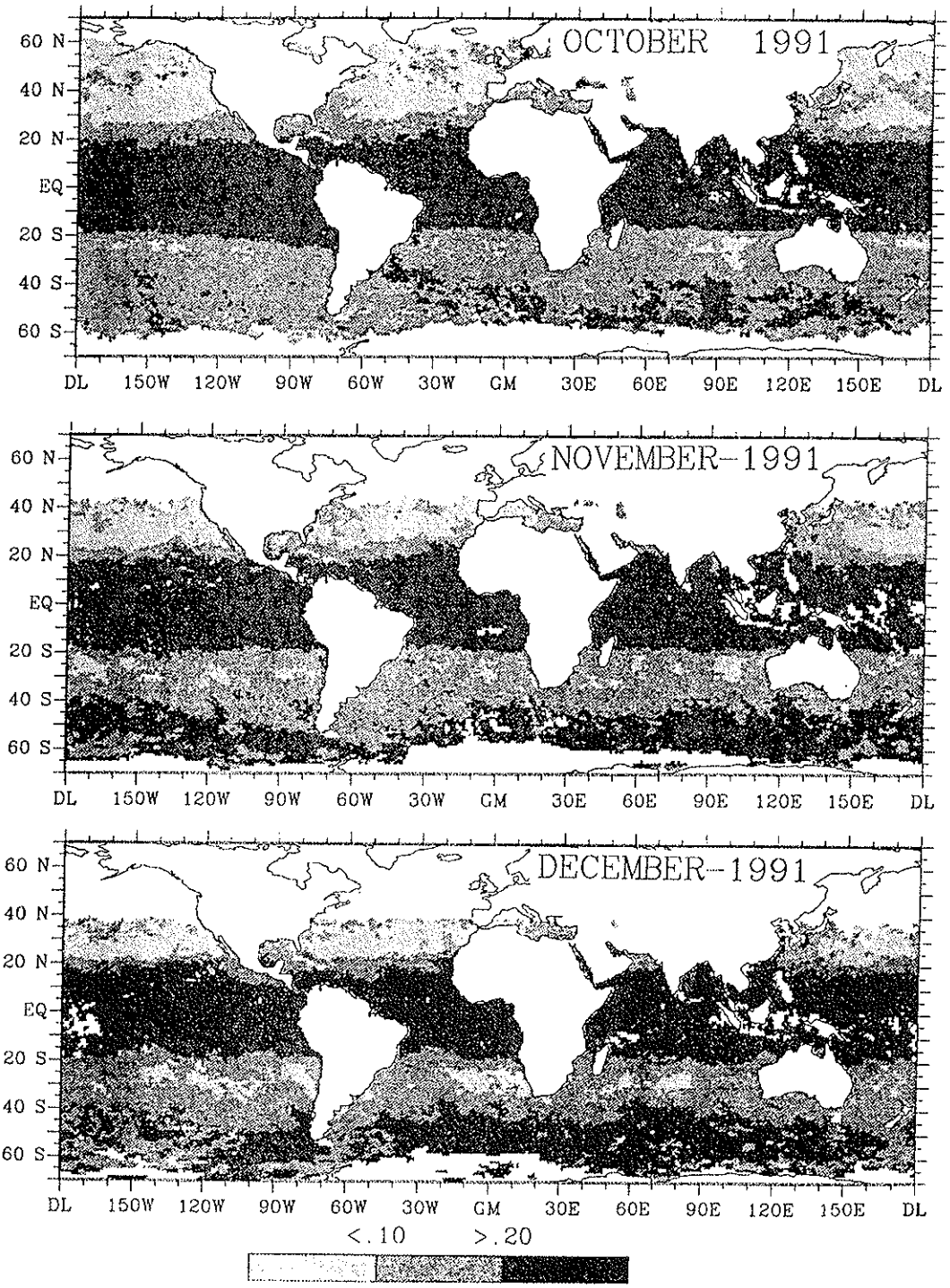

Fig. 48. Monthly mean aerosol optical thickness at a wavelength of 0.5 micrometers as derived from the AVHRR instrument on the NOAA-11 satellite for October through December of 1991. White represents no measurements possible, either due to poor solar illumination, persistent cloud cover, or land areas.

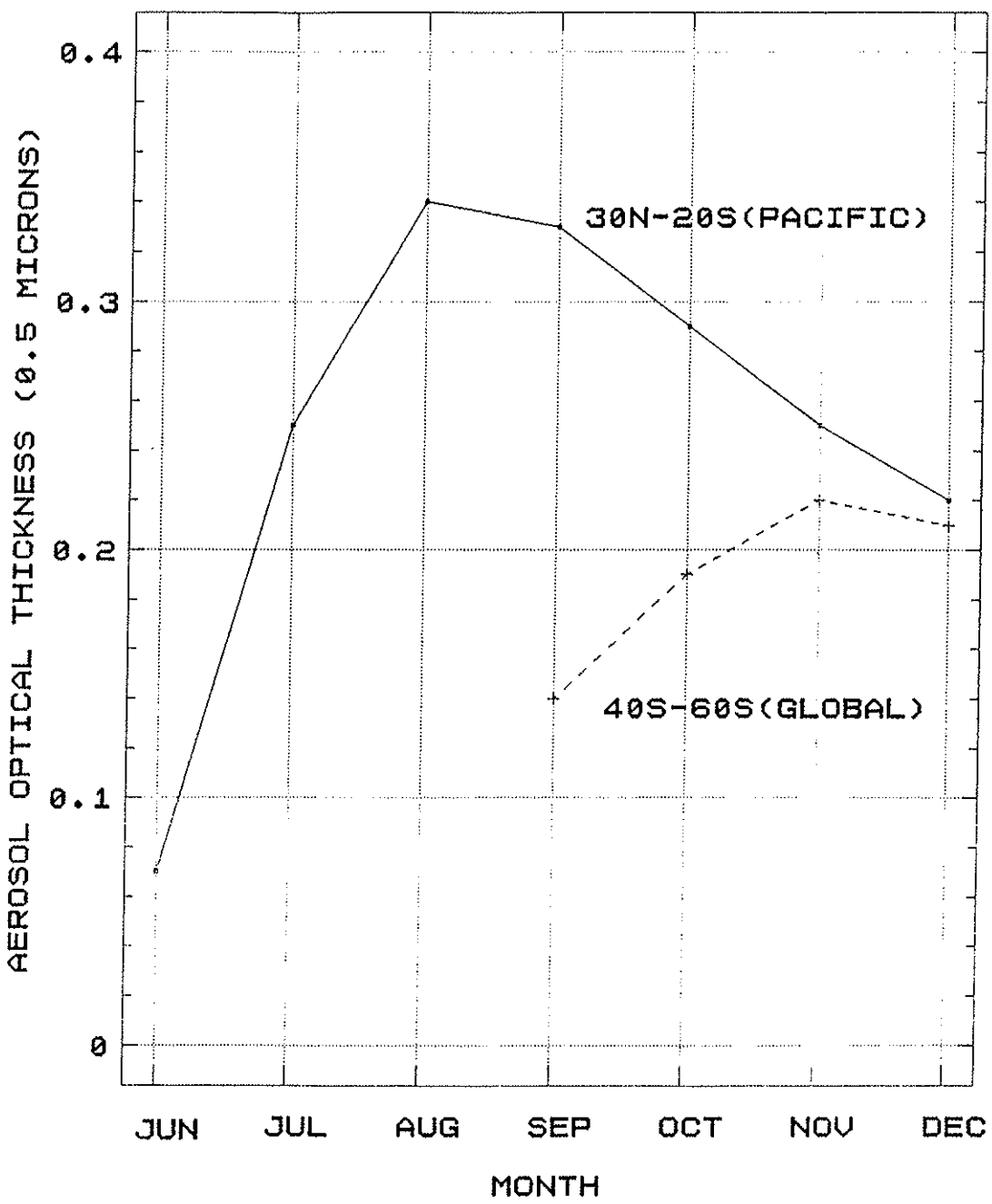

Fig. 49. Total monthly mean aerosol optical thickness as function of month for two latitude bands, one confined to the Pacific Ocean between 20°S and 30°N containing the Mt. Pinatubo aerosol layer, and another from 40°S to 60°S, containing both Mt. Pinatubo and Mt. Hudson aerosol.

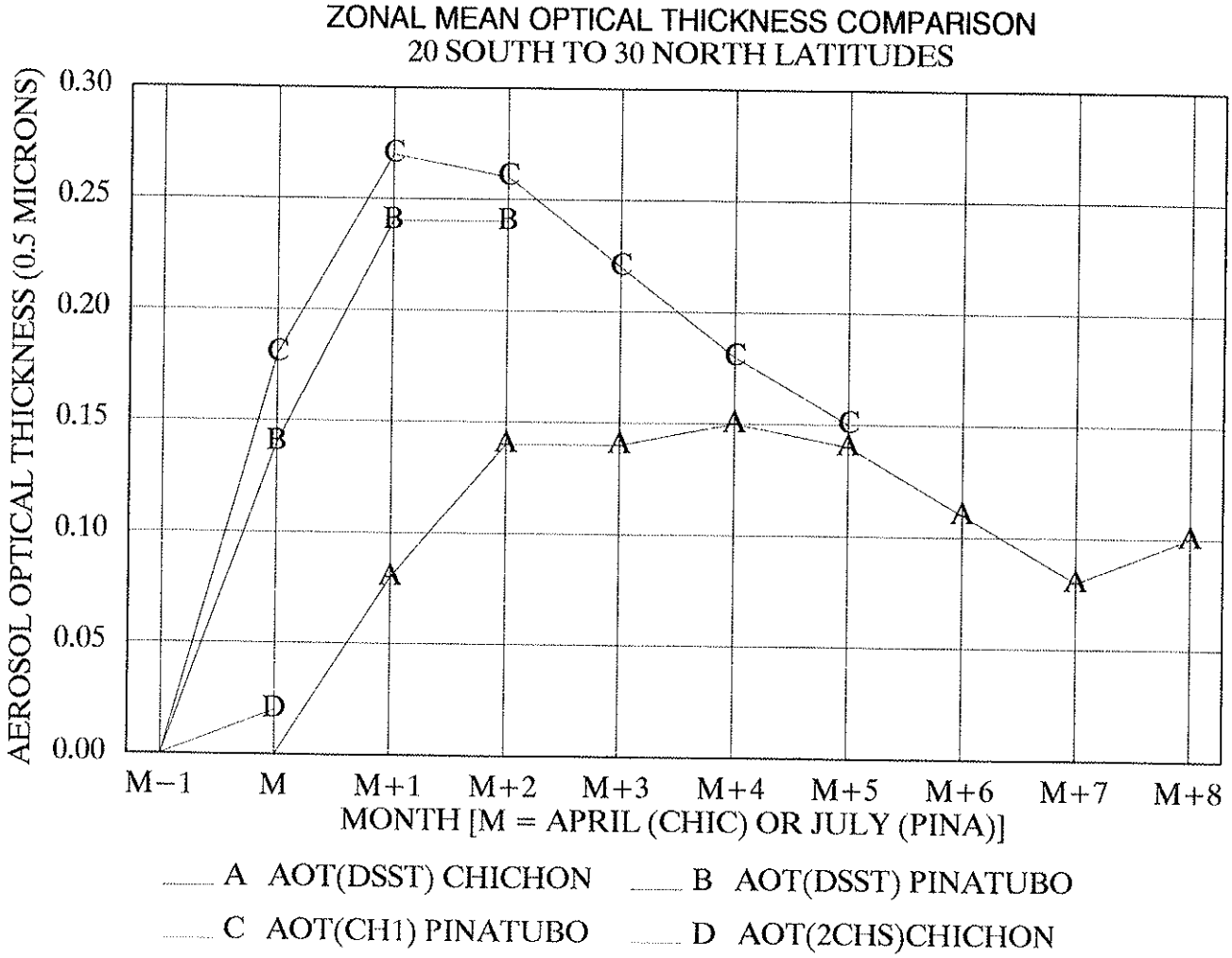

Fig. 50. Monthly mean stratospheric aerosol optical thickness (tropospheric mean of 0.07 removed) as a function of month for the latitude band 20°S to 30°N after El Chichon and Mt. Pinatubo. Curves A and B were derived from sea surface temperature error analyses, and curves C and D from reflected radiation retrieval algorithms.

Atmospheric Blocking

The most prominent anomalous circulation pattern in the middle latitudes during 1991 occurred between April and June over the south-central South Pacific Ocean (**Figs. 51-53**). Individual monthly mean 500 mb heights and anomalies for the period April-June 1991 (**Fig. 51**) show a meridional dipole of persistent height anomalies over the central and eastern South Pacific, flanked by persistent negative anomalies both upstream over New Zealand and downstream over the Scotia and Weddell Sea's. The wave pattern over the South Pacific intensified during May (**Figs. 51c,d**) and June (**Figs. 51e,f**), with strong flow diffluence observed throughout the central South Pacific during the entire period.

The three-month mean height anomaly pattern during this period exhibits marked asymmetries, with strong mean diffluence and maximum meridional flow speeds located upstream of the block. The implication is that much of the flow structure immediately upstream of the mean block position was strongly associated with intermonthly time scale variability (periods greater than 30 days) in this case. Moreover, both the structure and evolution of the blocking episode was strongly coupled with intermonthly fluctuations. The contribution from intermonthly fluctuations to the observed positive height anomaly over the mean block position at the time of maximum block intensity, for example, was greater than 75% (**Figs. 52a,b**). The primary contribution to the overall blocking episode apparently came from persistent positive planetary scale (total wave numbers 0-6) height anomalies (**Fig. 53**) that dominated the region throughout the period.

On the intra-monthly time scales, five well-defined periodic fluctuations in amplitude, corresponding to individual blocking events, are evident (**Fig. 53**). These blocking events were generally associated with large modulations in both the planetary scale and subplanetary scale (total wave numbers 7-12) flow.

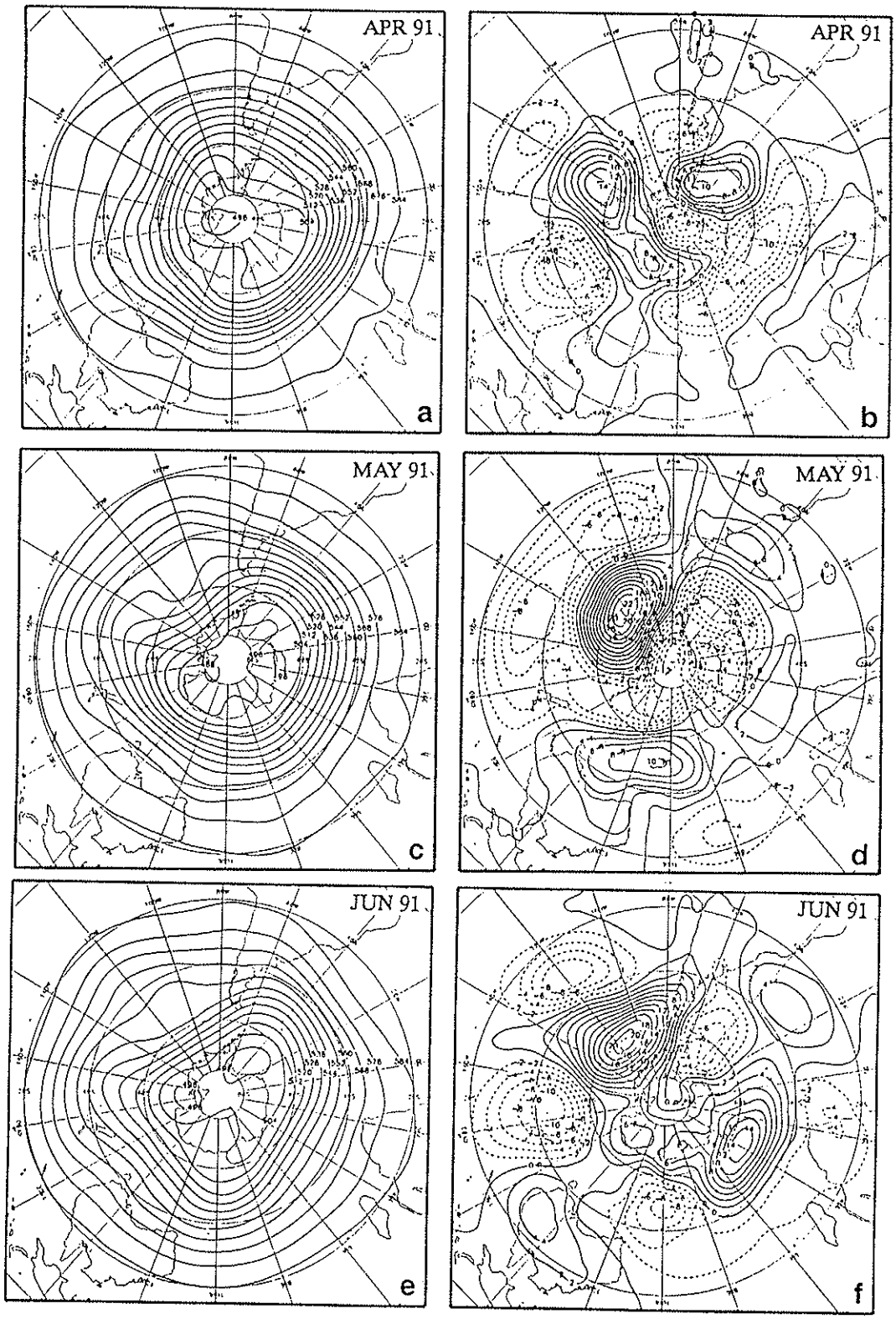

Fig. 51. Monthly mean 500 mb heights (interval is 80 m) and anomalies (interval is 20 m) for (a,b) April 1991, (c,d) May 1991 and (e,f) June 1991, respectively.

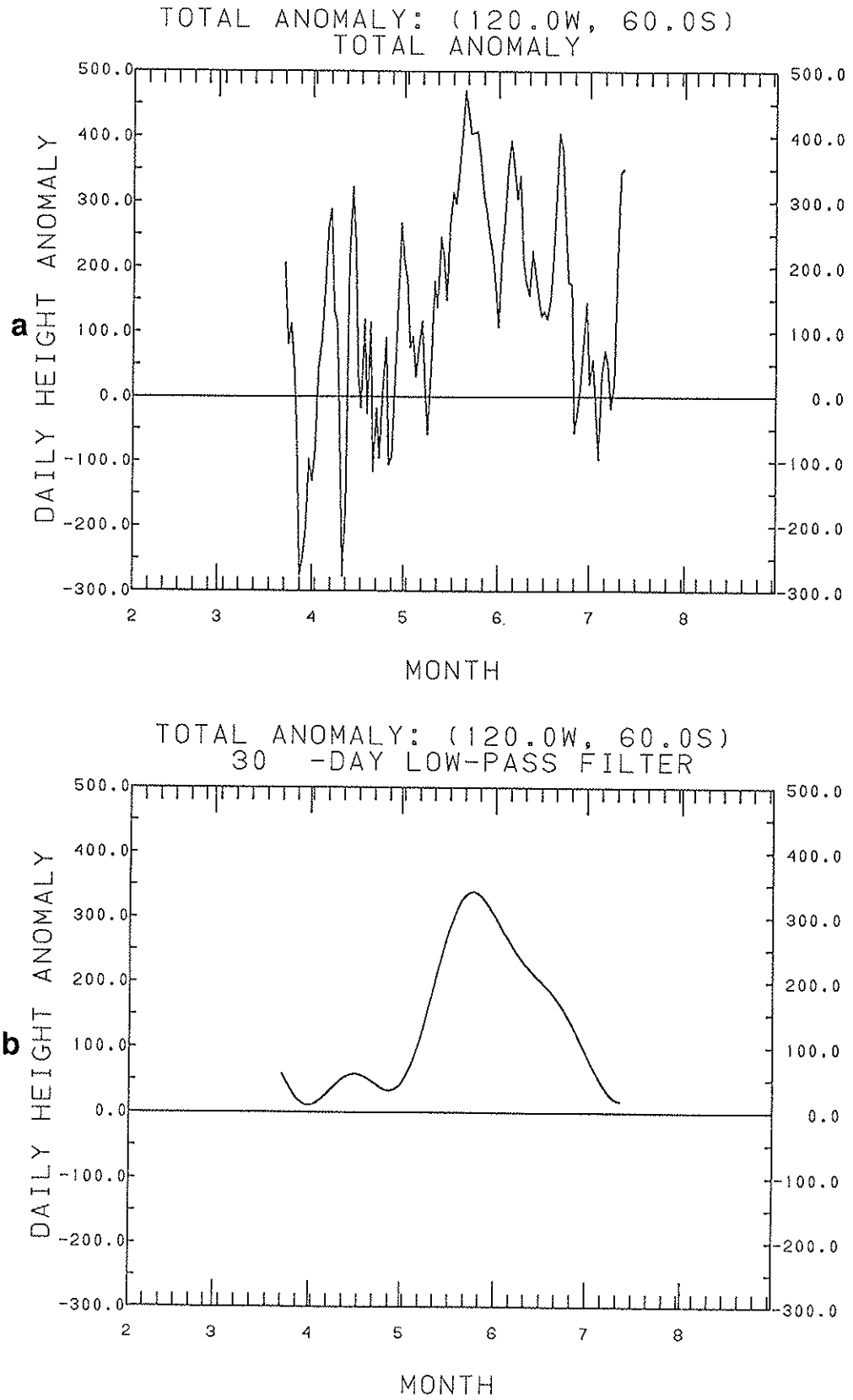

Fig. 52. Time series of daily (a) total height anomalies and (b) intermonthly (periods greater than 30 days) height anomalies during April-June 1991. Units of anomalies are meters.

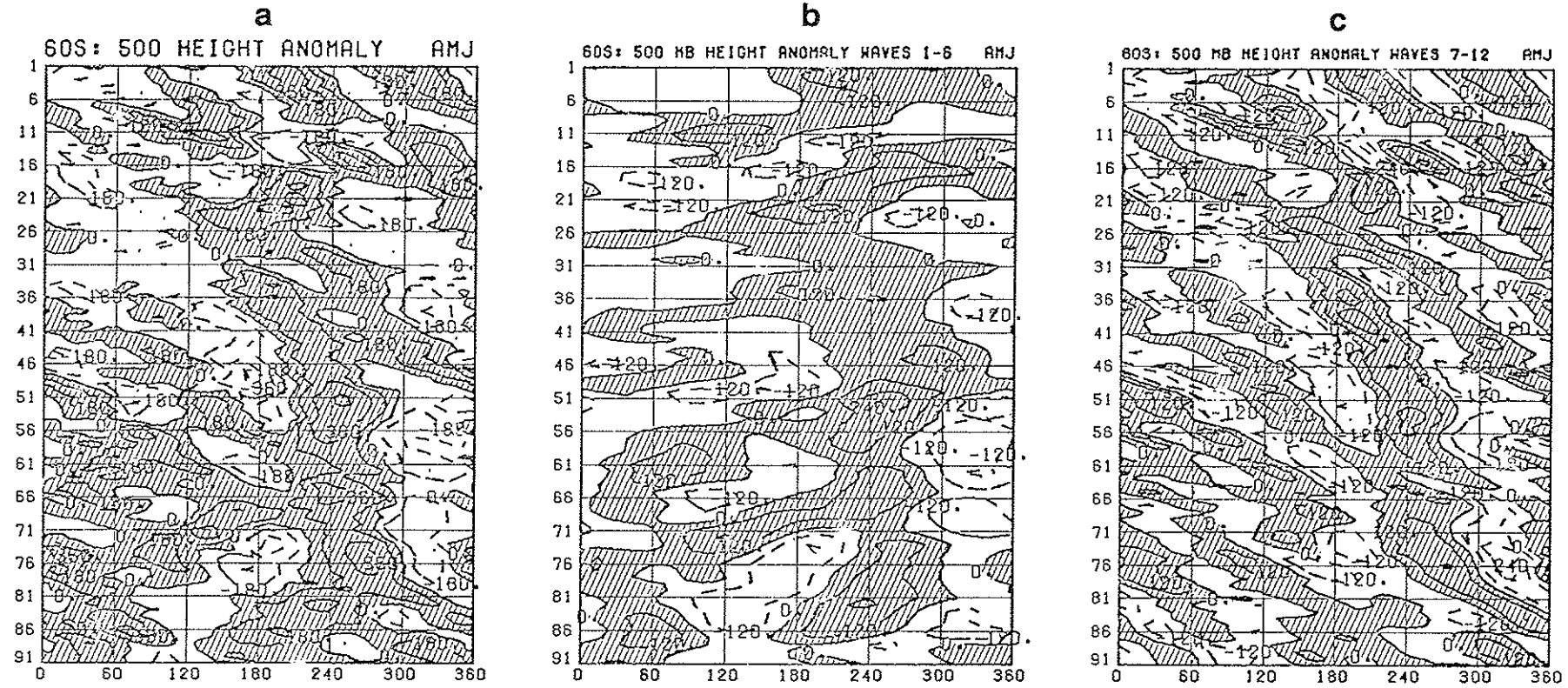

Fig. 53. Time longitude section at 60°S of daily 500 mb height anomalies for the period April - June 1991. Panel (a) shows the full height anomaly field (interval is 180 m). Panel (b) shows the planetary scale (two-dimensional wavenumbers 1-6) height anomaly field and panel (c) shows the sub-planetary scale (two-dimensional wavenumbers 7-12) height anomaly field. Contour interval in panels (b) and (c) is 120 m. Anomalies are computed with respect to the 1979-1988 base period. Wave groups are identical to those specified by Blackmon (1976). Positive height anomalies are shaded in all panels.

MAJOR CLIMATE ANOMALIES

MAJOR CLIMATIC EVENTS AND ANOMALIES AROUND THE WORLD DURING 1991

1. California:

HEAVY MARCH RAINS FOLLOW A FIFTH CONSECUTIVE DRY WINTER.

The southern Pacific Coast experienced a fifth consecutive subnormal rainy season during late 1990 and early 1991. January and February brought exceptionally low precipitation totals before the "March Miracle," when California observed its heaviest precipitation in five years. Parts of the northern Sierra Nevadas measured over 1000 mm of precipitation during the month, and much of the southern and west-central sections of the state received enough rain to eliminate moisture shortages that had accumulated during the previous five months. This precipitation brought significant relief to the region, but was not nearly enough to counteract five years of drought as the state's streamflow levels and reservoir storages improved from "desperate" to "critically low", according to the Western Regional Climate Center. Unfortunately, the 1991-92 rainy season started slowly, with sizable moisture shortages accumulating during October - December. Both short and long-term dryness were blamed for a series of destructive wildfires that scorched the Oakland vicinity in October and for a freakish dust storm in November that reduced visibilities to near zero along route I-5 near Coalinga, CA, causing a chain-reaction 104-vehicle pileup that took 17 lives and injured over 150 individuals, according to press reports.

2. Texas

HEAVY DECEMBER RAINS GENERATE WIDESPREAD, SEVERE FLOODING.

Torrential downpours deluged much of central Texas around mid-December and combined with above normal totals during the rest of the month to generate some of the century's worst flooding along the Guadalupe, Trinity, Brazos, and Colorado Rivers. Weekly totals of 200-415 mm fell from Austin southward to San Antonio, and many locations in central and eastern Texas received nearly half the normal annual rainfall in less than a week. According to the National Climatic Data Center, precipitation averaged across Texas during December 1991 was greater than during any previous December since records began in 1895 despite near to below normal amounts in southern and western parts of the state.

3. Northern and Eastern Australia:

WET EARLY IN THE YEAR, THEN VERY DRY.

Cyclone Joy set the stage for almost two months of excessively heavy rain in northern Australia, which finally ended in early March. By late March, however, moisture deficits were widespread as the Australian wet season came to a premature end. In September, the approach of spring failed to bring the typical increase in rain as sizable moisture deficits expanded across most of eastern Australia. A brief respite in early November failed to eliminate moisture deficits, but heavy rains soaked the northern areas in late November. Moderate rains during December ended the short-term moisture deficits, but he rainy season as a whole remained abnormally dry. The slow start to the 1991-92 wet season correlates well with the typical low-index (warm) El-Nino Southern Oscillation (ENSO) precipitation signal in the region.

4. Europe and the Middle East:

DRY WINTER, WET SPRING.

Short-term dryness was widespread across eastern Europe and the Middle East as the year began. Bitterly cold air invaded the continent during late January and early February as heavy snow blanketed many areas. When the cold snap eased, however, precipitation deficits remained. In early March, beneficial rains had commenced, diminishing the dry spell. Late season rains drenched the Middle East and southeastern Europe throughout April and May, then drier, more typical weather returned in June.

5. Southern Africa:

SHORT BUT VERY WET RAINY SEASON.

Rainfall surpluses followed a slow start to the rainy season as exceptionally heavy rains commenced in late January. High temperatures and dry weather temporarily ended the wet spell in March, but the unusually moist conditions were re-established at the end of the month. Very dry weather in April signaled the abrupt, premature end of a short but wet 1990-91 rainy season.

6. Indonesia and Malaysia:

DRYNESS ENGENDERS LARGE WILDFIRES.

Exceptionally dry conditions commenced during the late Spring across Indonesia and persisted into October, creating ideal conditions for extensive wildfires in the western half of the country. Spotty rains in late October and most of November provided limited relief, and more general moderate to heavy rainfall alleviated the dryness by the middle of December. This anomaly pattern is consistent with the typical low-index (warm) ENSO response in the region.

7. Europe, Northern Africa, and the Western Middle East:

COLD WAVE BLASTS REGION.

A late April cold wave invaded much of Europe after unusual March warmth and caused considerable crop damage. Cold and damp weather throughout May hampered the growth of surviving crops. The widespread chill shifted southeastward during June and more seasonable temperatures failed to return until the end of the month. The same southeastern areas were again afflicted by cold and wet weather in December.

8. Alaska, Northwestern Canada, and Eastern Siberia:

LATE SPRING AND EARLY SUMMER HEAT WAVE.

Mild weather engulfed northern Alaska and northwestern Canada during May. The mild and dry weather promoted wildfires in Alaska. After a brief spell of chilly weather in June, hot weather resumed and spread across all of northwestern North America and well into eastern Siberia. Cooler air moved into Alaska by mid-July, and ended the heat wave by spreading into eastern Siberia.

9. Central Mexico:

WIDESPREAD FLOODING FROM HEAVY RAINS.

Soaking rains in late June and most of July plagued the region, and extensive flooding was reported. Near normal conditions returned during August.

10. New Zealand:

PROLONGED WETNESS OBSERVED.

Very heavy precipitation drenched much of New Zealand from late July to early September. Drier conditions returned as September progressed.

11. Bangladesh:

SEVERE CYCLONE DECIMATES REGION.

In late April, a devastating, intense cyclone swept across the country as waves of six meters in height were whipped up by 270 kph winds, taking over 139,000 lives according to reports. Sporadic heavy rains throughout May hampered rescue and recovery operations.

12. Sri Lanka and Southern India:

TROPICAL CYCLONE 4B FOLLOWS A WET MONSOON SEASON.

A strong 1991 monsoon season was observed as heavy rains inundated Sri Lanka and much of southwestern India. Deluging rains brought widespread flooding and landslides in mid-June, and above normal totals continued to plague the region throughout July which eventually spread into northwestern and central India where widespread heavy rains had been lacking. Following the wet monsoon season, Tropical Cyclone 4B, packing winds over 100 kph, dumped as much as 580 mm of rain on parts of Sri Lanka and southern India in mid-November. Several weeks of wet weather before and after the system's landfall brought rainfall totals during late October through early December to over 700 mm at some locations.

SIGNIFICANT GLOBAL CLIMATE ANOMALIES DURING 1991

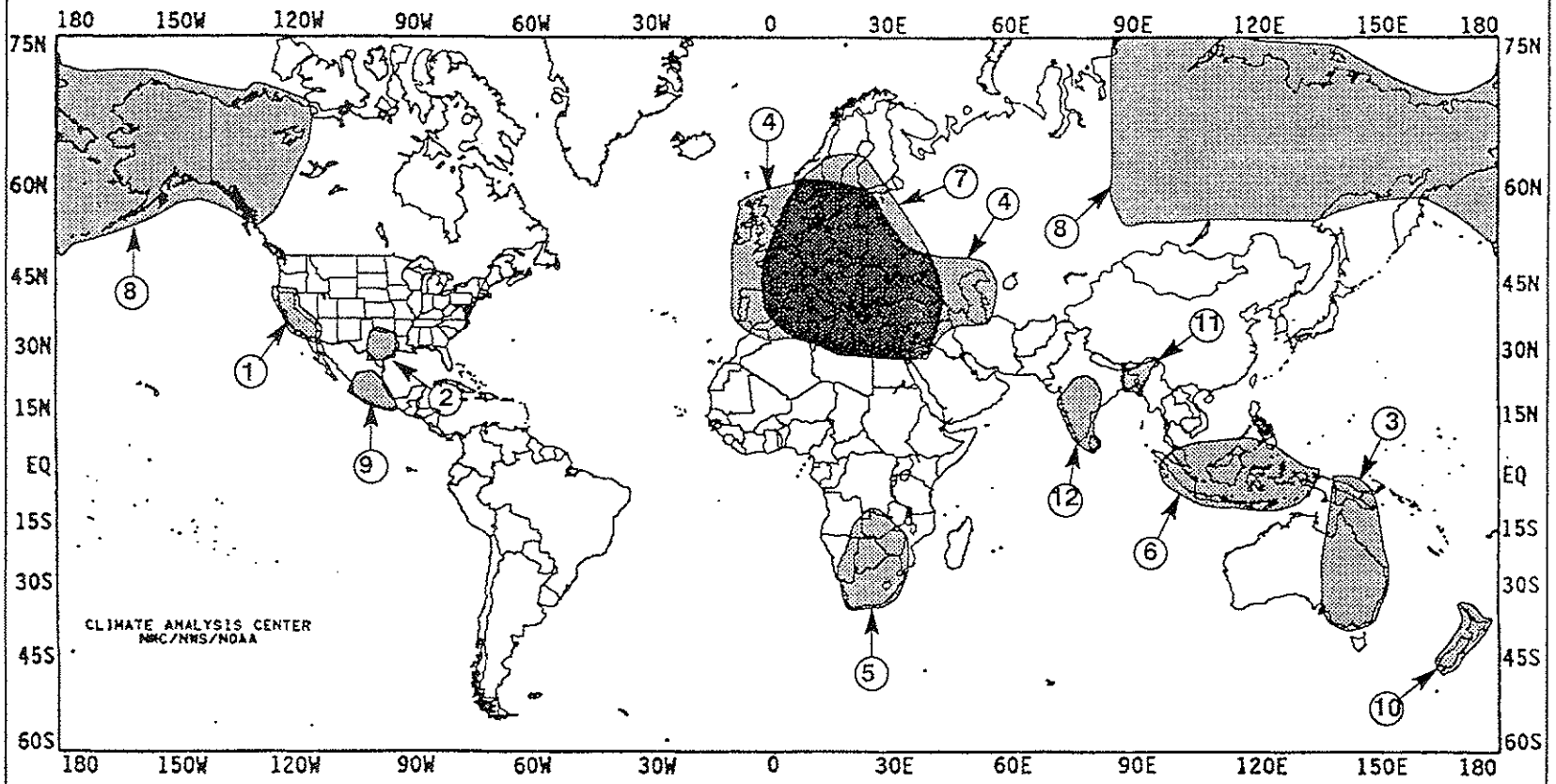

Numbers refer to specific items in the Major Climate Anomalies text.

REFERENCES

Arkin, P. A. and B. N. Meisner, 1987: The relationship between large-scale convective rainfall and cold cloud over the western hemisphere during 1982-1984. Mon. Wea. Rev., 115, 51-74.

Blackmon, M. L., 1976: A climatological spectral study of the 500 mb geopotential height of the Northern Hemisphere. J. Atmos. Sci., **33**, 1607-1623.

Halpert, M. S. and C. F. Ropelewski [Eds.], 1991, Climate Assessment: A Decadal Review, 1981-1990. [U. S. Govt. Printing Office: 1991 - 281-557/40426, 109 pp.

Janowiak, J. E. and P. A. Arkin, 1991: Rainfall variations in the tropics during 1986-89, as estimated from observations of cloud-top temperature., J. Geophys. Res., 96, 3359-3373.

Leetmaa, A., and M. Ji, 1989: Operational hindcasting of the tropical Pacific. Dyn. Atmos. Oceans, **14**, 465-490.

Rao, C. R. N., L. L. Stowe, and E. P. McClain, 1989: Remote sensing of aerosols over the oceans using AVHRR data. Theory, practice and applications. Int. J. Remote Sens., 10, (4,5); 743-749.

Reynolds, R. W., 1988: A real-time global sea surface temperature analysis. J. Climate, **1**, 75-86.

Ropelewski, C. F. and M. S. Halpert, 1986: North American precipitation and temperature patterns associated with the El Niño/Southern Oscillation (ENSO). Mon. Wea. Rev., **114**, 2352-2362.

_____, and _____, 1987: Global and Regional Scale Precipitation Patterns Associated with the El Niño/Southern Oscillation. Mon. Wea. Rev., **115**, 1606-1626.

Spencer R. W., and J. R. Christy, 1990: Precise monitoring of global temperature trends from satellites. Science, **247**, 1558-1562.

Stowe, L. L., 1991: Cloud and aerosol products at NOAA/NESDIS. Paleogeogr., Paleoclimatol., Paleoecol. (Global Planetary Change Sec.), 90: 25-32.

Stowe, L. L., R. M. Carey and P. P. Pellegrino, 1992: Monitoring the Mr. Pinatubo aerosol layer with NOAA-11 AVHRR data. Geophys. Res. Letters, 19, 2, 159-162.